Durham E-Theses

Improving the Logarithmic Accuracy of the Angular-Ordered Parton Shower

BEWICK, GAVIN

Improving the Logarithmic Accuracy of the Angular-Ordered Parton Shower

Gavin Bewick

A Thesis presented for the degree of
Doctor of Philosophy

Institute for Particle Physics Phenomenology
Department of Physics
Durham University
United Kingdom

April 2022

Improving the Logarithmic Accuracy of the Angular-Ordered Parton Shower

Gavin Bewick

Submitted for the degree of Doctor of Philosophy

April 2022

Abstract: Monte Carlo event generators are a key tool for making theoretical predictions that can be compared with the results of collider experiments, our most accurate probes of fundamental particle physics. New developments in the way parton shower accuracy is assessed have led us to re-examine the accuracy of the angular-ordered parton shower in the HERWIG 7 event generator, focussing on the way recoil is handled after successive emissions. We first discuss how the evolution variable is defined in the HERWIG angular-ordered shower and how the choice of this definition determines the recoil scheme. We then show how the recoil scheme can affect the logarithmic accuracy of final-state radiation produced by the algorithm. As part of this investigation we consider a new interpretation of the evolution variable intended to mitigate problems with previous iterations of the shower. To test this, simulated events for each scheme are compared with experimental data from both LEP and the LHC. Next we extend our analysis to initial-state radiation and perform the same process of assessing the logarithmic accuracy of different interpretations of the evolution variable. This time, we compare simulated events for each scheme with LHC data for the vector boson production. Additionally, we consider the impact that the choice of NLO matching scheme has on the accuracy of these simulations, with reference to the same LHC data.

Contents

List of Figures

List of Tables

Declaration

The work in this thesis is based on research carried out at the Institute for Particle Physics Phenomenology in the Department of Physics of Durham University in collaboration with Professor Peter Richardson, Professor Michael Seymour, Doctor Silvia Ferrario Ravasio and other members of the HERWIG collaboration. Parts of this thesis have been previously published:

- Chapter 2 is based on research published in:

  G. Bewick, S. Ferrario Ravasio, P. Richardson and M. H. Seymour, *Logarithmic Accuracy of Angular-Ordered Parton Showers* , *JHEP* **04** (2020) 019 [1904.11866]

- Chapter 3 is based on research published in:

  G. Bewick, S. Ferrario Ravasio, P. Richardson and M. H. Seymour, *Initial-State Radiation in the Herwig 7 Angular-Ordered Parton Shower*, *JHEP* **01** (2022) 026 [2107.04051]

No part of this thesis has been submitted elsewhere for any degree or qualification.

Acknowledgements

Chapter 1

Introduction

The Large Hadron Collider (LHC) at CERN has been colliding particles at centre-of-mass (CoM) energies from 7-13 TeV since 2010, producing huge quantities of high-quality measurements. So far these measurements have only corroborated the Standard Model (SM) of particle physics[1], with the most dramatic discovery being the observation of the Higgs boson in 2012 [13, 14]. Despite the SM's success in collider experiments, its failure to provide a candidate for dark matter or account for massive neutrinos means that it is considered an incomplete description of nature[2]. With no higher energy collider feasible in the immediate future, the outlook for the field of high energy physics is that any signature of Beyond Standard Model (BSM) physics will come in the form of small deviations from SM predictions. This will either emerge from data already collected at the LHC or from new measurements made at the proposed High Luminosity LHC. This can be seen as a movement of the field away from the "high energy frontier" of the previous era where the energy scale of the collision would allow the observation of new physics and towards the "precision frontier" where reducing the theoretical and experimental uncertainty on measurements at the current scale will reveal new physics.

---

[1]There are inconsistencies between LHCb measurements and the SM predictions of the branching ratios of B mesons [11, 12], however at the time of writing, the possibility that these discrepancies are due to lack of statistics or systematic uncertainties has not been ruled out.

[2]There is also evidence from Fermilab that the measured value of the muon magnetic moment does not match the SM prediction, but this too has yet to reach the threshold for significance [15].

The emphasis on precision has refocussed efforts within the field to improve the accuracy of Monte Carlo (MC) event generators, since they are the only way to simulate the complete final states produced in particle collisions. This allows for accurate predictions of SM processes and proposed BSM models in a form that can be directly compared to data from a detector like ATLAS or CMS. The most versatile of these tools are general-purpose Monte Carlo (GPMC) event generators [16], which combine 3 processes: a fixed-order approach to calculate the high energy scattering process; followed by a Markovian technique to dress the event with additional radiation of coloured particles (partons), called a parton shower (PS); and finally, a model to convert partons into hadrons and for their subsequent evolution/decay. It is now standard to include techniques to improve the description of high energy radiation while avoiding double counting of radiation from the PS, which are broadly categorised as either higher-order matching or multi-jet merging schemes. Additionally models for multiple parton interactions (MPI) and underlying event (UE) simulation have also become standard inclusions. The output of a GPMC is a final state of the kind that would be recorded in a detector. The hard scattering and PS stages of event generation are both formally derived from perturbative Quantum Chromodynamics (QCD), while the others are based on phenomenological models tuned to experimental data. Attempts to improve the formal accuracy of GPMCs are therefore restricted to the hard scattering process (and the subsequent matching and merging procedures) [17–35] and the PS [36–43].

The focus of this thesis is on the recent attempts to improve the logarithmic accuracy of the angular-ordered (AO) PS in the GPMC event generator HERWIG [44, 45]. In particular we examine how the definition of the evolution variable can determine the effect that recoil from successive emissions has on the accuracy of the shower. We further try to determine if it is possible to select an evolution variable which has the desired level of logarithmic accuracy and maintains good agreement with experimental data.

In this chapter we give an overview of Quantum Chromodynamics, the underlying

theory for the simulations discussed in this work. We describe the different parts of a hadronic collider event and how the development of different tools to accurately describe each of them is a consequence of how this theory behaves under the different energy scales or kinematics involved in a given stage of a collision. We then show how this theoretical background informs the construction of MC event generators, and give an overview of how each stage of an event is simulated. In particular we show how a parton shower algorithm is constructed and give a formal introduction to the concept of logarithmic accuracy.

In Chapter 2 we assess the effect that the definition of the evolution variable has on the logarithmic accuracy of the HERWIG AO PS for final-state radiation (FSR). Our motivation comes from a recent paper on dipole showers [41] and we outline how we have adapted elements of their technique relevant to the angular-ordered shower into our own analysis. We assess the impact that previous definitions of the evolution variable have on the handling of recoil and therefore logarithmic accuracy. In addition, we present a new interpretation of the evolution variable that is intended to mitigate problems with the previous ones. We then present comparisons of HERWIG runs using each recoil scheme to experimental data from LEP and the LHC to determine which gives the best agreement with these data.

Next, in Chapter 3 we present the effects of the new recoil scheme on initial-state radiation (ISR) and resonances. We consider the differences between the initial- and final-state showers and determine if the analysis of logarithmic accuracy carried out in Chapter 2 still holds for ISR. We then present a comparison between the old and new recoil schemes for ISR and their agreement with LHC data for vector boson production. As part of this comparison we also consider the impact of higher order matching schemes on the ability of the shower to reproduce experimental data.

In the final chapter we summarise the results presented in this thesis. We draw conclusions about the success of our endeavour to improve the logarithmic accuracy of the HERWIG AO PS and whether this work presents avenues for further improvements to be made within the angular-ordered formalism in the future.

1.1 Quantum Chromodynamics

Quantum Chromodynamics is the theory governing the interactions of quarks and gluons [46, 47], so called because of the 3 "colour" charges of the theory which give rise to "colourless" stable hadrons in analogy with RGB colour perception. This property of QCD comes from the underlying non-Abelian $SU(N_C)$ gauge symmetry of the theory, where N_C is the number of colour degrees of freedom. In the exact theory $N_C = 3$, however useful approximations can be derived from considering the limit of $N_C \rightarrow \infty$ and for this reason the N_C dependence of terms is kept in the following discussion.

The gauge structure of QCD gives rise to the Yang-Mills Lagrangian density

$$\mathcal{L}_{YM} = -\frac{1}{4} F_{\mu\nu}^a F^{a\mu\nu} + \sum_{\text{flavours}} \bar{q}_i \left(i\gamma^\mu D_\mu - m_q \right)_{ij} q_j, \tag{1.1.1}$$

where Einstein summation convention has been used and will be used for the rest of this thesis.

The first term in the Lagrangian describes the gauge bosons of the theory (the gluons) and their self interactions. The field strength tensor is given by

$$F_{\mu\nu}^a = \partial_\mu A_\nu^a - \partial_\nu A_\mu^a - g_S f^{abc} A_\mu^b A_\nu^c, \tag{1.1.2}$$

where A_μ^a are the gluon fields, g_S is the gauge coupling and f^{abc} are the structure constants of the gauge group. The gluons are in the adjoint representation with colour indices $a = 1, \ldots, (N_C^2 - 1)$.

The interactions between the quarks and gluons come from the second term in the Lagrangian. Here q_i is a quark field of mass m_q, γ^μ are the Dirac matrices and the covariant derivative is given by

$$\left(D_\mu \right)_{ij} = \delta_{ij} \partial_\mu + i g_S t_{ij}^a A_\mu^a, \tag{1.1.3}$$

where t_{ij}^a are the generators of the Lie group. Quarks are in the fundamental representation of the group and have colour indices $i = 1, \ldots, N_C$. A further feature

of quarks is that there are six species of them called flavours. Each quark flavour has its own mass, with u, d and s being much lighter than c, b and t. These flavours also differ in their interactions under the electroweak symmetry of the SM, with u, c and t having the same electroweak charges and with d,s and b sharing a different set. These flavours are all identical under QCD interactions, the effects of flavour mainly make themselves known through the quark masses (the t mass is so high that it cannot be neglected even at LHC centre-of-mass energies), the quark decay widths and in hadronic properties such as parton distribution functions.

The generators of the Lie group and the structure constants are related by the Lie algebra

$$[t^a, t^b] = t^a t^b - t^b t^a = i f^{abc} t^c. \tag{1.1.4}$$

The normalisation of the generators

$$\text{Tr}\left(t^a t^b\right) = \delta^{ab} T_R, \tag{1.1.5}$$

is chosen by convention to be $T_R = 1/2$. This in turn sets the values of the Casimirs of the group, defined by

$$t^a_{ij} t^a_{jk} = \delta_{ik} C_F, \tag{1.1.6}$$

$$f^{abc} f^{abd} = \delta^{cd} C_A, \tag{1.1.7}$$

to be $C_F = (N_C^2 - 1)/2 N_C$ and $C_A = N_C$. The quantities T_R, C_F and C_A are called colour factors and appear frequently in quantities derived from QCD calculations.

For the sake of completeness, it should be noted that in order to perform calculations in perturbative QCD a specific gauge must be chosen, which introduces a gauge fixing term into the Lagrangian. For certain choices of gauge this will lead to the introduction of "ghost" fields, which act to cancel unphysical degrees of freedom. These ghost fields only appear in higher-order calculations containing closed gluon loops. Furthermore, the final results of all QCD calculations are independent of the choice of gauge used, as required by the gauge symmetry. In this chapter we

make use of the results of higher-order calculations but since we do not calculate any ourselves, an in-depth discussion of gauges is not necessary for this thesis. There is also a final term which can be added to the Lagrangian consistent with the $SU(N_C)$ gauge symmetry that introduces charge parity (CP) violating effects. These effects are constrained by experimental observations to be vanishingly small, but this in turn requires an explanation from field theory as to why this is the case. Such questions are well beyond the scope of the work presented here, however.

1.1.1 Fixed Order QCD

Most fixed-order perturbative calculations in Quantum Field Theory (QFT) are done in the approximation where the initial state consists of free particles at a great distance from each other, that then interact weakly at the point of collision and finally the products of the reaction are scattered off far away from each other and again behave as free particles.

The equation for the cross section for a $2 \to n$ scattering process in this formalism is given by

$$\hat{\sigma} = \int \mathrm{d}\Phi_n \frac{1}{\varphi\left(p_a, p_b\right)} \left|\mathcal{M}_{ab \to n}\right|^2 \left(\Phi_n; \mu_{\mathrm{R}}\right), \qquad (1.1.8)$$

where $\varphi\left(p_a, p_b\right)$ is the flux of incoming particles, μ_{R} is the renormalisation scale (which will be discussed later) and Φ_n is the n-body phase space with differential element

$$\mathrm{d}\Phi_n = \prod_{i=1}^{n} \frac{\mathrm{d}^3 \vec{p_i}}{(2\pi)^3 2E_i} \cdot (2\pi)^4 \delta^{(4)} \left(p_a + p_b - \sum_{i=1}^{n} p_i\right), \qquad (1.1.9)$$

where p_a and p_b are the momenta of the incoming point particles and p_i, $\vec{p_i}$ and E_i are the 4-momentum, 3-momentum and energy of the ith outgoing particle. The term $\mathcal{M}$ is the matrix element (ME), or amplitude, for the process. In the equation above the matrix element has been averaged over the initial spin and colour states and summed over final spin and colour states. This is to account for the unpolarised beams and the fact that these quantum states are not measured by the detectors.

This picture is untrue for fundamental particles in QCD. Either they enter the

collision as part of a hadronic initial state (*e.g.* protons at the LHC) or they are produced in the final state and quickly form into collimated clusters of hadrons called jets. However, this formalism of fixed order matrix elements can still be used to describe the collision of two very hard[1] partons by making use of the factorisation property of QCD. This means that low energy regions of the calculation are decoupled from the high energy region and this allows for the non-perturbative effects arising from the incoming partons being bound in hadrons to be contained in terms called parton distribution functions (PDFs). The equation for the parton-level cross section can therefore be modified to give the hadron-level cross section

$$
\begin{aligned}
\sigma = \sum_{a,b} \int_0^1 \mathrm{d}x_a \ \mathrm{d}x_b \int \mathrm{d}\Phi_n f_a^{h_1}\left(x_a, \mu_F\right) f_b^{h_2}\left(x_b, \mu_F\right) \\
\times \frac{1}{\varphi\left(p_a, p_b\right)} \left|\mathcal{M}_{ab \to n}\right|^2 \left(\Phi_n; \mu_F, \mu_R\right),
\end{aligned}
\tag{1.1.10}
$$

where $f_a^{h_i}(x_a, \mu_F^2)$ is the PDF for parton a in the ith hadron, μ_F is the factorisation scale (which will be discussed later), x_a is the momentum fraction of the ith hadron carried by parton a and the sum runs over all possible parton species. The "hat" notation is used to denote parton-level quantities, so that the incident partonic flux is given by $\varphi\left(p_a, p_b\right) = 2\hat{s} = 2x_a x_b s$, where s is the hadronic CoM energy squared.

The squared ME is calculated in perturbation theory using Feynman rules derived from the QCD Lagrangian. It can therefore be written as an expansion in powers of the strong coupling

$$
\alpha_S = \frac{g_S^2}{4\pi}.
\tag{1.1.11}
$$

The point at which the series is truncated determines the accuracy of the calculation with leading order[2] (LO) keeping only the lowest order terms. This approximation is followed by next-to-leading order (NLO) and then next-to-next-to-leading order (N[2]LO) and so on. In this way there is a clear metric for assessing the accuracy of a given calculation and, just as importantly, a clear rubric for reaching the next level of accuracy. Currently NLO calculations are the highest level in common use

---

[1]The terms "hard" and "soft" are used to denote high and low energy respectively.

[2]The lowest order cross section is often called the Born cross section

in GPMC simulations so they will be the only higher order calculations considered explicitly in this thesis.

The origin of the scales μ_F and μ_R will be discussed in the following subsections. It is important to note here that they are chosen by convention and are not physically meaningful, with the explicit dependence shown in the cross sections defined above arising from the fact that such calculations must be truncated at a finite order. The choice of factorisation scale also determines which processes are described by the PDF and which are described by the ME.

The quantities calculated here are inclusive quantities, meaning that they relate to the probability of producing *at least n* final-state particles. This means that at N^mLO the calculation must include matrix elements with up to $(n + m)$ final-state particles and the corresponding higher multiplicity phase spaces. To calculate an exclusive quantity, the final-state evolution should be incorporated into the cross section, as will be discussed in the next section. The fact that this can be done in a straightforward way is another consequence of the factorisation property of QCD.

Renormalisation

When performing higher order calculations, loop diagrams must be evaluated. These diagrams translate into integrals that diverge at high energy and the theory must be renormalised to remove such ultraviolet (UV) divergences. The renormalisation process of dimensional regularisation introduces an unphysical renormalisation scale, μ_R. High energy physics above μ_R is reabsorbed into the definitions of constants, such as α_S. Since this is an arbitrary scale, physical observables must have the same value regardless of the choice of μ_R. For example, for a single scale process

$$\mu_R^2 \frac{d}{d\mu_R^2} X\left(Q^2/\mu_R^2, \alpha_S\right) \equiv \left[\mu_R^2 \frac{\partial}{\partial \mu_R^2} + \mu_R^2 \frac{\partial \alpha_S}{\partial \mu_R^2} \frac{\partial}{\partial \alpha_S}\right] X = 0, \qquad (1.1.12)$$

where Q is the energy scale at which the observable, X, is measured. From this requirement the renormalisation group equation, which describes the μ_R dependence

of α_S, is derived

$$\mu_R^2 \frac{\partial \alpha_S}{\partial \mu_R^2} = \beta\left(\alpha_S\right), \qquad (1.1.13)$$

where $\beta\left(\alpha_S\right)$ is a function which can be expressed as a perturbative series

$$-\beta(\alpha_S) = \sum_{n=0}^{\infty} b_n \alpha_S^{2+n} = \frac{\beta_0}{4\pi}\alpha_S^2 + \frac{\beta_1}{\left(4\pi\right)^2}\alpha_S^3 + \ldots \qquad (1.1.14)$$

Each order in this expansion represents a set of loop diagrams which contribute quantum corrections to the value α_S, consistent with the interpretation of renormalisation as a process of absorbing high energy physics into the definition of α_S. Examples of diagrams absorbed at 1-loop order are shown in Fig. 1.1.
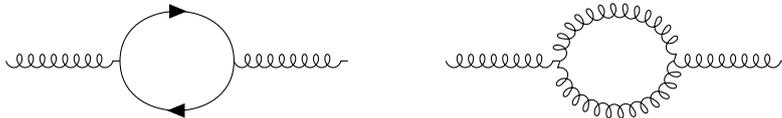
Figure 1.1: Corrections absorbed into the definition of α_S at 1-loop order.

The choice of the value of μ_R used in a given calculation depends on the process under consideration. For fixed order calculations the centre-of-mass energy of the collision is typically used to reduce the size of $\log\left(Q^2/\mu_R^2\right)$ terms which enter the calculation as coefficients of α_S. For the emission of soft and collinear radiation, which will be important for parton showers, the transverse momentum of such emissions is the natural choice of scale. This is due to the fact that the transverse momentum gives the upper limit to the logarithmically enhanced region of gluon emission [48].

If the choice is made to identify μ_R with the physical scale at which a process occurs, then the β function can be viewed as the evolution of the strong force over those physical energy scales. Unlike QED, the QCD β function is negative meaning the coupling is weak at high energy scales and strong at low energy scales[1]. Therefore perturbation theory is applicable for hard scattering processes but breaks down for soft processes.

---

[1]This explains the QCD properties of asymptotic freedom, where quarks and gluons are approximately free at high energies, and confinement, where quarks and gluons must be bound into quarks at low energies.

There is some freedom in how a renormalised quantity is defined, which is determined by the choice of renormalisation scheme that is employed. The most straightforward one is the modified minimal subtraction scheme, $\overline{\text{MS}}$, which absorbs only the divergent term plus a universal constant. For PS splitting kernels there is a set of process independent corrections that can be resummed to all orders by absorbing them into the definition of α_S, which leads to the use of the Catani-Marchesini-Webber (CMW) scheme [49] in such cases. This effectively amounts to rescaling the $\overline{\text{MS}}$ definition of the coupling, $\alpha_S^{(\overline{\text{MS}})}$, by

$$\alpha_S^{(\text{CMW})} = \alpha_S^{(\overline{\text{MS}})} \left(1 + K \frac{\alpha_S^{(\overline{\text{MS}})}}{2\pi} \right), \tag{1.1.15}$$

where K is given by

$$K = C_A \left(\frac{67}{18} - \frac{1}{6}\pi^2 \right) - \frac{5}{9}N_f, \tag{1.1.16}$$

where N_f is the number of active quark flavours. The number of active flavours is determined by the energy scale α_S is evaluated at, as quarks with masses very much larger than the relevant scale give negligible contributions to the calculation.

Subtraction

The other set of divergences that are encountered when performing higher order calculations are infrared (IR) divergences, which arise when accounting for the contributions of soft or collinear particles. The Bloch-Nordsieck [50] and Kinoshita-Lee-Nauenberg [51, 52] theorems prove that IR divergences from real and virtual sources will cancel each other out to give an overall finite cross section. However, the appearance of such divergent terms can prevent intermediate steps of a calculation from being performed so techniques such as phase space slicing and subtraction have been devised to deal with them. The most widely used and relevant to this thesis is Catani-Seymour dipole subtraction [53].

NLO calculations are often carried out in the following formalism. The Born cross

section for a $2 \to n$ process can be written as

$$\sigma^{(\text{LO})} = \int \mathrm{d}\Phi_{\mathcal{B}} \mathcal{B}_n \left(\Phi_{\mathcal{B}}; \mu_F, \mu_R \right),\tag{1.1.17}$$

where $\mathcal{B}_n$ is the Born amplitude and $\Phi_{\mathcal{B}}$ is the n-particle phase space. In order to promote this to a NLO cross section the contribution from diagrams with an extra internal (virtual) particle and an extra external (real) particle must be added. Therefore the NLO cross section can be written as

$$\sigma^{\text{NLO}} = \int \mathrm{d}\Phi_{\mathcal{B}} \left[\mathcal{B}_n \left(\Phi_{\mathcal{B}}; \mu_F, \mu_R \right) + \mathcal{V}_n \left(\Phi_{\mathcal{B}}; \mu_F, \mu_R \right) \right]$$
$$+ \int \mathrm{d}\Phi_{\mathcal{R}} \mathcal{R}_n \left(\Phi_{\mathcal{R}}; \mu_F, \mu_R \right)\tag{1.1.18}$$

where the term $\mathcal{V}_n$ contains all the contributions from an extra virtual particle, and has already been renormalised to remove UV divergences, and $\mathcal{R}$ contains all the real emission contributions. $\mathcal{V}_n$ is integrated over the n-body phase space, $\Phi_{\mathcal{B}}$, while $\mathcal{R}_n$ is integrated over the $(n+1)$-body phase space, $\Phi_{\mathcal{R}}$. The IR divergences arise in the phase space integrals of $\mathcal{V}_n$ and $\mathcal{R}$ when the additional particle is very soft or collinear to another particle. Since these integrals are not analytically solvable and must be carried out numerically in a fixed integer number of dimensions, the usual methods of dimensional regularisation are not applicable here. The motivation behind subtraction schemes is that the divergences in Eqn. 1.1.18 can be removed by inserting two subtraction terms

$$\sigma^{(\text{NLO})} = \int \mathrm{d}\Phi_{\mathcal{B}} \left[\mathcal{B}_n \left(\Phi_{\mathcal{B}}; \mu_F, \mu_R \right) + \mathcal{V}_n \left(\Phi_{\mathcal{B}}; \mu_F, \mu_R \right) + \mathcal{I}_n^{(\mathcal{S})} \left(\Phi_{\mathcal{B}}; \mu_F, \mu_R \right) \right]$$
$$+ \int \mathrm{d}\Phi_{\mathcal{R}} \left[\mathcal{R}_n \left(\Phi_{\mathcal{R}}; \mu_F, \mu_R \right) - \mathcal{S}_n \left(\Phi_{\mathcal{R}}; \mu_F, \mu_R \right) \right],\tag{1.1.19}$$

where $\mathcal{S}_n$ is called the real subtraction term and $\mathcal{I}_n$ is called the integrated subtraction term. These terms must fulfil the condition that they do not affect the overall answer, *i.e.* that

$$0 \equiv \int \mathrm{d}\Phi_{\mathcal{B}} \mathcal{I}_n^{(\mathcal{S})} \left(\Phi_{\mathcal{B}}; \mu_F, \mu_R \right) - \int \mathrm{d}\Phi_{\mathcal{R}} \mathcal{S}_n \left(\Phi_{\mathcal{R}}; \mu_F, \mu_R \right).\tag{1.1.20}$$

Catani-Seymour dipole subtraction applies the factorisation properties of the cross section calculation to derive a process independent form of these subtraction terms.

In the soft or collinear limit the amplitude factorises into the Born part and a "splitting kernel" describing the emission of an extra parton. If $2 \to 3$ kinematic mapping is also used (allowing all particles to be on their mass shells) then the phase space factorises as well, allowing the construction of the subtraction terms as follows

$$
\begin{aligned}
\mathcal{S}\left(\Phi_{\mathcal{R}}\right) &= \sum_{\text{dipoles}} \mathcal{D}\left(p_a, p_b; p_1, p_2, \ldots, p_{n+1}\right) \\
&= \sum_{ij,k} \mathcal{B}_{ij;k}\left(\Phi_{\mathcal{B}}\right) \otimes \widetilde{\mathcal{D}}_{ij;k}\left(\Phi_1\right)
\end{aligned}
\tag{1.1.21}
$$

and

$$
\begin{aligned}
\mathcal{I}^{(\mathcal{S})}\left(\Phi_{\mathcal{B}}, \varepsilon\right) &= \sum_{\text{dipoles}} \mathcal{I}^{(\mathcal{D})}\left(p_a, p_b; p_1, p_2, \ldots, p_{i-1}, p_{i+1}, \ldots, p_{n+1}\right) \\
&= \sum_{ij,k} \mathcal{B}_{ij;k}\left(\Phi_{\mathcal{B}}\right) \otimes \widetilde{\mathcal{I}}_{ij;k}^{(\mathcal{D})}\left(\Phi_{\mathcal{B}}\right)
\end{aligned}
\tag{1.1.22}
$$

where the terms denoted $\tilde{\mathcal{D}}_{ij;k}$ are the dipole splitting kernels, so called because they treat each pair of external coloured particles as a dipole from which the additional particle is produced. The dipole terms belong to a single particle phase space, Φ_1, which allows them to be integrated analytically to give the $\widetilde{\mathcal{I}}_{ij;k}^{(\mathcal{D})}$ terms.

Parton Distribution Functions

Although the interactions inside hadrons take place at energies below the scale where perturbation theory breaks down, the factorisation formula shown at the start of this section is valid. This is due to the fact that, at the high energy scales at which protons collide, the timescales of the hard collision are much larger than the timescales of interactions that characterise the internal structure of the protons. This effectively means that the two protons see a snapshot of each other as a set of (approximately) free partons at the moment of collision. This allows the partonic cross section to be calculated as if between free partons in fixed order QCD, with the distributions of partons given by parton distribution functions (PDFs). The parton distribution function introduces the factorisation scale, μ_{F}, which sets a cutoff below which any physics is absorbed into the definition of the PDF (*c.f.* μ_{R} in renormalisation). Due

to their non-perturbative nature PDFs cannot be determined from first principles, but their evolution with μ_F can be derived from perturbation theory and is given by the Dokshitser–Gribov–Lipatov–Altarelli–Parisi (DGLAP) equations [54–56]

$$
\frac{\partial}{\partial \log \mu_F^2}
\begin{pmatrix}
f_{q/h}\left(x, \mu_F^2\right) \\
f_{g/h}\left(x, \mu_F^2\right)
\end{pmatrix}
$$
$$
= \frac{\alpha_S\left(\mu_R^2\right)}{2\pi} \int_x^1 \frac{dz}{z}
\begin{pmatrix}
\mathcal{P}_{q\to q}\left(\frac{x}{z}\right) & \mathcal{P}_{g\to q}\left(\frac{x}{z}\right) \\
\mathcal{P}_{q\to g}\left(\frac{x}{z}\right) & \mathcal{P}_{g\to g}\left(\frac{x}{z}\right)
\end{pmatrix}
\begin{pmatrix}
f_{q/h}\left(z, \mu_F^2\right) \\
f_{g/h}\left(z, \mu_F^2\right)
\end{pmatrix}
\tag{1.1.23}
$$

where $\mathcal{P}_{a\to b}\left(\frac{x}{z}\right)$ are the (regularised) Altarelli-Parisi splitting kernels which give the probability of finding a parton of type b with a momentum fraction, x, of parton a after parton a undergoes a splitting process. The accuracy of the PDF depends on the order to which these splitting kernels are given. At leading order these are the probability that a parton a will go to parton of type b by emitting c in the collinear approximation, beyond leading order the identity of c is not uniquely determined by a and b so has been left implicit in Eqn. 1.1.23. In this way the evolution of a parton inside the hadron can be viewed as the result of individual emissions where a fraction of the parton's momentum is carried away by the emittied particle. As with μ_R, it is convenient to choose a value of μ_F close to the energy scale of the physical process. Indeed for many fixed order processes both scales are chosen to be the centre-of-mass energy.

1.1.2   Resummation

To consider the effect of additional QCD radiation beyond fixed order, it is useful to consider the following process. For a cross section with coloured partons in the final state, there is a probability to emit a further parton. In the soft-collinear limit the cross section factorises as follows

$$
d\sigma \approx \sigma_0 \frac{dk_\perp^2}{k_\perp^2} \frac{\alpha_S}{2\pi} P(z) dz d\phi,
\tag{1.1.24}
$$

where σ_0 is the LO cross section, $k_\perp$, z and ϕ paramaterise the phase space for the additional emission and $P(z)$ is the (unregularised) Altarelli-Parisi splitting kernel

$$P(z) = C_F \frac{1 + z^2}{1 - z}, \tag{1.1.25}$$

where for this example the kernel for the process $q \to qg$ in the massless limit has been used. This splitting kernel has been spin-averaged so there is no dependence on the azimuthal angle, ϕ. Integrating this kernel over the energy fraction retained by the quark, z, gives

$$\begin{aligned}
\int_0^{1-\varepsilon} \mathrm{d}z P(z) &= C_F \int_0^{1-\varepsilon} \mathrm{d}z \frac{1 + z^2}{1 - z} \approx C_F \left[\int_0^{1-\varepsilon} \mathrm{d}z \frac{2}{1 - z} - \int_0^1 \mathrm{d}z(1 + z) \right] \\
&= 2C_F \left[\log \frac{Q^2}{k_\perp^2} - \frac{3}{4} \right],
\end{aligned} \tag{1.1.26}$$

where $\varepsilon = k_\perp^2/Q^2$ has been used to set the upper bound on z for a gluon emission of $k_\perp$ (with $k_\perp^2 > Q_0^2$ defining the smallest possible "resolvable" emission and preventing the integral from diverging). Integration over the transverse momentum, $k_\perp$, gives

$$\int_{Q_0^2}^{Q^2} \frac{\mathrm{d}k_\perp^2}{k_\perp^2} \left(2C_F \log \frac{Q^2}{k_\perp^2} \right) = C_F \log^2 \frac{Q^2}{Q_0^2}, \tag{1.1.27}$$

where only leading logarithmic terms have been kept and the running of α_S has been ignored for simplicity. This process can be applied recursively, with each emission contributing an extra power of $\alpha_S L^2$ to the Born cross section, where $L = \log(Q^2/Q_0^2)$. The 2-jet cross section for the hard process $e^+ e^- \to q\bar{q}$ is determined by the probability of every emission *not* happening above a jet resolution scale (which in this case we have taken to be Q_0)

$$\sigma = \sigma_0 \left[1 - \frac{\alpha_S}{2\pi} C_F L^2 + \frac{1}{2!} \left(\frac{\alpha_S}{2\pi} C_F L^2 \right)^2 + \dots \right]. \tag{1.1.28}$$

The large argument of these logs spoils the convergence of the series which means *all* orders of α_S must be accounted for. This can be done as follows

$$\Delta(Q, Q_0) = \sum_{n=0}^{\infty} \frac{1}{n!} \left[-\frac{\alpha_S}{2\pi} C_F \log^2 \frac{Q^2}{Q_0^2} \right]^n = \exp \left[-\frac{\alpha_S}{2\pi} C_F \log^2 \frac{Q^2}{Q_0^2} \right], \tag{1.1.29}$$

where $\Delta\left(Q, Q_0\right)$ is the Sudakov form factor and gives the non-emission probability between Q and Q_0. Since it is derived from the sum of emission probabilities to all orders this process is called resummation.

Taking the $k_\perp$ dependence of α_{S} back into account gives the more commonly used expression for the Sudakov form factor of an arbitrary splitting process

$$\Delta\left(Q, Q_0\right) = \exp\left[-\int_{Q_0^2}^{Q^2} \frac{\mathrm{d}k_\perp^2}{k_\perp^2}\left(\frac{\alpha_{\mathrm{S}}\left(k_\perp^2\right)}{2\pi}\int_0^{1-\varepsilon}\mathrm{d}z P_{ab\to c}(z)\right)\right] \tag{1.1.30}$$

This form still only takes into account the most dominant of contributions where each is emission soft and collinear relative to the previous one. This is the double leading logarithmic approximation (because of the 2 powers of L for each power of α_{S}). Additional subleading terms also contribute from radiation that is soft *or* collinear but not both[1], giving single logarithmic terms (one power of L for each power of α_{S}). Smaller contributions come from terms with smaller powers of L relative to α_{S}.

To see how the accuracy of such a calculation can be quantified, we consider an arbitrary observable, X, which may be written as

$$X = \sum_{n=0}^{\infty}\sum_{m=0}^{2n} c_{m,n}\alpha_{\mathrm{S}}^n L^m + \mathcal{O}(\alpha_{\mathrm{S}}e^{-L}), \tag{1.1.31}$$

where the terms of order $\alpha_{\mathrm{S}}^n L^{2n}$ are the double logarithmic terms and those of order $\alpha_{\mathrm{S}}^n L^{2n-1}$ are the single logarithmic terms, with the further subleading terms ranging from those of order $\alpha_{\mathrm{S}}^n L^{2n-2}$ down to those of α_{S}^n. The class of terms with the highest powers of L are called leading logarithmc (LL), followed by the next-to-leading (NLL) terms and so on. As long as $c_{2n,n} \neq 0$ then this counting begins at the double logarithmic terms, as is the case for all observables considered in this thesis, but double and leading logarithms are not synonymous in general. If X can be written as an exponential, then an alternative form of logarithmic counting can

---

[1]Radiation in this instance may still be soft and collinear relative to the partons produced in the hard process, but the soft or collinear approximation is broken if radiation is not strongly ordered in energy or angle respectively

be employed

$$X = \exp\left[Lg_1\left(\alpha_{\mathrm{S}}L\right) + g_2\left(\alpha_{\mathrm{S}}L\right) + \alpha_{\mathrm{S}}g_3\left(\alpha_{\mathrm{S}}L\right) + \cdots\right] + \mathcal{O}(\alpha_{\mathrm{S}}e^{-L}), \qquad (1.1.32)$$

where $g_1\left(\alpha_{\mathrm{S}}L\right)$ (if non-zero) contains the LL contributions of order $\alpha_{\mathrm{S}}^n L^{n+1}$, $g_2\left(\alpha_{\mathrm{S}}L\right)$ contains the NLL contributions of order $\alpha_{\mathrm{S}}^n L^n$ *etc.* The formal "logarithmic" accuracy of a resummation calculation can therefore be defined by the level of the logarithmic terms that are taken into account, in analogy with the way that accuracy is defined for a fixed order calculation relative to leading order.

A further consideration comes from the definition of α_{S}. If the argument of the strong coupling is $k_\perp$ and the CMW scheme is adopted, then some NLL terms are included into the LL definition of the Sudakov form factor.

The Sudakov form factor has uses beyond resummation calculations. Its main application in this thesis will be in the implementation of PS algorithms in event generators. The Sudakov form factor gives the non-emission probability between two scales, q^2 and Q^2, which can be linked to the emission probability by unitarity[1], *i.e.* by the fact that the sum of emission and non-emission probabilities must be 1

$$\mathsf{P}_{\mathrm{emission}} = 1 - \mathsf{P}_{\mathrm{no\,emission}} = 1 - \Delta(Q^2, q^2). \qquad (1.1.33)$$

This is an important result because the relatively straightforward calculation of the effect of all resolvable emissions ($\Delta(Q^2, Q_0^2)$) can be used to determine the effect of all non-resolvable emissions and loops ($1 - \Delta(Q^2, Q_0^2)$) without having to evaluate these contributions directly.

Leading Colour Approximation

As mentioned at the beginning of this chapter, QCD calculations can be simplified by the approximation that $N_C \to \infty$. This is equivalent to neglecting terms suppressed

---

[1]This is only strictly true for soft or collinear emissions, which we are mainly concerned with in this regime. Contributions from hard non-collinear loops at higher orders affect the total cross section, but the following unitarity argument is still valid to NLO as these contributions can be taken account of in the normalisation of the cross section.

by $1/N_C^2$, which occur in many QCD calculations. If these terms are neglected the calculation is said to take place in the leading colour approximation. Since $N_C = 3$ for QCD, these terms represent, at most, a correction of about 10% so are safe to neglect as a first approximation. The large-N_C limit also allows the gluon's charge to be modelled as the combined charge of a quark and an anti-quark, which in turn leads to a simplification of the way colour flows through a QCD process and the approximation of QCD as interactions between colour-anticolour pairs[1].

This approximation is particularly useful for describing the logarithmically enhanced region and is frequently used in the construction of PS algorithms.

1.1.3   Hadronisation and soft QCD

Using the renormalisation group equations it is possible to define a scale, $\Lambda_{\mathrm{QCD}} \approx 250$ MeV, at which the strong coupling would diverge if perturbation theory could be extrapolated to that point. In practice, at scales $Q \sim \Lambda_{\mathrm{QCD}}$ the coupling becomes so large that perturbation theory breaks down completely and coloured particles are forced into colourless bound states called hadrons. This process is currently beyond any first-principles description, so experimental observations are used to identify some of the properties of how hadrons form.

The distribution of hadrons within a jet is dependent on whether a quark or gluon initiated the jet, but independent of the type of hard process that produced the hard parton and of the nature of the colliding particles (e^+e^-, $p\bar{p}$, *etc.*), implying that the hadronisation process is universal. The theoretical motivation for this is that, at the later stages of the event, partons can be grouped into colourless regions and either this net-zero colour charge or causality prevents these regions from interacting with each other. Therefore hadronisation takes place locally within these regions unaffected by the wider event.

The success of perturbative calculations in describing hadronic spectra in jets implies

---

[1]Such a pair is called a dipole, as already seen in the context of NLO subtraction schemes.

that observables at the hadron level will roughly follow their distribution at the parton level, a concept known as local parton-hadron duality [57].

A further indication of how to model hadronisation comes from the string effect which emerges from the semiclassical description of the self interaction of gluons. The field between two quarks increases linearly as a function of separation and the gluon field pulls itself into a one dimensional "string" between the two poles. Sufficiently hard gluons (those that were emitted during the perturbative phase) distort this straight line, so that it bends around their location. Hadrons tend to be produced along these strings, so that for a $qg\bar{q}$ system, hadrons are preferentially formed between qg or $g\bar{q}$ and not between $q\bar{q}$.

In addition to hadron formation, in order to build up a complete picture of a collision event, it is important to consider the contribution of the underlying event (UE). The UE can be defined as any final-state particles produced in the same collision as the hard process, but not originating from the hard process. Such additional activity arises because protons are extended objects containing many partons, therefore softer scatterings will occur simultaneously to the hard collision (multiple parton interactions, MPI). A further possible UE process is for the remnants of the initial-state protons (the beam remnant) to be scattered into the detector.

1.2   Monte Carlo Event Generators

GPMCs are used to simulate final states at colliders such as the LHC [16]. Though the focus on this thesis is on the HERWIG event generator, the broad features of the simulation are shared with other generators such as SHERPA [58, 59] and PYTHIA [60, 61]. The event consists of 3 main stages: the hard process; the parton shower; and hadronisation.

1.2.1 Hard Process Simulation

The first stage of an event simulation is to produce a set of particles from a hard matrix element calculated using perturbative QCD. For simple processes (leading order and with a low multiplicity of final-state particles), the GPMC will draw from a library of matrix elements which have been calculated through the standard textbook method of adding together the contributions from the relevant Feynman diagrams. For more complicated processes numerical methods are employed to generate the matrix element, leading to the use of such dedicated tools as Matchbox [62] and MadGraph [63]. However it is calculated, the squared matrix element must then be convoluted with PDFs taken from libraries based on experimental data (since PDFs cannot be calculated from first principles). The last step is integrating over allowed phase space for the initial- and final-state particles using Monte Carlo integration.

The Monte Carlo integration step has two purposes. Firstly, this is a method of calculating the overall event rate to be compared with experiment. Secondly, this is a way of generating the set of kinematic variables that are used to set the starting point for the parton shower. This is done through a process of unweighting where final-state kinematic variables, x_i, are generated by a uniform distribution then accepted with a probability of $f/f_{\max}$, where $f(x_i)$ is the integrand of the MC integration.

1.2.2 Parton Showers

The next stage of the event is the parton shower, which is a MC technique for generating additional jets, as well as jet substructure, from a hard process involving coloured particles. These features of an event are determined by processes that occur below the energy scale of the hard process and above the scales where non-perturbative effects become so large that phenomenological models must be used. The PS approach is motivated by resummation techniques, which are also used to describe QCD at these intermediate energy scales. All types of shower rely on the interpretation of the Sudakov form factor as the non-emission probability between

two evolution scales in order to generate an additional parton using an approximation of the single-emission probability in the relevant kinematic regime, called the splitting kernel. This allows a parton shower algorithm, using the veto algorithm detailed in Appendix A, to successively generate additional partons down to a soft cut-off scale. There are different types of shower algorithm, which can be categorised by the following:

- the choice of splitting kernel used;

- the choice of evolution scale and splitting variables;

- the method used to construct the kinematics of a splitting.

The two shower algorithms used in HERWIG (the dipole and angular-ordered showers discussed below) use different choices for each of these categories.

Splitting Kernels

The splitting kernels are the functions that determine the branching probability and are therefore derived from the soft or collinear limits of QCD matrix elements. In principle any function that can reproduce the soft and collinear singularities of the real emission QCD matrix element for a given process at leading colour can be used as a splitting kernel. However, all shower algorithms developed so far use either the Altarelli-Parisi splitting functions or Catani-Seymour dipole kernels, due to their success in describing PDF evolution and NLO calculations, respectively. Showers which use AP kernels are often simply called parton showers, while those that use CS kernels are called dipole showers (or antenna showers if they do not distinguish between emitter and spectator).

Evolution Scales

Parton showers require an ordering scale, t, to evolve over and a splitting parameter, z, to determine the energy fraction carried by the emitted parton. These

parameters also form the basis for the kinematics of the splitting. When calculating the probability of emitting an additional parton in the collinear limit, the following quantities become equivalent parameterisations for the phase space: the virtuality of the emitter, q; the transverse momentum of the emitted parton with respect to the emitter, $p_\perp$; and the opening angle between the emitter and emitted, θ

$$\frac{\mathrm{d}\theta^2}{\theta^2} = \frac{\mathrm{d}q^2}{q^2} = \frac{\mathrm{d}k_\perp^2}{k_\perp^2}. \tag{1.2.1}$$

Therefore $t = q^2$, $t = \theta^2$ or $t = p_\perp^2$ are equivalent choices at leading logarithmic accuracy and differences between these variables manifest in subleading logarithmic terms.

A cut-off value of this scale must also be chosen in order to determine when the shower algorithm will terminate. This value is chosen with reference to a minimum $p_\perp$ that defines the smallest possible resolvable emission[1].

Kinematics

The final component of a parton shower algorithm is a scheme to define how to map the parameters t and z onto a set of kinematics and to handle recoil to preserve momentum conservation.

The parameters t and z unambiguously define the kinematics for a single branching, using the relation between possible choices θ, q and $p_\perp$ that applies in the collinear limit, *e.g.* for massless partons

$$p_\perp^2 = z(1-z)q^2 = z^2(1-z)^2\theta^2 E^2, \tag{1.2.2}$$

where E is the energy of the branching parton. However t is open to interpretation upon successive branchings, as will be discussed in Chapter 2. The final kinematic quantity is the azimuthal angle ϕ. When spin averaged kernels are typically used (as is typically the case), ϕ can be generated from a uniform distribution.

---

[1]A minimum virtuality could be used for this instead, although all modern implementations use $p_\perp$ to define the cutoff scale

The problem of momentum conservation can be seen by examining the following process. Consider a hard process with a final state consisting of two on-shell massless partons, $\widetilde{ij}$ and k, as shown in Fig. 1.2. If an emission is generated by the shower for $\widetilde{ij}$, the massless child partons i and j are now required to be on shell. However, a massless on-shell particle cannot decay into two other on shell particles, so momentum must be reshuffled from elsewhere in the final state. This, of course, applies recursively if i or j goes on to branch. The way recoil is handled is a matter of convention, with some algorithms using a local recoil scheme where momentum is mapped between emitter, emitted and spectator partons while others use a global recoil scheme where each emission means momentum must be reallocated throughout the shower.
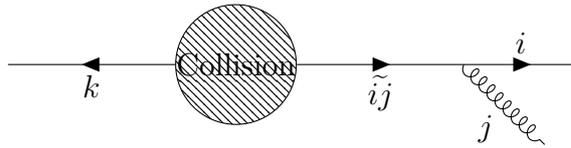
Figure 1.2: The branching of a final-state parton $\widetilde{ij}$ into partons i and j.

The Herwig Angular-Ordered Shower

For the HERWIG angular-ordered shower [64], the evolution variable, $\tilde{q}$, is (in the massless limit) given by the opening angle, θ, scaled by the energy, E, of the emitting particle

$$\tilde{q}^2 = \theta^2 E^2 = \frac{q^2}{z(1-z)}, \tag{1.2.3}$$

and the splitting parameter, z, is the light-cone momentum fraction. A modified version of $\tilde{q}$, which includes the mass, is now used in order to give a correct description of the "dead cone" region where gluon emission is suppressed around a massive quark

$$\tilde{q}^2 = \frac{q^2 - m^2}{z(1-z)}. \tag{1.2.4}$$

The AO parton shower uses $1 \to 2$ kinematics and spin-averaged Altarelli-Parisi splitting functions

$$
\begin{aligned}
P_{q \to qg} &= \frac{C_F}{1-z} \left[1 + z^2 - \frac{2m_q^2}{z\tilde{q}^2} \right], \\
P_{g \to gg} &= C_A \left[\frac{z}{1-z} + \frac{1-z}{z} + z(1-z) \right], \\
P_{g \to q\bar{q}} &= T_R \left[1 - 2z(1-z) + \frac{2m_q^2}{z(1-z)\tilde{q}^2} \right],
\end{aligned}
\tag{1.2.5}
$$

as its splitting kernels and imposes the AO condition through a veto procedure, *e.g.* for massless successive branchings, n and $(n+1)$

$$
\tilde{q}_{(n+1)}^2 < z_n^2 \tilde{q}_n^2.
\tag{1.2.6}
$$

This construction lends itself to the use of global recoil as each parton is showered individually, so there is no obvious counterpart to share recoil with. This in turn means that the kinematics of each branching are not finalised until the showering process has been terminated (and an additional Lorentz boost has been applied to ensure overall momentum conservation).

This type of shower is based on properties of gluon emission matrix elements in the soft limit. In this limit gluon emission from an ensemble of coloured particles can be described by

$$
W = \sum_{i,j} C_{ij} W_{ij},
\tag{1.2.7}
$$

where the sum runs over every pair of external partons, C_{ij} are colour factors and W_{ij} are eikonal radiation functions. For massless emitters, the eikonal radiation function is given by

$$
W_{ij} = \frac{\omega^2 p_i \cdot p_j}{p_i \cdot q\, p_j \cdot q} = \frac{1 - \cos\theta_{ij}}{\left(1 - \cos\theta_{iq}\right)\left(1 - \cos\theta_{jq}\right)},
\tag{1.2.8}
$$

where ω is the energy of the emitted gluon, q is its momentum, p_i and p_j are the momenta of partons i and j respectively, θ_i and θ_j are the angles between the emitted gluon and parton i and j respectively and θ_{ij} is the angle between i and j. These eikonal radiation functions can be split into collinear singular contributions from

each parton in the dipole[1]. When azimuthally averaged, these terms have the form

$$\left\langle W_{ij}^i \right\rangle = \frac{1}{2\left(1 - \cos\theta_i\right)} \left[1 + \frac{\cos\theta_i - \cos\theta_{ij}}{|\cos\theta_i - \cos\theta_{ij}|} \right]. \tag{1.2.9}$$

The function $\left\langle W_{ij}^i \right\rangle$ effectively contains a $\Theta(\theta_{ij} - \theta_i)$ term suppressing radiation outside of the opening angle of the emitting dipole. By considering the whole pattern of radiation, W, again it becomes apparent that emission at wider angles is identical to that of a single particle with a colour charge equal to the net charge of the dipole. The angular ordering condition comes as a natural way to simulate colour coherence in the parton shower, since a wide angle emission generated before a collinear splitting has the same probability as a coherent emission from a collinear pair, it is therefore sufficient to enforce that only the former can happen in the algorithm.

The advantage of an angular-ordered shower is its ability to capture NLL behaviour originating from soft, wide-angle emissions [49]. AO showers also include subleading colour effects that are neglected in the dipole shower. The disadvantage is that it fills a smaller region of phase space compared to other PS algorithms. This stems from its inability to generate hard wide-angle emissions and leaves an area known as a dead zone which must be filled with hard matrix element corrections (MEC). This process is effectively a special case of a multijet merging algorithm where the cut off scale is fixed. This is only done for LO matrix elements, at NLO the matching scheme will provide the emissions which fill the dead zone.

The Herwig Dipole Shower

The other shower implemented in HERWIG is the dipole shower [62]. The dipole shower uses $p_\perp$ as an ordering variable and uses a leading colour approximation to generate $2 \to 3$ splittings. The splitting kernels are spin-averaged Catani-Seymour

---

[1]here we just use dipole to mean any pairing of two coloured partons, not necessarily ones that are colour partners in the large-N_C limit

dipole kernels

$$
K_{qg,k}^{(FF)} = C_F \left[\frac{2}{1 - z_i \left(1 - y_{ij;k} \right)} - (1 + z_i) \right],
$$

$$
K_{gg,k}^{(FF)} = 2C_A \left[\frac{1}{1 - z_i \left(1 - y_{ij;k} \right)} + \frac{1}{1 - (1 - z_i) \left(1 + y_{ij;k} \right)} - 2 + z_i \left(1 - z_i \right) \right],
$$

$$
K_{q\bar{q},k}^{(FF)} = T_R \left[1 - 2z_i \left(1 - z_i \right) \right],
$$

$$
\tag{1.2.10}
$$

where z_i is the splitting parameter and $y_{ij;k}$ is the recoil parameter

$$
y_{ij;k} = \frac{p_i p_j}{p_i p_j + p_i p_k + p_j p_k},
$$

$$
z_i = \frac{p_i p_k}{p_i p_k + p_j p_k} = 1 - z_j.
$$

$$
\tag{1.2.11}
$$

For the sake of brevity, we have only shown the kernels for final-final dipoles (those dipoles where both partons are final-state particles), there are separate splitting kernels for final-initial dipoles and initial-initial dipoles. Massive splitting kernels have been developed and implemented in the HERWIG dipole shower, though we have given the massless kernels above, again, for the sake of brevity. The grouping of partons into dipoles lends itself naturally to the use of local recoil. In the dipole formalism, each emitter comes with a colour-connected spectator to absorb recoil and ensure that the momentum is conserved at the level of each dipole.

This shower has the advantage of using $p_\perp$ as an ordering variable, which allows for easier matching with NLO calculations, as will be discussed in Section 1.2.3. This shower also has the advantage of being able to populate a larger region of phase space than the AO PS, eliminating the need for MEC. Because of this a dipole shower is now the default in PYTHIA [65] and SHERPA [66].

Initial-State Radiation

The picture used to describe PS algorithms up until now has been one of additional emissions off of final state partons. However, the PS shower formalism is also required to describe soft and collinear radiation from initial-state partons, which

is more complicated than in the final-state case. For practical event generation, the kinematics of the hard process (*e.g.* the momentum fraction, x, of each parton entering the hard process) are selected first, which leaves the PS algorithm for ISR with the task of producing probable evolution histories for the incoming partons given these fixed values. This is achieved by a process of backward evolution that uses the DGLAP evolution of the PDF to give the probability of each emission. Evolving downwards in Q and upwards in x the emissions are generated in the same way as in FSR but with the Sudakov form factor weighted by the PDF

$$\Delta(Q^2, q^2)/f(x, q^2), \tag{1.2.12}$$

where q is the lower energy scale.
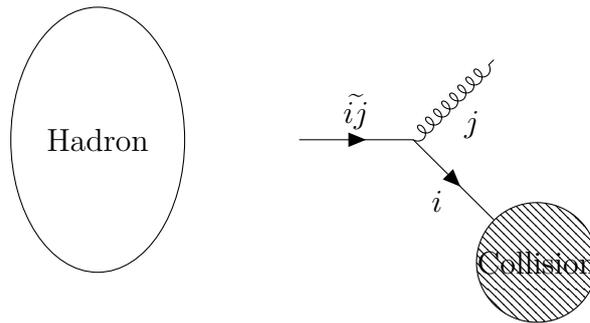
Figure 1.3: Initial-state radiation, showing the branching of parton $\widetilde{ij}$ into space-like parton i and time-like parton j. In practice, the branching is generated backwards, so that $\widetilde{ij}$ and j are added onto shower progenitor i, which acquires a negative virtuality.

This process applies to the chain of partons connecting the hard process to the incoming hadron, as shown in Fig. 1.3. Such partons are called "space-like" because they aqcuire a negative virtuality when they undergo a backwards branching, as opposed to "time-like" partons, such as those in final-state showers, which acquire a positive virtuality from forward branchings. In each step of the backwards shower, a space-like child is given a space-like parent and a time-like sibling, which is showered forward separately.

Resonances and Decays

If the final state contains particles that are unstable over the timescale of a collider event then the simulation of these decays must also be handled by the GPMC. For unstable particles with lifetimes longer than typical hadronisation timescales (*e.g.* the b quark) the decays are handled during the hadronisation phase. However, for particles that decay on shorter timescales (*e.g.* the t quark) then the decay must be handled during the shower phase. The narrow width approximation is used to inform the way that the shower proceeds in such cases.
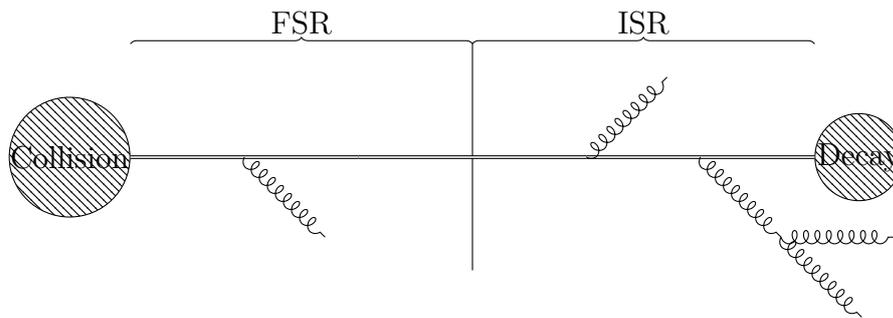
Figure 1.4: A resonance shower in the narrow width approximation. The vertical line marks the point at which the heavy particle becomes on-shell.

The resonance propagator is divided into two sections, as shown in Fig. 1.4, with the midpoint representing the point where the resonance goes on shell. The first section is connected to the hard process and is showered as a final-state shower progenitor, while the second is connected to the decay and is treated as an initial-state shower progenitor (though it is showered without using PDFs, since the evolution must go back to an on-shell parton and not a bound state). The narrow width approximation states that there is no interference between these two regimes. If the decay products are coloured then they must be subsequently showered. This algorithm may also handle resonances like weak vector bosons as these may decay to coloured particles, which must be showered, but will not undergo QCD showering themselves.

Logarithmic Accuracy

Because parton showers are designed to reproduce the results of resummation calculations they can be classified according to the logarithmic accuracy formalism. Since the showers discussed within this thesis use the leading logarithmic approximation in the construction of their splitting kernels and evolution variables, they are formally only accurate to leading logarithmic accuracy. A parton shower is only NLL accurate if it describes all sources of NLL terms, a property that has only been demonstrated by the PANSCALES parton shower algorithms [42] which are not yet implemented in a GPMC. However, by including effects which give rise to sub-leading logarithms (this is the motivation behind the angular ordering condition) or by using certain recoil schemes in preference to others, it may be possible to bring a LL algorithm closer to NLL accuracy. The effect that these choices have on the logarithmic accuracy is the main motivation for the research presented in this thesis.

1.2.3   Matching and Merging

Dressing a LO ME with a parton shower is straightforward. However, when showering a NLO ME the contribution from the real emission term, $\mathcal{R}_n$, must be carefully accounted for to avoid double counting. This has led to the development of "matching" schemes, in which the real emission term from the NLO calculation provides 1 hard emission that is integrated into the parton shower. This is typically done to ensure that the formal accuracy of both the PS and the fixed order calculation of the hard ME are maintained. The two matching schemes used in HERWIG (though these are implemented in most other GPMCs as well) are POWHEG [23] and MC@NLO [20].

The related concept of "merging" comes from the observation that emissions leading to new jets are best described by a hard ME, while parton showers best describe the pattern of radiation within a jet. Rather than producing a single emission from a full NLO calculation, merging schemes use tree level matrix elements to provide several extra emissions. In such schemes the emission phase space is divided in two

by choosing a value of a suitable scale. Above this scale, matrix elements are used to generate emissions and below it the parton shower is used.

POWHEG is a method for generating the hardest emission of a parton shower without requiring detailed knowledge of the algorithm being used. The NLO differential cross section (the integrand from Eqn. 1.1.19) is used as a starting point, integrating over the 1-particle phase space gives the NLO-weighted Born contribution

$$\overline{\mathcal{B}}_n\left(\Phi_{\mathcal{B}}\right) = \mathcal{B}\left(\Phi_{\mathcal{B}}\right) + \tilde{\mathcal{V}}_n\left(\Phi_{\mathcal{B}}\right) + \int d\Phi_1\left[\mathcal{R}_n\left(\Phi_{\mathcal{B}}\otimes\Phi_1\right) - \mathcal{S}_n\left(\Phi_{\mathcal{B}}\otimes\Phi_1\right)\right], \quad (1.2.13)$$

where the renormalised and infrared subtracted virtual term is given by

$$\tilde{\mathcal{V}}_n\left(\Phi_{\mathcal{B}}\right) = \mathcal{V}_n\left(\Phi_{\mathcal{B}}\right) + \mathcal{I}_n^{(\mathcal{S})}\left(\Phi_{\mathcal{B}}\right). \quad (1.2.14)$$

The "Born-like" term, $\overline{\mathcal{B}}_n$, is so called because it now describes a final state of n rather than $(n+1)$ particles because of the integration over the 1-particle emission phase space. The first emission is then generated in the same way as an emission in a parton shower, using the ratio

$$\mathcal{R}_n\left(\Phi_{\mathcal{B}}\otimes\Phi_1\right)/\mathcal{B}_n\left(\Phi_{\mathcal{B}}\right), \quad (1.2.15)$$

in place of the splitting kernel in the Sudakov form factor (which we denote as $\Delta_n^{(\mathcal{R}/\mathcal{B})}$). This ratio can be used instead of $\mathcal{R}/\overline{\mathcal{B}}$ because the extra emission term only needs to be accurate to first order in $\alpha_{\rm S}$ to achieve NLO accuracy. The POWHEG probability distribution up to the first emission is given by

$$\begin{aligned}
d\sigma_n^{(\rm NLO)} = {} & d\Phi_{\mathcal{B}}\overline{\mathcal{B}}_n\left(\Phi_{\mathcal{B}}\right) \\
& \times \left\{\Delta_n^{(\mathcal{R}/\mathcal{B})}\left(Q^2, Q_0^2\right) + \int_{Q_0^2}^{Q^2} d\Phi_1\left[\frac{\mathcal{R}_n\left(\Phi_{\mathcal{B}}\otimes\Phi_1\right)}{\mathcal{B}_n\left(\Phi_{\mathcal{B}}\right)}\Delta_n^{(\mathcal{R}/\mathcal{B})}\left(Q^2, t\left(\Phi_1\right)\right)\right]\right\}.
\end{aligned}$$
$$(1.2.16)$$

The term in curly brackets integrates to unity, so does not affect the overall cross section. This method is much easier for $p_\perp$-ordered showers than for angular-ordered showers, as the former can begin from the $p_\perp$ scale of the first emission while the latter require the use of a truncated shower. The truncated shower proceeds as follows:

first the shower variables for the POWHEG emission, t_P and z_P, are reconstructed; then shower is allowed to evolve as normal from the maximum scale, Q^2, down to t_P; at this point the POWHEG emission is inserted; after this has been done the shower evolution down to the cut off scale, Q_0^2, continues as normal. In addition to this any emission produced by the parton shower which would be harder than the POWHEG one must be vetoed. In this way the kinematics and colour structure of the parton shower is maintained.

The MC@NLO method requires a detailed knowledge of the PS algorithm it is matching the NLO calculation to and uses this insight to avoid double counting of the first emission from the shower and the real emission from the matrix element. This is done by decomposing the real emission term into hard, $\mathcal{H}_n$, and soft, $\mathcal{S}_n$, components

$$\mathcal{R}_n \left(\Phi_\mathcal{R}\right) = \mathcal{R}_n^{(\mathrm{S})} \left(\Phi_\mathcal{R}\right) + \mathcal{R}_n^{(\mathrm{H})} \left(\Phi_\mathcal{R}\right) = \mathcal{S}_n \left(\Phi_\mathcal{B} \otimes \Phi_1\right) + \mathcal{H}_n \left(\Phi_\mathcal{R}\right), \qquad (1.2.17)$$

and then equating the soft part with the subtraction term (hence the notation, $\mathcal{S}_n$). The subtraction term is further identified with the parton shower kernels, $\mathcal{K}_{ij;k}$, as follows

$$\mathcal{S}_n \left(\Phi_\mathcal{B} \otimes \Phi_1\right) \equiv \sum_{ijk} \mathcal{B}_n \left(\Phi_\mathcal{B}\right) \otimes \mathcal{K}_{ij;k} \left(\Phi_1\right) = \mathcal{B}_n \left(\Phi_\mathcal{B}\right) \otimes \mathcal{K} \left(\Phi_1\right), \qquad (1.2.18)$$

this is well motivated by the fact that PS kernels and subtraction terms are both designed to describe the probability of parton emission in singular limits, it is for this reason that CS dipoles were adapted for use as PS kernels. The MC@NLO differential cross section (up to the first emission) is given by

$$\mathrm{d}\sigma_n^{(\mathrm{NLO})} = \mathrm{d}\Phi_\mathcal{B} \tilde{\mathcal{B}}_n \left(\Phi_\mathcal{B}\right) \left\{ \Delta_n^{(\mathcal{K})} \left(Q^2, Q_0^2\right) + \int_{Q_0^2}^{Q^2} \mathrm{d}\Phi_1 \mathcal{K} \left(\Phi_1\right) \Delta_n^{(\mathcal{K})} \left(Q^2, t \left(\Phi_1\right)\right) \right\}$$
$$+ \mathrm{d}\Phi_\mathcal{R} \mathcal{H}_n \left(\Phi_\mathcal{R}\right),$$
$$(1.2.19)$$

where the Born-like term is given by

$$\tilde{\mathcal{B}}_n \left(\Phi_\mathcal{B}\right) = \mathcal{B}_n \left(\Phi_\mathcal{B}\right) + \tilde{\mathcal{V}}_n \left(\Phi_\mathcal{B}\right). \qquad (1.2.20)$$

The MC@NLO method is implemented as an algorithm by handing the parton shower an $(n + 1)$-particle state with a probability determined by $\mathcal{H}_n$ and an appropriate modification to the starting point of the shower. Otherwise the shower is handed an n-particle state and the first emission is generated by the parton shower. The emissions generated by the hard remainder term fill regions of phase space not filled by the parton shower and ensure that the overall cross section is accurate to NLO. These hard emissions do not affect the logarithmic accuracy of the parton shower since, by construction, $\mathcal{H}_n = \mathcal{R}_n - \mathcal{S}_n$ and therefore in regions of phase space where $\mathcal{S}_n$ is a good approximation of the emission probability $\mathcal{H}_n$ will be zero.

An example of a multi-jet merging scheme is the CKKW scheme [17], where the parton shower can be used to generate sufficiently soft or collinear jets in addition to generating jet substructure. This process uses a jet resolution parameter, y_{cut}, as defined by a jet clustering algorithm, to divide the emission phase space. A certain value of this parameter y_{ini} is used to set a scale above which jets are generated by hard MEs and below which jets are generated by parton shower emissions. The value of y_{ini} is selected by tuning to experimental data, but should be in the overlap region where both the PS and ME approaches are valid in order to ensure smooth matching between these two regimes. A hard jet configuration is selected by the following probability distribution

$$\mathsf{P}(n, i) = \frac{\sigma_{n,i}^{(LO)}}{\sum_{k,j}^{k=N} \sigma_{k,j}^{(LO)}}, \tag{1.2.21}$$

where $\sigma_{n,i}^{(LO)}$ is the tree-level cross section of multiplicity, n, and parton composition, i. Once a configuration has been chosen, the Born cross section is modified with Sudakov form factors to reweight it (the Sudakov form factor's role as the no-emission probability means that this reweighting transforms an inclusive quantity into an exclusive one). The parton shower can then run, but must veto forbidden emissions (*i.e.* emissions with too high $p_\perp$) to avoid producing any more jets separated by more than y_{ini}. This veto procedure ensures that the probability of a given jet multiplicity is independent of the arbitrary scale, y_{ini}, to NLL accuracy in the cross section.

1.2.4   Hadronisation

There are two main classes of models employed by GPMCs to simulate hadronisation: cluster models and string models. HERWIG [67] and SHERPA [68] use the former, while the latter is used in PYTHIA [69].

These models share the same broad features of grouping quarks and antiquarks into bound states to produce mesons and the creation of $q\bar{q}$ pairs non-perturbatively to ensure this process continues until a final state consisting only of hadrons is reached. However, since the large-N_C limit is used, these models cannot produce colourless bound states consisting of 3 quarks. To be able to describe the production of baryons, they rely on objects called "diquarks", where a set of either two quarks or two antiquarks is treated as a single particle. A baryon is therefore formed when a quark is grouped into a bound state with an antidiquark (or *vice versa*). In this way, the hadronisation model only needs to specify a mechanism for meson production and baryon production can be introduced by allowing the non-perturbative generation of quark-antiquark pairs to also produce diquark-antidiquark pairs. We therefore take this approach in the descriptions of the models that follow.

The cluster model is based on a property of parton showers called preconfinement, which arose from the observation that partons produced by the shower can be grouped into colour singlets with an asymptotically invariant mass spectrum independent of the hard scale. The first stage of this model is to take the partonic state from the end of the showering phase, force the gluons to split into quark-antiquark pairs and then group the resulting set of quarks into colour-singlet "clusters". Low mass clusters are interpreted as hadrons after some momentum shuffling to force them onto their mass shell. High mass clusters are interpreted as excited states of hadrons and undergo decays until the decay products reach suitably low masses to be considered hadrons. These decays proceed by producing a non-perturbative quark-antiquark pair to split a heavy cluster into two lower mass clusters. The resulting hadronic spectra closely match the partonic ones as expected by LHPD.

The string model is based on the string effect and involves treating mesons as massless quark-antiquark pairs connected by strings (the strong force is treated as a classical potential of the form $V(r) \approx \sigma r$). At the end of the showering phase, the colour structure of the whole event is used to determine the initial placement of these strings. The energy of the strings from this initial configuration will likely be too high, so they must undergo fragmentation via the creation of quark-antiquark pairs to produce low energy strings that can be identified with hadrons. Gluons are treated as kinks in these strings (or equivalently as point particles, each connected by two strings to two quarks).

1.2.5 The Underlying Event

In order to fully simulate hadronic collisions GPMCs must account for effects arising from the UE. The most significant of these arises from additional partons scattering during the same hadronic collision as the hard process (MPI). The motivation for MPI models comes from the fact that the cross section for $2 \to 2$ parton scattering (above some cut-off $p_{\perp,\text{min}}$), $\sigma_{2\to2}$, is larger than the total proton-proton cross-section, σ_{pp}. Therefore more than one partonic scattering must occur per proton-proton collision, with the ratio of the two cross sections giving the average number of scatters per event

$$\left\langle N_{\text{scatters}}\left(p_{\perp,\text{min}}\right)\right\rangle \equiv \frac{\sigma_{2\to2}\left(p_{\perp,\text{min}}\right)}{\sigma_{pp}} \geq 1. \tag{1.2.22}$$

Models based on this insight adopt the following procedure: once the hard process has been showered, additional independent pairs of back-to-back partons are generated based on the distribution of $\langle N_{\text{scatters}} \rangle - 1$. These additional scatters are showered independently, but the overall colour structure of the event must be considered before hadronisation takes place.

The MPI model used in HERWIG [70] uses the cross section of the hard process to give an estimation of the impact parameter, which in turn informs the probability of additional scatters. The effect of this is to produce a broader distribution for

$\langle N_{\mathrm{scatters}} \rangle - 1$ than would be obtained by a naive Poissonian. The theoretical motivation for this is that the number of scatters is dependent on the impact parameter and a rarer hard process implies a more direct collision between the two protons. This model also includes a simulation of soft scattering that makes up the remainder of σ_{pp} once all the scatters above $p_{\perp,\mathrm{min}}$ have been generated. The model found in PYTHIA [71] takes a different approach and instead uses a parton-shower-like algorithm based on the non-scattering probability between two energy scales.

The final state also contains particles from the beam remnant, although they will only significantly appear in the very forward regions of an event. For general-purpose pp experiments, like ATLAS and CMS, no measurement is made in these regions, either due to phase-space cuts or detector geometry. Therefore, in a GPMC event, the beam remnant is only modelled to ensure overall energy-momentum conservation and to achieve the correct colour structure of the final state [72].

It is also possible for final- and initial-state particles to interact with each other outside of the hard process, an effect known as rescattering. While a model has been implemented in PYTHIA for pp collisions [73], the effects of rescattering only become significant in heavy-ion collisions and are therefore of negligible impact on the research presented in this thesis.

Chapter 2

Logarithmic Accuracy in Final-State Radiation

2.1 Introduction

Most of the progress made in improving the formal accuracy of GPMCs over the last decade came from matching the parton shower approximation of QCD radiation with fixed-order matrix elements. This increased the accuracy of the cross-section calculation and improved the description of hard radiation, which is not adequately described by the soft and collinear approximations used in parton shower algorithms. In the last few years however there has been a revival of work [74–77] to improve the accuracy of the parton shower algorithm in antenna [78–80] and dipole [81–83] showers, as well as work on amplitude-based evolution to treat subleading colour effects [84, 85].

A recent work [41] attempted to introduce a more rigorous way to assess logarithmic accuracy and showed that two popular dipole shower algorithms, used in Pythia 8 [65] and Dire [86], have issues even at leading-logarithmic accuracy due to the way the singular emissions are split between different dipole contributions and how recoils are handled. In this chapter we will use a similar approach to that of Ref. [41]

to analyse the behaviour of the improved angular-ordered shower of Ref. [64]. While some of the issues considered in Ref. [41] are irrelevant for parton showers using $1 \to 2$ kinematics and global recoil, some of the underlying physics issues addressed can occur in the angular-ordered parton shower, although they manifest themselves in different ways.

In the next section we summarise the findings of Ref. [41] and introduce a definition of logarithmic accuracy that will guide our analysis. In section 2.3 we present the definitions of the parton momenta and kinematics used in the angular-ordered parton shower. These are then used to construct three different interpretations of the evolution variable and consider the logarithmic accuracy of each. We then discuss the tuning procedure used for the HERWIG 7 angular-ordered parton shower to ensure a like-for-like comparison between new and old evolution variables. Finally we present our conclusions. In Appendix B.1 we discuss a technical detail related to the splitting $g \to q\bar{q}$ and in Appendix B.2 we explicitly show that the default recoil scheme implemented in HERWIG 7.1 only correctly describes the double-logarithmically enhanced terms, thus justifying the proposal of a new recoil prescription.

2.2   Definition of Logarithmic Accuracy

It is difficult to define the overall logarithmic accuracy of a parton shower algorithm, a problem that stems from the fact that parton showers are used to provide predictions for a wide range of observables and processes. This is in contrast to fixed-order calculations, where a given calculation is only performed for a specific process. In Ref. [41] the authors tackled this issue by proposing a definition of logarithmic accuracy based on the following metrics:

1. The ability of a shower to reproduce tree-level matrix elements in the strongly ordered limits, *e.g.* ordered in angle and energy for LL accuracy.

2. The ability of a shower to reproduce analytic resummation results, to a given
   logarithmic accuracy, for all observables where such calculations exist.

Parton shower algorithms are designed around soft-collinear matrix elements for
a single emission on the basis that once these can be correctly reproduced then
the correct probability for an arbitrary number of emissions will follow due to the
factorisation of QCD MEs. This in turn means that the PS will correctly reproduce
the large logarithms which appear in resummation calculations and therefore will
give accurate predictions of experimental observables. However, the recoil gener-
ated by successive emissions may spoil the correspondence between the shower and
analytic n-emission probabilities. There are also problems caused by the leading
colour approximation for dipole showers that only manifest themselves after multiple
emissions. The failure to match these matrix elements can then be classified by the
order of the logarithmic terms that the PS algorithm (or a calculation based on
said algorithm) gets wrong when compared to a resummation calculation. Previous
studies have examined the ability of PS algorithms to reproduce resummation calcu-
lations to a given logarithmic order [49] or made numerical comparisons between the
PS emission probability and multi-parton matrix elements [87–90]. The innovation
of the approach taken in Ref. [41] is to make a more systematic comparison between
the exact and PS multi-parton matrix elements and then link any failure of the PS to
reproduce the real ME in a given limit to an inability to reproduce a corresponding
set of logarithmic terms in a resummation calculation.

Ref. [41] examined two parton shower algorithms PYTHIA 8 [65] and DIRE [86] and
found that they both fail to reproduce the emission probability in some enhanced
regions for 2 emissions, even though they both give the correct probability in the soft
wide-angle regime, hard collinear regime and soft collinear regime for 1 emission.

The authors considered an initial $q - \bar{q}$ dipole and the emission of two gluons g_1 and
g_2 that are both soft and collinear to either of the hard partons and widely separated
in rapidity from each other. Given these requirements, the two emissions must be

independent and the double-emission probability is

$$dP_{\text{soft}}^{(2)} = \frac{1}{2!} \prod_{i=1}^{2} \left[C_F \frac{\alpha_{\text{S}}(p_{\perp i})}{\pi} \frac{d\phi_i}{2\pi} \frac{dp_{\perp i}^2}{p_{\perp i}^2} dy_i \right], \qquad (2.2.1)$$

where y_i is the rapidity of gluon i and $p_{\perp i}$ is its transverse momentum, all computed in the original $q - \bar{q}$ dipole frame, where the z axis is aligned with the q direction. The second gluon, g_2, can be emitted either from the $\bar{q} - g_1$ or from the $q - g_1$ dipole.

The problem with the PS algorithms considered stems from the fact that subsequent emissions are constructed in separate frames where the emitter and spectator are back-to-back. By construction the emitted parton is closer in angle to the emitter than the spectator in such a frame. This is not a Lorentz invariant statement however, so upon boosting back to the original frame, the emitted parton can be closer to the spectator than the emitter. Since the emitter determines the splitting kernel this corresponds to an incorrect splitting probability. In the example given, where 2 gluons are emitted from a $q\bar{q}$ pair, the algorithm can generate g_2 as an emission from g_1, but with g_2 being collinear to q (or $\bar{q}$) in the $q - \bar{q}$ frame. This results in an incorrect colour factor, since $C_A/2$ is assigned instead of C_F. This mistake has no effect at leading colour, since $C_F \to C_A/2$ in the large number of colours limit, though it does correspond to an error in the subleading colour contribution. This causes problems for logarithmic accuracy because the $g \to gg$ splitting kernel is soft-collinear enhanced in the relevant region of phase space and therefore this corresponds to a LL error. Indeed this is born out by calculating the probability of an event shape variable having a value smaller than e^{-L}, denoted $\Sigma(L)$. At the 2-emission level for the thrust (this in fact works for a general class of observables to which thrust belongs), the difference between the analytic and PS values of $\Sigma(L)$, denoted $\delta\Sigma(L)$, gives a term which is proportional to $\alpha_{\text{S}}^2 L^4$, but colour suppressed by a factor of $1/(N_C^2 - 1)$. However, this error does not appear in other observables, such as jet broadening, emphasising the importance of considering all event shape variables, rather than one.

The handling of recoil also causes problems in the regions where the g_2 can be emitted

from g_1 but ends up being collinear to q or $\bar{q}$. The emitter receives the transverse recoil in these showers, therefore

$$\mathbf{p}_{\perp 1} \to \mathbf{p}_{\perp 1} - \mathbf{p}_{\perp 2}, \qquad (2.2.2)$$

where the bold symbol indicates it is a two-momentum. This implies that $p_{\perp 1}$ can receive a substantial modification if the transverse momentum of the second gluon is only marginally smaller than that of the first emission, thus violating Eqn. (2.2.1). Therefore the two emissions are not independent of each other and the algorithm fails to reproduce the correct splitting probability in this area of phase space. The quantitative effects are not readily apparent, however, so in Ref. [41] the ratio of PS and analytic MEs was presented as a function of $p_{\perp}$ and ϕ so that regions of phase space where the PS approximation breaks down were clearly highlighted . These include empty zones the PS cannot fill and large areas where the disagreement between the two MEs is of the order of 50%. For the 2-jet rate defined by the Cambridge algorithm, the $\delta\Sigma(L)$ between the analytic and PS momentum mappings (again for 2 emissions) has a value proportional to $\alpha_{\mathrm{S}}^2 L^2$ at leading colour, corresponding to a NLL error.

Based on these observations, a necessary (but not sufficient) condition for an algorithm to be NLL accurate is that the singularity structure of the spectrum in Eqn. (2.2.1) is reproduced in all the regions of the Lund plane [91], which describes the available phase space in terms of the transverse momenta and rapidities of the emitted gluons relative to a suitably-defined frame/axis. As was first pointed out in Ref. [91], and exploited in Ref. [41] to understand the logarithmic accuracy of parton showers, the leading-logarithmic gluon emission probability is uniform in the plane defined by the logarithm of transverse momentum and rapidity. Specific corrections to the uniform distribution can be made in specific phase space regions, to promote this description to next-to-leading logarithmic accuracy. To be exact, as the cut-off of a parton shower, or value of an event shape observable, is made logarithmically smaller ($\mathcal{O} < e^{-L}$), the area of the Lund plane increases as the square of this log-

arithm, $\sim L^2$. If a parton shower algorithm makes an order 1 error over an *area* of the Lund plane, *i.e.* a region that grows at rate proportional to L^2, we say that it is not leading-logarithmically accurate. Conversely, if it does not make such an error, we say that it has the potential to be leading-logarithmically accurate. If a parton shower algorithm makes an order 1 error only along a *line* in the Lund plane, *i.e.* a region that grows at rate proportional to L, we say that it is leading-logarithmically accurate but not next-to-leading-logarithmically accurate. Our aim is to construct an algorithm that makes order 1 errors only at isolated *points* in the Lund plane, *i.e.* regions that do not grow with L, and therefore give rise only to errors in event shape distributions of either next-to-next-to-leading logarithmic or power-suppressed order. The emission of two gluons of similar transverse momenta corresponds to a line in the Lund plane and therefore careful consideration of this configuration is required to reach next-to-leading logarithmic accuracy. The importance of recoil effects for the correct description of this region was first pointed out in Ref. [87].

We wish to adapt this form of analysis in order to assess the behaviour of the HERWIG angular-ordered shower. The subleading colour issue does not affect an angular-ordered parton shower, which implements colour coherence by construction, so that in the above example g_2 can only be emitted, with the correct colour factor, in a cone around q or g_1 that is smaller than the angle that separates q and g_1. However, the effects of recoil must be carefully taken into account and this is therefore where we will focus our efforts[1]. In particular we wish to see if the recoil scheme adopted in Ref. [93] has the potential to be NLL accurate and, if not, whether other recoil schemes meet this criterion. In the following we will consider three recoil scheme prescriptions, one of which leads to an incorrect kinematic mapping in the soft limit. In Appendix. B.2 we explicitly show how this leads to incorrect NLL contributions in the thrust distribution as an example event shape observable.

---

[1] The AO shower does also fail to reproduce NLL terms for inter-jet observables arising from soft, but non-collinear emissions [92]. However this problem is highly subleading for global event shapes and for the properites of jets themselves. Addressing this issue would require an improvement of the way that azimuthal correlations are handled, entirely separate from the issues arising from recoil. For these two reasons this source of inaccuracy is therefore not part of our investigation.

2.3   Kinematics

We define all momenta in terms of the Sudakov basis such that the 4-momentum of particle l is

$$q_l = \alpha_l p + \beta_l n + k_{\perp l}, \tag{2.3.1}$$

where the reference vectors p and n are the momentum of the parent parton with on-shell mass m_0 and a light-like vector that points in the direction of its colour partner. They obey

$$p^2 = m_0^2, \qquad p \cdot n \neq 0, \qquad n^2 = 0, \qquad p \cdot k_{\perp l} = n \cdot k_{\perp l} = 0, \tag{2.3.2}$$

so that the transverse momenta are defined with reference to the axis of p and n and the transverse momentum 4-vector $k_{\perp l}$ is space-like. If we consider a particle $\widetilde{ij}$ that splits into a pair of particles i and j, the light-cone momentum fractions of particles i and j are defined as

$$z_i = \frac{q_i \cdot n}{q_{\widetilde{ij}} \cdot n} = \frac{\alpha_i}{\alpha_{\widetilde{ij}}} = 1 - z_j. \tag{2.3.3}$$

The relative transverse momentum of the branching is given by

$$q_{\perp i} \equiv k_{\perp i} - z_i k_{\perp \widetilde{ij}} = - \left(k_{\perp j} - z_j k_{\perp \widetilde{ij}} \right), \tag{2.3.4}$$

and the magnitude of the spatial component is therefore given by

$$p_{\perp i}^2 \equiv \mathbf{p}_{\perp i}^2 = -q_{\perp i}^2. \tag{2.3.5}$$

The parton shower evolution terminates when

$$p_{\perp i}^2 < p_{\perp \min}^2, \tag{2.3.6}$$

where $p_{\perp \min}^2$ is an infrared cutoff tuned to data of the order of 1 GeV.

For many results we do not need a specific representation of the reference vectors. Where we do need a representation we use the choice made in Ref. [64] for final-state

radiation with a final-state colour partner, *i.e.*

$$p = \frac{Q}{2}\left[1 + b - c, 0, 0, \lambda\right]; \tag{2.3.7a}$$

$$n = \frac{Q}{2}\left[\lambda, 0, 0, -\lambda\right]; \tag{2.3.7b}$$

where Q is the invariant mass of the radiating particle and its colour partner, $b = m_0^2/Q^2$, $c = m_s^2/Q^2$, λ is the Källén function

$$\lambda = \lambda(1, b, c) \equiv \sqrt{1 + b^2 + c^2 - 2b - 2c - 2bc}, \tag{2.3.8}$$

and m_0, m_s are the masses of the radiating particle and its colour partner, respectively.

2.3.1   Single Emission

For the branching $0 \to 1, 2$, with no further emission we have:

$$q_0 = p + \beta_0 n; \tag{2.3.9a}$$

$$q_1 = zp + \beta_1 n + q_\perp; \tag{2.3.9b}$$

$$q_2 = (1 - z)p + \beta_2 n - q_\perp; \tag{2.3.9c}$$

where, $q_\perp$ is the transverse momentum 4-vector, $m_{0,1,2}$ are the on-shell masses of the particles, z is the light-cone momentum defined in Eqn. 2.3.3, $\beta_{1,2}$ are determined by the on-shell condition $q_{1,2}^2 = m_{1,2}^2$ and β_0 by momentum conservation. The virtuality of the parton initiating the branching is therefore

$$q_0^2 = \frac{p_\perp^2}{z(1-z)} + \frac{m_1^2}{z} + \frac{m_2^2}{(1-z)}, \tag{2.3.10}$$

where $q_\perp^2 = -p_\perp^2$.

2.3.2   Second Emission

We now consider two emissions, the first with z_1, $\tilde{q}_1$, ϕ_1 and the second from the first outgoing parton of the first branching with z_2, $\tilde{q}_2$, ϕ_2, as shown in Fig. 2.1.
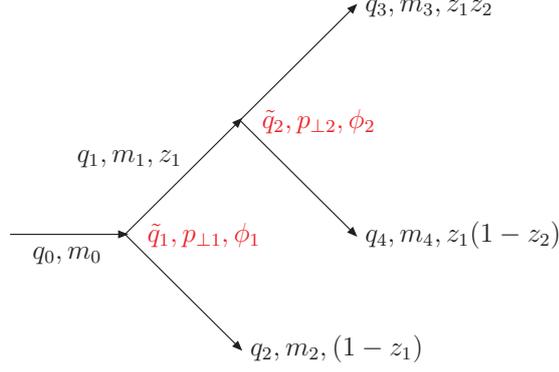
Figure 2.1: The kinematics of two branchings in the angular-ordered parton shower. The off-shell momenta (q_i), on-shell masses (m_i) and light-cone momentum fractions of the partons are shown together with the evolution variable ($\tilde{q}_i$), transverse momentum ($p_{\perp i}$) and azimuthal angle (ϕ_i) of each branching.

We define the off-shell momenta of the four partons after the branchings as:

$$q_0 = p + \beta_0 n; \tag{2.3.11a}$$

$$q_1 = z_1 p + \beta_1 n + q_{\perp 1}; \tag{2.3.11b}$$

$$q_2 = (1 - z_1) p + \beta_2 n - q_{\perp 1}; \tag{2.3.11c}$$

$$q_3 = z_1 z_2 p + \beta_3 n + z_2 q_{\perp 1} + q_{\perp 2}; \tag{2.3.11d}$$

$$q_4 = z_1 (1 - z_2) p + \beta_4 n + (1 - z_2) q_{\perp 1} - q_{\perp 2}; \tag{2.3.11e}$$

where $p^2 = m_0^2$, the β_i coefficients are fixed by the on-shell condition and momentum conservation and the space-like transverse momentum is given by

$$q_{\perp i} = [0; \mathbf{p}_{\perp i}, 0] = [0; p_{\perp i} \cos \phi_i, p_{\perp i} \sin \phi, 0], \tag{2.3.12}$$

such that $q_{\perp i}^2 = -\mathbf{p}_{\perp i}^2 = -p_{\perp i}^2$. The virtualities of the branching partons are:

$$q_0^2 = \frac{p_{\perp 1}^2}{z_1 (1 - z_1)} + \frac{q_1^2}{z_1} + \frac{m_2^2}{1 - z_1}; \tag{2.3.13a}$$

$$q_1^2 = \frac{p_{\perp 2}^2}{z_2 (1 - z_2)} + \frac{m_3^2}{z_2} + \frac{m_4^2}{1 - z_2}. \tag{2.3.13b}$$

In all the cases we consider parton 4 is a gluon, $m_4 = 0$, so that partons 1 and 3 must have the same mass, $i.e.$ $m_1 = m_3$. It is also useful to define a unit vector in

the direction of the transverse momentum, *i.e.*

$$\hat{\mathbf{n}}_i = [\cos\phi_i, \sin\phi_i] \, . \tag{2.3.14}$$

2.4   Interpretation of the Evolution Variable

In Ref. [64] the extension of the original angular-ordered parton shower [94] to include mass effects and longitudinal boost invariance along the jet axis was presented. In this algorithm the evolution variable is

$$\tilde{q}^2 = \frac{q_0^2 - m_0^2}{z(1-z)}, \tag{2.4.1}$$

in order to include mass effects (in particular the correct mass in the propagator), retain angular-ordering and have a simple single emission probability

$$\mathrm{dP} = \frac{\mathrm{d}\tilde{q}^2}{\tilde{q}^2} \frac{\alpha_{\mathrm{S}}}{2\pi} \frac{\mathrm{d}\phi}{2\pi} \mathrm{d}z P_{i \to jk}(z, \tilde{q}), \tag{2.4.2}$$

where $P_{i \to jk}(z, \tilde{q})$ is the quasi-collinear splitting function [95], z is the light-cone momentum fraction and ϕ is the azimuthal angle of the transverse momentum generated in the splitting. The strong coupling α_{S} is evaluated at the scale

$$\mu = z(1-z)\tilde{q}; \tag{2.4.3}$$

from Eqns. (2.4.1) and (2.3.10) we can see that μ coincides with the transverse momentum of the splitting [44, 49], which we label $p_\perp$, if $m_1 = m_2 = 0$.

For a single emission (or the last emission in an extended shower) where the children are on their mass shell, the kinematics are unambiguously defined by Eqn. 2.4.1 and the ordering variable can be expressed equivalently in terms of q^2 and $p_\perp^2$:

$$\tilde{q}^2 = \frac{q_0^2 - m_0^2}{z(1-z)} = \frac{p_\perp^2 + (1-z)m_1^2 + zm_2^2 - z(1-z)m_0^2}{z^2(1-z)^2}. \tag{2.4.4}$$

However, when the children of a branching go on to branch further they become off-shell, and it is clear from Eqn. (2.3.13) that we cannot simultaneously preserve

q_0^2 and $p_\perp^2$. The choice of the preserved quantity will determine the interpretation of $\tilde{q}^2$. The procedure used by HERWIG is to generate values of $\tilde{q}^2$, z and ϕ for each branching and then calculate the preserved kinematic variable from these values. Then the upper limit of $\tilde{q}^2$ is calculated for each of the children and the shower proceeds to the next branching. Only at the end of the whole shower evolution is the generation of each branching completed by constructing its kinematics from its (now off-shell) children's momenta, using the preserved kinematic variable that had been constructed from $\tilde{q}^2$. Thus any other kinematic variables are shifted slightly, to accommodate the change from on-shell to off-shell kinematics. Further details concerning the kinematic reconstruction can be found in Sec. 6.1 of Ref. [44]. As the virtuality acquired from the new partons does not depend upon the azimuthal angle, as can be seen from Eqn. (2.3.13), we can already anticipate that the shift in the other kinematic variables is not affected by the value of ϕ.

We now present our investigation into the three different choices for the preserved kinematic variable.

2.4.1 $p_\perp$ Preserving Scheme

The original choice of Ref. [64] was to use Eqn. 2.4.1 together with the expression for the virtuality in Eqn. 2.3.10, to define the transverse momentum of the branching $0 \to 1, 2$ as

$$p_\perp^2 = z^2(1-z)^2\tilde{q}^2 + m_0^2 z(1-z) - m_1^2(1-z) - m_2^2 z, \qquad (2.4.5)$$

where on-shell masses, $m_{1,2}$, are used[1] for the particles produced in the branching.

As observed in Ref. [93] this choice tends to lead to too much hard radiation from the parton shower, as the virtuality of the parent parton can arbitrarily grow after

---

[1] By default a cut-off on the transverse momentum of the splitting is applied, as described at the beginning of Sec. 2.3. However it is possible to choose a cut-off on the virtuality of the emitting parton: if this choice is adopted, $m_{1,2}$ are set to the value of the minimum virtualities allowed for particles 1 and 2.

multiple emissions.

2.4.2 q^2 Preserving Scheme

Ref. [93] suggested that the virtuality of the branching should be determined using the virtualities that the particles produced in the branching develop after subsequent evolution, such that

$$p_\perp^2 = z^2(1-z)^2\tilde{q}^2 + m_0^2 z(1-z) - q_1^2(1-z) - q_2^2 z. \qquad (2.4.6)$$

Clearly this is the same as Eqn. 2.4.5 if there is no further emission, *i.e.* $q_{1,2}^2 = m_{1,2}^2$.

This choice, however, has the problem that the subsequent evolution of the partons is not guaranteed to result in a physical, *i.e.* a $p_\perp^2 \geq 0$, solution of Eqn. 2.4.6. In Ref. [93] it was noted that vetoing emissions that give non-physical solutions affected the evolution of the total number of particles at the leading logarithmic level. Hence, if there is no physical solution the transverse momentum is set to zero such that the virtuality of the branching particle is

$$q_0^2 = \frac{q_1^2}{z} + \frac{q_2^2}{(1-z)}. \qquad (2.4.7)$$

We remark that, even if the transverse momentum of the previous emission changes, the strong coupling for that splitting remains evaluated at $z_1(1 - z_1)\tilde{q}_1$, *i.e.* the original transverse momentum for a massless splitting. Additionally, each emission can only be vetoed when it is generated to ensure that the veto is not affected by subsequent emissions.

2.4.3 Dot-Product Preserving Scheme

Motivated by the original massless angular-ordered parton shower of Ref. [94], where the evolution variable was related to the dot product of the outgoing momenta, we

investigate the choice

$$\tilde{q}^2 = \frac{2q_1 \cdot q_2 + m_1^2 + m_2^2 - m_0^2}{z(1-z)}, \tag{2.4.8}$$

where the inclusion of the masses is required to give the correct propagator in the general case. However, it is not needed for gluon emission, $m_0 = m_1$ and $m_2 = 0$, and only becomes relevant in $g \to q\bar{q}$ branching.

In this case

$$p_\perp^2 = z^2(1-z)^2\tilde{q}^2 - q_1^2(1-z)^2 - q_2^2 z^2 + z(1-z)\left[m_0^2 - m_1^2 - m_2^2\right]. \tag{2.4.9}$$

As before, this reduces to Eqn. 2.4.5 in the case of no further emission.

The major advantage of the original massless algorithm [94] was that subsequent evolution would always leave a given branching with a physical solution for the transverse momentum. If we consider gluon emission, the condition

$$\tilde{q}^2 > 2\max\left(\frac{q_1^2}{z^2}, \frac{q_2^2}{(1-z)^2}\right), \tag{2.4.10}$$

is sufficient, but not necessary, for there to be a solution for the transverse momentum in Eqn. 2.4.9. If this inequality is satisfied, the virtuality of the branching parton is

$$q_0^2 = q_1^2 + q_2^2 + z(1-z)\tilde{q}^2 \leq \frac{\tilde{q}^2}{2}. \tag{2.4.11}$$

Assuming that the branching parton was produced in a previous branching with light-cone momentum fraction, z_i, and evolution scale, $\tilde{q}_i$, the angular-ordering condition ensures that $\tilde{q} < z_i\tilde{q}_i$. Hence

$$q_0^2 \leq \frac{z_i^2\tilde{q}_i^2}{2}, \tag{2.4.12}$$

so that if Eqn. 2.4.10 is satisfied for one branching it will also be satisfied for previous branchings. Therefore, provided that we require

$$\tilde{q}^2 > 2\max\left(\frac{m_1^2}{z^2}, \frac{m_2^2}{(1-z)^2}\right), \tag{2.4.13}$$

where $m_{1,2}$ are either the physical or cut-off masses of the partons, the subsequent evolution will be guaranteed to have a physical solution for the transverse momentum.

There are, however, two issues with this choice. The first is that if we impose Eqn. 2.4.13 on radiation from a heavy quark with mass m, the transverse momentum of the branching must satisfy

$$p_\perp \geq (1-z)m, \qquad (2.4.14)$$

which, since $p_\perp \sim (1-z)E\theta$, corresponds to $\theta \geq m/E$, *i.e.* the hard dead-cone [96,97] the new algorithm was designed to avoid [64]. In practice we use a cut-off on the transverse momentum of the emission, which is fine for radiation from gluons, light quarks and even the charm quark since the cut-off is close to the charm mass. For the $3^{\rm rd}$ generation quarks we get a small fraction of events where the kinematics cannot be reconstructed ($\lesssim 0.2$ per mille and $\lesssim 0.5\%$ of $q \to qg$ branchings for bottom and top quarks, respectively, hardly varying with centre-of-mass energy). However this region is subleading, *i.e.* does not give rise to either soft or collinear logarithms, and therefore we adopt the approach of setting the transverse momentum of the emission to zero, as outlined for the q^2 preserving scheme, in such cases.

The second, although less important, issue involves the $g \to q\bar{q}$ branching process. The limit on $\tilde{q}^2$ for this case is presented in Appendix B.1. For massive quarks, in particular the bottom quark, this limit is stricter than the one arising from the cut-off on transverse momentum that we use. We therefore have some $g \to b\bar{b}$ branchings where we are forced to set the transverse momentum to zero. As before, this region is subleading ($\lesssim 0.5\%$ of $g \to b\bar{b}$ branchings, again hardly varying with centre-of-mass energy) and therefore does not affect the logarithmic accuracy. The $g \to q\bar{q}$ process only gives logarithms of the quark mass, and the neglected region does not contribute to these logarithms.

A full study of these mass effects is beyond the scope of this work, although they are very important and we hope to return to this topic in the future.
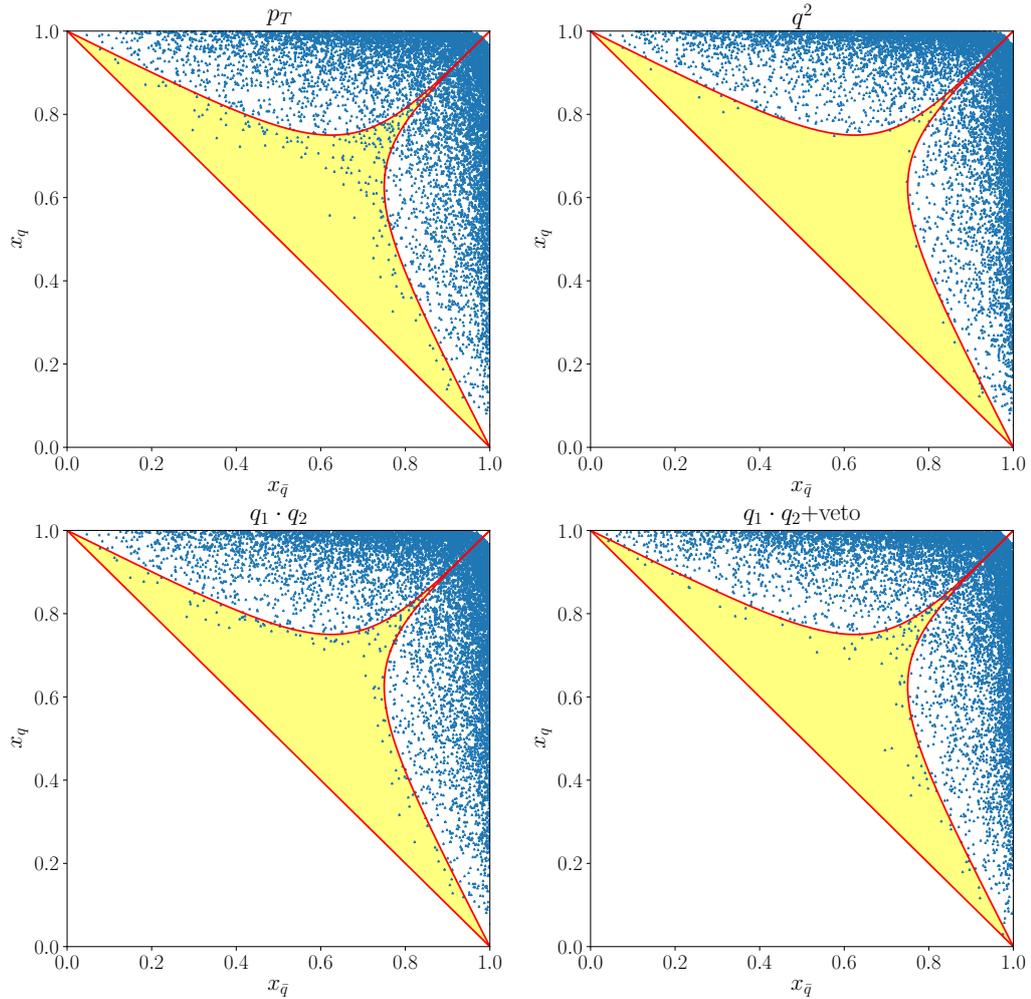
Figure 2.2: Dalitz plots for $e^+e^- \to q\bar{q}$ showing the region of phase space filled after multiple emissions from the quark and anti-quark in the angular-ordered parton shower for several choices of the preserved quantity: $p_\perp$ (upper-left panel), q^2 (upper-right panel), dot product (lower-left panel) and dot product plus q^2 veto (lower-right panel). The red line illustrates the limits for the first parton shower emission and the yellow region corresponds to the dead zone. The variable x_i is defined to be $2E_i/Q$, where E_i is the energy of parton i and Q is the total energy, all defined in the centre-of-mass frame of the collision.

Phase Space Corrections

The angular ordering of the parton shower, which allows for a consistent treatment of colour coherence effects, leads to a region of phase space without any gluon emissions, the so-called "dead zone".

The choice of the preserved quantity in the presence of multiple emissions can significantly affect the phase-space region that is filled by the shower. Fig. 2.2 illustrates the Dalitz plots for $e^+e^- \to q\bar{q}$. We have clustered the partons using

the FastJet [98] implementation of the k_T jet algorithm [99] and we have switched off $g \to q\bar{q}$ splittings in order to unambiguously define the q and $\bar{q}$ jets. We can appreciate how little the q^2 preserving scheme populates the dead zone, coloured in yellow, in contrast to the $p_\perp$ preserving scheme. This feature is essential when matching to higher order computations, like matrix element corrections, since they are designed to fill this hard region of the phase space instead of the shower. We notice that the dot-product preserving scheme (bottom-left panel) displays intermediate behaviour compared to the two other schemes, with the number of points in the dead zone for the dot-product preserving scheme about half of that in $p_\perp$ preserving scheme.

In order to reinforce the advantageous properties the dot-product preserving scheme shares with the q^2 preserving scheme, the HERWIG 7.1 default, we have implemented a rejection veto to avoid generating virtualities that are too large. Indeed the virtuality of the shower progenitor increases when multiple emissions are generated, unless the q^2 preserving scheme is used. To this end, let us consider the two-body phase space for the process $e^+ e^- \to q\bar{q}$, which reads

$$d\Phi_2(s, m^2, m^2) = \frac{d\Omega}{32\pi^2} \lambda\left(1, \frac{m^2}{s}, \frac{m^2}{s}\right), \qquad (2.4.15)$$

where Ω is the solid angle that describes the direction of the quark and λ is the Källén function introduced in Eqn. (2.3.8). When n emissions are generated the phase space becomes

$$d\Phi_{n+2} = d\Phi_2(s, k_q^2, k_{\bar{q}}^2) \prod_{i=1}^{n} \frac{d\tilde{q}_i^2}{(4\pi)^2} z_i(1 - z_i) dz_i \frac{d\phi_i}{2\pi}, \qquad (2.4.16)$$

where k_l^2 is the virtuality developed by the shower progenitor $l = q, \bar{q}$. Thus, if we want to factorise the n-body phase space over the original two-body one, we need to include the Jacobian factor

$$J = \frac{d\Phi_2(s, k_q^2, k_{\bar{q}}^2)}{d\Phi_2(s, m^2, m^2)} = \frac{\lambda(s, k_q^2, k_{\bar{q}}^2)}{\lambda(s, m^2, m^2)}. \qquad (2.4.17)$$

Since $J < 1$, we can simply implement a reweighting procedure: at the end of the

showering phase we generate a random number, r, smaller than 1 and we accept the event only if $r < J$, otherwise we shower the event anew. Looking at the Dalitz plots (bottom-right panel of Fig. 2.2), we see that while this has only a modest effect, it does produce about a 10% reduction of events in the dead zone. Note that these plots are all made with the same set of parameters.

2.5 Assessing the Logarithmic Accuracy

The angular-ordered parton shower has the correct single-emission probability by construction. However, it is still instructive to calculate the Lund variables (*i.e.* the transverse momentum, $k_\perp$, and rapidity, y) to see how the HERWIG variables relate to the physical ones. For a single gluon emission, $m_0 = m_1 = m$ and $m_2 = 0$, all three choices for the interpretation of the evolution variable are identical, giving

$$k_\perp^2 = p_\perp^2 = (1-z)^2 \left(z^2 \tilde{q}^2 - m^2 \right) \qquad \approx z^2(1-z)^2\tilde{q}^2 \qquad \approx \epsilon^2\tilde{q}^2, \qquad (2.5.1a)$$

$$y = \frac{1}{2}\ln\left[\frac{(1+b-c+\lambda)^2 Q^2 (1-z)^2}{4p_\perp^2} \right] \qquad \approx \ln\left[\frac{Q(1-z)}{p_\perp} \right] \qquad \approx \ln\left[\frac{Q}{\tilde{q}} \right], \quad (2.5.1b)$$

where $\lambda = \lambda(1,b,c)$. The first approximation is that both the radiating particle and the spectator are massless, *i.e.* $m \to 0$, and the second approximation is that the emitted gluon is soft, *i.e.* $z = 1 - \epsilon$ with $\epsilon \to 0$. We also consider $\tilde{q}/Q \to 0$, *i.e.* that the emission occurs within the logarithmically enhanced region of phase space. The HERWIG soft-collinear gluon emission probability from a massless quark line is given by

$$\mathrm{dP}_{\mathrm{soft}}^{\mathtt{Hw7}} = C_F \frac{\mathrm{d}\tilde{q}^2}{\tilde{q}^2} \frac{\alpha_S(z(1-z)\tilde{q})}{2\pi} \mathrm{d}z \frac{(1+z^2)}{1-z} \frac{\mathrm{d}\phi}{2\pi} \approx C_F \frac{\mathrm{d}\tilde{q}^2}{\tilde{q}^2} \frac{\alpha_S(\epsilon\tilde{q})}{\pi} \frac{\mathrm{d}\epsilon}{\epsilon} \frac{\mathrm{d}\phi}{2\pi}, \qquad (2.5.2)$$

if we rearrange the above expression in terms of the Lund variables $k_\perp$ and y we reproduce the correct form of the soft-collinear emission probability

$$\mathrm{dP} = C_F \frac{\alpha_S(k_\perp)}{\pi} \frac{\mathrm{d}k_\perp^2}{k_\perp^2} \mathrm{d}y \frac{\mathrm{d}\phi}{2\pi}. \qquad (2.5.3)$$

We now need to investigate the accuracy for two successive gluon emissions, *i.e.*

$m_{0,1,3} = m$, $m_{2,4} = 0$. In particular, in angular-ordered parton showers, one can obtain strongly disordered regions in which a second emission is much harder (in energy, contribution to jet virtuality or transverse momentum) than the first. We therefore have to check that the kinematics of the softer first gluon are not disturbed by the second harder one.

The different schemes only affect the relationship between the relative transverse momentum of each branching and the evolution variable, this means that the kinematics are the same in all three schemes when expressed in terms of transverse momenta. The Lund variables for the two emissions are therefore:

$$k_{\perp 1}^2 = p_{\perp 1}^2; \tag{2.5.4a}$$

$$y_1 = \frac{1}{2} \ln \left[\frac{(1 + b - c + \lambda)^2 Q^2 (1 - z_1)^2}{4 k_{\perp 1}^2} \right]; \tag{2.5.4b}$$

$$k_{\perp 2}^2 = (\mathbf{p}_{\perp 2} - (1 - z_2)\mathbf{p}_{\perp 1})^2; \tag{2.5.4c}$$

$$y_2 = \frac{1}{2} \ln \left[\frac{(1 + b - c + \lambda)^2 Q^2 z_1^2 (1 - z_2)^2}{4 k_{\perp 2}^2} \right]. \tag{2.5.4d}$$

All three choices of evolution variable are identical for the final emission in a shower, therefore

$$p_{\perp 2}^2 = (1 - z_2)^2 \left[z_2^2 \tilde{q}_2^2 - m^2 \right], \tag{2.5.5}$$

and the virtuality of the branching parton is

$$q_1^2 = z_2(1 - z_2)\tilde{q}_2^2 + m^2. \tag{2.5.6}$$

For the first branching the relationships depend on our choice of reconstruction scheme.

2.5.1 $p_\perp$ Preserving Scheme

If we use the $p_\perp$ preserving scheme then the transverse momentum of the first branching is

$$k_{\perp 1}^2 = p_{\perp 1}^2 = (1 - z_1)^2 \left[z_1^2 \tilde{q}_1^2 - m^2 \right], \tag{2.5.7}$$

the final virtual mass of the original parton is

$$q_0^2 = \frac{p_{\perp 1}^2}{z_1(1 - z_1)} + \frac{q_1^2}{z_1} = z_1(1 - z_1)\tilde{q}_1^2 + \frac{z_2(1 - z_2)\tilde{q}_2^2}{z_1} + m^2, \qquad (2.5.8)$$

and the transverse momentum of the second branching is

$$k_{\perp 2}^2 = (1 - z_2)^2 \left(z_2 \sqrt{\tilde{q}_2^2 - \frac{m^2}{z_2^2}} \hat{\mathbf{n}}_2 - z_1(1 - z_1)\sqrt{\tilde{q}_1^2 - \frac{m^2}{z_1^2}} \hat{\mathbf{n}}_1 \right)^2, \qquad (2.5.9)$$

where we recall that $\hat{\mathbf{n}}_i$ is a unit vector parallel to $\mathbf{p}_{\perp i}$, see Eqn. (2.3.14).

In the massless and soft limits: $z_{1,2} \to 1$ such that $z_{1,2} = 1 - \epsilon_{1,2}$ and $\epsilon_{1,2} \ll 1$; and $\tilde{q}_{1,2}/Q \ll 1$, with no further assumptions about the value of $\tilde{q}_2$ relative to $\tilde{q}_1$ beyond the angular-ordering condition, so that there are regions of parameter space where *e.g.* $\tilde{q}_2 \sim \epsilon_1\tilde{q}_1$. Therefore the Lund variables are

$$k_{\perp 1}^2 \approx \epsilon_1^2\tilde{q}_1^2; \qquad (2.5.10\text{a})$$

$$y_1 \approx \ln\left[\frac{Q}{\tilde{q}_1}\right] \qquad (2.5.10\text{b})$$

$$k_{\perp 2}^2 \approx \epsilon_2^2(\tilde{q}_2\hat{\mathbf{n}}_2 - \epsilon_1\tilde{q}_1\hat{\mathbf{n}}_1)^2; \qquad (2.5.10\text{c})$$

$$y_2 \approx \frac{1}{2}\ln\left[\frac{Q^2}{(\tilde{q}_2\hat{\mathbf{n}}_2 - \epsilon_1\tilde{q}_1\hat{\mathbf{n}}_1)^2}\right]; \qquad (2.5.10\text{d})$$

In the soft limit

$$q_0^2 = \epsilon_1\tilde{q}_1^2 + \epsilon_2\tilde{q}_2^2 + m^2. \qquad (2.5.11)$$

As the limit from angular-ordering is $\tilde{q}_1 \geq \tilde{q}_2$, we see that for

$$\epsilon_2\tilde{q}_2^2 > \epsilon_1\tilde{q}_1^2, \qquad (2.5.12)$$

there is a disordered region where a second, harder, gluon gives the dominant contribution to the virtuality of the original parton. In this disordered region, $k_{\perp 2} \gg k_{\perp 1}$, therefore $\epsilon_1\tilde{q}_1$ is negligible relative to $\tilde{q}_2$ and the kinematics are effectively independent. However, if instead $\tilde{q}_2 < \epsilon_1\tilde{q}_1 = k_{\perp 1}$ then the transverse momentum of the first emission overwhelms that of the second. This is the region in which the emission angle of the second gluon is smaller than the recoil angle of the quark from the first
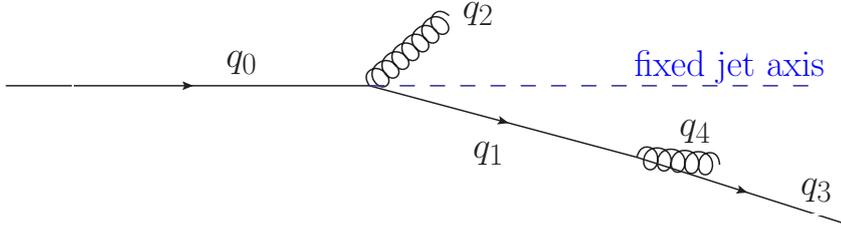
Figure 2.3: Region in which the emission angle of the second gluon is smaller than the recoil angle of the quark from the first-gluon emission.

gluon (Fig. 2.3). The kinematics in this region appear to be interdependent because the transverse momentum and rapidity are being measured relative to the fixed jet axis, not the local axis of emission[1]. If we calculate the Lund variables using q_3 as the axis then they are:

$$k_{\perp 1}^2 \approx \epsilon_1^2 (\tilde{q}_1 \hat{\mathbf{n}}_1 + \epsilon_2 \tilde{q}_2 \hat{\mathbf{n}}_2)^2; \qquad (2.5.13\text{a})$$

$$y_1 \approx \frac{1}{2} \ln \left[\frac{Q^2}{(\tilde{q}_1 \hat{\mathbf{n}}_1 + \epsilon_2 \tilde{q}_2 \hat{\mathbf{n}}_2)^2} \right]; \qquad (2.5.13\text{b})$$

$$k_{\perp 2}^2 \approx \epsilon_2^2 \tilde{q}_2^2; \qquad (2.5.13\text{c})$$

$$y_2 \approx \ln \left[\frac{Q}{\tilde{q}_2} \right]. \qquad (2.5.13\text{d})$$

The second gluon variables are now the same as the single emission case, Eqn. 2.5.1, thus retaining the correct behaviour in the soft limit. The first gluon variables are correct this time, because $\tilde{q}_2$ is always smaller than $\tilde{q}_1$ and the factor of ϵ_2 makes $\epsilon_2 \tilde{q}_2$ negligibly small compared to $\tilde{q}_1$. Thus, this scheme is accurate to leading logarithmic order as it reproduces the correct behaviour of the soft-collinear splitting function.

---

[1]Similar issues were discussed in the context of CAESAR resummation, see Ref. [100] Appendix C.

2.5.2 q^2 Preserving Scheme

For the q^2 preserving scheme

$$
\begin{aligned}
k_{\perp 1}^2 = p_{\perp 1}^2 &= \max\left(z_1^2(1-z_1)^2\tilde{q}_1^2 + m^2 z_1(1-z_1) - q_1^2(1-z_1), 0\right) \\
&= \max\left((1-z_1)\left[(1-z_1)(z_1^2\tilde{q}_1^2 - m^2) - z_2(1-z_2)\tilde{q}_2^2\right], 0\right),
\end{aligned}
\tag{2.5.14}
$$

so that the transverse momentum is non-zero if

$$
(1-z_1)(z_1^2\tilde{q}_1^2 - m^2) > z_2(1-z_2)\tilde{q}_2^2.
\tag{2.5.15}
$$

In the limit that both $z_{1,2} \to 1$ then

$$
p_{\perp 1}^2 = \max\left(\epsilon_1(\epsilon_1(\tilde{q}_1^2 - m^2) - \epsilon_2\tilde{q}_2^2), 0\right),
\tag{2.5.16}
$$

so that in the soft limit the transverse momentum is non-zero for massless partons if

$$
\epsilon_1\tilde{q}_1^2 > \epsilon_2\tilde{q}_2^2,
\tag{2.5.17}
$$

which is effectively the requirement that the generated virtualities are ordered, which is clearly violated in the disordered region we are concerned about.

In the ordered region in which a solution is possible, the Lund variables, calculated relative to the q_3 axis are:

$$
k_{\perp 1}^2 \approx \epsilon_1^2\tilde{q}_1^2 - \epsilon_1\epsilon_2\tilde{q}_2^2;
\tag{2.5.18a}
$$

$$
y_1 \approx \frac{1}{2}\ln\left[\frac{Q^2}{\tilde{q}_1^2 - \tilde{q}_2^2\frac{\epsilon_2}{\epsilon_1}}\right];
\tag{2.5.18b}
$$

$$
k_{\perp 2}^2 \approx \epsilon_2^2\tilde{q}_2^2;
\tag{2.5.18c}
$$

$$
y_2 \approx \ln\left[\frac{Q}{\tilde{q}_2}\right].
\tag{2.5.18d}
$$

In the bulk of the soft region, the $\tilde{q}_2^2$ terms are negligible. However, along the "line" $\epsilon_2\tilde{q}_2^2 \sim \epsilon_1\tilde{q}_1^2$ the generated $k_{\perp 1}^2$ value is wrong by a factor of order 1. Moreover, for most reasonable event shapes, *e.g.* thrust, the first gluon is the dominant one. Therefore this is a next-to-leading-logarithmic (NLL) error, *i.e.* the double logar-

ithmic behaviour is correct, while the single soft logarithm is incorrect. An explicit derivation for the case of the thrust is given in Appendix B.2.

In the disordered region, $p_{\perp 1} = 0$, therefore the Lund variables are:

$$k_{\perp 1}^2 \approx \epsilon_1^2 p_{\perp 2}^2 \qquad\qquad \approx \epsilon_1^2 \epsilon_2^2 \tilde{q}_2^2; \qquad\qquad (2.5.19a)$$

$$y_1 \approx \frac{1}{2} \ln \left[\frac{Q^2}{p_{\perp 2}^2} \right] \qquad\qquad \approx \frac{1}{2} \ln \left[\frac{Q^2}{\epsilon_2^2 \tilde{q}_2^2} \right]; \qquad\qquad (2.5.19b)$$

with $k_{\perp 2}^2$ and y_2 given by Eqn. 2.5.18. While the kinematics of the second gluon are correct, kinematics of the first gluon are completely wrong in this region of the Lund plane. This could, in principle, be a leading-log effect. However, for the example of the thrust distribution, in this region the second gluon is the hardest one and the first gluon gives a sub-leading contribution to the observable. Therefore, again, this effect is only significant along the line at the edge of this region and only leads to a NLL error. We conclude that the q^2 preserving is undesirable, as it reconstructs incorrect kinematics over a finite area of the Lund plane. In practice this leads to a NLL error in the thrust distribution (see Appendix B.2). Related problems with the q^2 preserving scheme were also noted in Ref. [101].

2.5.3   Dot-Product Preserving Scheme

In the dot-product preserving scheme, the transverse momentum of the first branching is

$$\begin{aligned}
k_{\perp 1}^2 = p_{\perp 1}^2 &= z_1^2 (1 - z_1)^2 \tilde{q}_1^2 - q_1^2 (1 - z_1)^2 \\
&= (1 - z_1)^2 \left[z_1^2 \tilde{q}_1^2 - z_2 (1 - z_2) \tilde{q}_2^2 - m^2 \right],
\end{aligned} \qquad (2.5.20)$$

the virtuality of the first parton is

$$q_0^2 = \tilde{q}_1^2 z_1 (1 - z_1) + \tilde{q}_2^2 z_2 (1 - z_2) + m^2, \qquad\qquad (2.5.21)$$

and the transverse momentum of the second branching is

$$k_{\perp 2}^2 = (1 - z_2)^2 \left(z_2 \sqrt{\tilde{q}_2^2 - \frac{m^2}{z_2^2}} \hat{\mathbf{n}}_2 - z_1(1 - z_1)\sqrt{\tilde{q}_1^2 - \frac{m^2}{z_1^2} - \frac{z_2(1 - z_2)\tilde{q}_2^2}{z_1^2}} \hat{\mathbf{n}}_1 \right)^2.$$

$$(2.5.22)$$

In the massless and soft limits, the Lund variables, with respect to the direction of p, are

$$k_{\perp 1}^2 \approx \epsilon_1^2(\tilde{q}_1^2 - \epsilon_2 \tilde{q}_2^2);$$

$$(2.5.23\text{a})$$

$$y_1 \approx \frac{1}{2} \ln \left[\frac{Q^2}{\tilde{q}_1^2 - \epsilon_2 \tilde{q}_2^2} \right]$$

$$(2.5.23\text{b})$$

$$k_{\perp 2}^2 \approx \epsilon_2^2(\tilde{q}_2 \hat{\mathbf{n}}_2 - \epsilon_1 \tilde{q}_1 \hat{\mathbf{n}}_1)^2;$$

$$(2.5.23\text{c})$$

$$y_2 \approx \frac{1}{2} \ln \left[\frac{Q^2}{(\tilde{q}_2 \hat{\mathbf{n}}_2 - \epsilon_1 \tilde{q}_1 \hat{\mathbf{n}}_1)^2} \right],$$

$$(2.5.23\text{d})$$

while with respect to the direction of q_3 they become

$$k_{\perp 1}^2 \approx \epsilon_1^2(\tilde{q}_1^2 + \epsilon_2 \tilde{q}_2^2);$$

$$(2.5.24\text{a})$$

$$y_1 \approx \frac{1}{2} \ln \left[\frac{Q^2}{\tilde{q}_1^2 + \epsilon_2 \tilde{q}_2^2} \right]$$

$$(2.5.24\text{b})$$

$$k_{\perp 2}^2 \approx \epsilon_2^2 \tilde{q}_2^2;$$

$$(2.5.24\text{c})$$

$$y_2 \approx \ln \left[\frac{Q}{\tilde{q}_2} \right].$$

$$(2.5.24\text{d})$$

We now see that although the difference between Eqn. 2.5.20 and Eqn. 2.5.14 looks minor, this translates into a crucial difference in the expressions for $k_{\perp 1}^2$ in the soft limit. In Eqn. 2.5.24, since $\tilde{q}_2^2$ has to be smaller than $\tilde{q}_1^2$, the factor of ϵ_2 makes $\epsilon_2 \tilde{q}_2^2$ parametrically smaller than $\tilde{q}_1^2$. Therefore, even though the virtuality can still be dominated by the second emission if $\epsilon_2 > \epsilon_1$, the second term of the expression for $k_{\perp 1}^2$ can never be as large as the first and the kinematics of the emissions are effectively independent. The dot-product preserving scheme therefore exhibits the same logarithmic accuracy as the $p_\perp$ preserving scheme.

2.5.4 Global Recoil

We also need to consider the impact that the implementation of global recoil in HERWIG 7 has on the logarithmic accuracy of the angular-ordered shower. For simplicity, here we will consider the case of two final-state particles, the generic case can be found in Ref. [44].

Consider a final state produced by particle a, with momentum

$$q_a = \sqrt{s}\,[1, 0, 0, 0]\,, \tag{2.5.25}$$

which splits into particles b and c, whose momenta are given by

$$
\begin{aligned}
p_b &= \frac{\sqrt{s}}{2}\,[1 + b - c, 0, 0, +\lambda\,(1, b, c)]\,, \\
p_c &= \frac{\sqrt{s}}{2}\,[1 - b + c, 0, 0, -\lambda\,(1, b, c)]\,,
\end{aligned}
\tag{2.5.26}
$$

where λ is the Källén function defined in Eqn. (2.3.8) and $b = m_b^2/s$, $c = m_c^2/s$. During the shower evolution, the particles acquire virtualities $q_b^2 = b's$ and $q_c^2 = c's$ and their momenta are modified to

$$q_b = p_b + \beta_b\,n_b\,, \quad q_c = p_c + \beta_c\,n_c, \tag{2.5.27}$$

where

$$
\begin{aligned}
n_b &= \frac{\sqrt{s}}{2}\lambda\,(1, b, c)\,[1, 0, 0, -1]\,, \\
n_c &= \frac{\sqrt{s}}{2}\lambda\,(1, b, c)\,[1, 0, 0, +1]\,,
\end{aligned}
\tag{2.5.28}
$$

and

$$\beta_b = \frac{s(b' - b)}{2p_b \cdot n_b} \quad \beta_c = \frac{s(c' - c)}{2p_c \cdot n_c}. \tag{2.5.29}$$

However, if we want to have two particles with invariant masses q_b^2 and q_c^2, whose three-momenta are parallel to the directions of p_b and p_c, respectively, then the two particles must have four-momenta equal to

$$
\begin{aligned}
q_b' &= \frac{\sqrt{s}}{2}\,\left[1 + b' - c', 0, 0, +\lambda\,\left(1, b', c'\right)\right]\,, \\
q_c' &= \frac{\sqrt{s}}{2}\,\left[1 - b' + c', 0, 0, -\lambda\,\left(1, b', c'\right)\right]\,.
\end{aligned}
\tag{2.5.30}
$$

Since $q_b + q_c = q_b' + q_c'$, then q_b (q_c) and q_b' (q_c') can be related by a Lorentz transform along the p_b (p_c) direction. The boost parameter for b is

$$v^{(b)} = \frac{((b+b')(1+b-c) + \lambda(b-b'))((b-b')(1+b-c) + \lambda(b+b')) - 4b^2\lambda'(1+b'-c')}{((b-b')(1+b-c) + \lambda(b+b'))^2 + 4b^2(1+b'-c')^2},$$

(2.5.31)

where we have used the shorthand notation $\lambda = \lambda(1, b, c)$ and $\lambda' = \lambda(1, b', c')$. The expression may look complicated, but if we consider that b, c, b' and c' are all much smaller than 1, we get

$$v^{(b)} \approx c' - c, \qquad\qquad v^{(c)} \approx b' - b. \qquad\qquad (2.5.32)$$

The partons that were produced during the shower also need to be boosted along the direction of their progenitor's momentum. This boost will leave the transverse momenta, the light-cone momentum fractions and the ordering variables (since $\tilde{q}$ is expressed in terms of scalar products and z) of the branchings invariant, but not the rapidities of the particles.

Indeed the rapidities of partons that have b as shower progenitor are slightly shifted towards smaller values

$$\Delta y_b = \frac{1}{2} \log\left(\frac{1 - v^{(b)}}{1 + v^{(b)}}\right) \approx -v^{(b)}, \qquad\qquad (2.5.33)$$

and the rapidities of partons produced by the c cascade are slightly shifted in the opposite direction

$$\Delta y_c = \frac{1}{2} \log\left(\frac{1 + v^{(c)}}{1 - v^{(c)}}\right) \approx v^{(c)}, \qquad\qquad (2.5.34)$$

where we have expanded the result because the boost parameter is generally much smaller than 1, being of the order of $(q^2 - m^2)/s$, where q^2 is the virtuality developed by the colour partner of the shower progenitor and m is its mass.

Let us now discuss the impact that this global recoil has on the logarithmic accuracy of soft emissions in the massless limit, *i.e.* for $b = c = 0$. Let us assume for simplicity that b is a quark and c is an anti-quark. If we use the default HERWIG 7 settings, partons originating from b will all have positive rapidity and the single emission

probability in the soft limit is

$$\mathrm{dP}_{q \to qg} = C_\mathrm{F} \frac{\alpha_\mathrm{S}(p_\perp)}{\pi} \frac{\mathrm{d}\phi}{2\pi} \frac{\mathrm{d}p_\perp^2}{p_\perp^2} \, \mathrm{d}y \, \Theta(y) \,, \tag{2.5.35}$$

while the probability of a soft-emission originating from c is given by

$$\mathrm{dP}_{\bar{q} \to \bar{q}g} = C_\mathrm{F} \frac{\alpha_\mathrm{S}(p_\perp)}{\pi} \frac{\mathrm{d}\phi}{2\pi} \frac{\mathrm{d}p_\perp^2}{p_\perp^2} \, \mathrm{d}y \, \Theta(-y) \,, \tag{2.5.36}$$

and the sum of the two contributions yields

$$\mathrm{dP}_\mathrm{soft} = C_\mathrm{F} \frac{\alpha_\mathrm{S}(p_\perp)}{\pi} \frac{\mathrm{d}\phi}{2\pi} \frac{\mathrm{d}p_\perp^2}{p_\perp^2} \, \mathrm{d}y. \tag{2.5.37}$$

However, when we apply our global recoil, the rapidity of the partons are shifted, to the left for partons coming from b and to the right for those coming from c, causing a double counting of the central-rapidity region. Therefore Eqn. (2.5.37) becomes

$$\mathrm{dP}_\mathrm{soft}^\mathtt{Hw7} = C_\mathrm{F} \frac{\alpha_\mathrm{S}(p_\perp)}{\pi} \frac{\mathrm{d}\phi}{2\pi} \frac{\mathrm{d}p_\perp^2}{p_\perp^2} \, \mathrm{d}y \left[1 + \Theta\left(|y| < \bar{v} \right) \right] , \tag{2.5.38}$$

where $\bar{v}$ is the average boost-parameter that is applied by the global recoil procedure. Nevertheless, given that $\bar{v}$ is of the order q^2/s and for soft emission q^2 is typically much smaller than s, this is a power-suppressed effect, *i.e.* non-logarithmic, and therefore does not alter the logarithmic accuracy of the parton shower.

2.6   Tuning

The new interpretation of the evolution variable means that the hadronisation parameters (which are highly sensitive to the specifics of the PS algorithm) have to be retuned. In order to do so, we follow the same strategy as that of Ref. [93]: simulated events are analysed with RIVET [102], which also enables a comparison with experimental results. The dependence of these results on the hadronisation and parton shower parameters [103] is interpolated by the PROFESSOR program [104], which also finds the set of values that best fits the experimental measurements. In our case, where observables were measured by multiple experiments, only the most

recent set of data is used. We have not included LHC data in the tuning dataset due to the high CPU-time requirement of simulating hadronic events. We only consider the transverse momentum (pTmin) as a cutoff parameter and ignore the virtuality.

In order to tune the shower and light quark hadronisation parameters we used data on jet rates and event shapes for centre-of-mass energies between 14 and 44 GeV [105–108], at LEP1 and SLD [1, 2, 107–110] and LEP2 [2, 107, 108, 110], particle multiplicities [1, 109] and spectra [1, 109, 111–123] at LEP 1, identified particle spectra below the $\Upsilon(4S)$ from Babar [124], the charged particle multiplicity and distributions from [125–130] for centre-of-mass energies between 14 and 61 GeV, the charged particle multiplicity [131, 132] and particle spectra [131, 133, 134] in light quark events at LEP1 and SLD, the charged particle multiplicity in light quark events at LEP2 [135, 136], the charged particle multiplicity distribution at LEP 1 [137–139], and hadron multiplicities at the Z-pole [140], and data on the properties of gluon jets [3, 141].

The hadronisation parameters for charm quarks were tuned using the charged multiplicity in charm events at HRS [127], SLD [132] and LEP2 [135,136], the light hadron spectra in charm events at LEP1 and SLD [131, 133, 134], the multiplicities of charm hadrons at the Z-pole [1, 140], and charm hadron spectra below the $\Upsilon(4S)$ [142–144] and at LEP1 [145].

The hadronisation parameters for bottom quarks were tuned using the charged multiplicity in bottom events at HRS [127], SLD [132] and LEP2 [135, 135, 136], the light hadron spectra and event shapes in bottom events at LEP1 and SLD [108, 131, 133, 134, 141], the multiplicities of charm and bottom hadrons at the Z-pole [1, 140], charm hadron spectra at LEP1 [113, 145] and the bottom fragmentation function measured at LEP1 and SLD [4, 146–148].

PROFESSOR offers the ability to weight each observable differently: we adopted the same weights as in Ref. [93]. Furthermore, as in [93], to prevent the fit being dominated by a few observables with very small experimental uncertainty, we imposed a minimum relative error of 5% in the computation of the chi-squared χ^2.

The following procedure was adopted to tune HERWIG 7.

1. The strong coupling computed in the CMW scheme [49] (α_S^{CMW}), the minimum transverse momentum allowed in the showering phase ($p_\perp^{\min}$) and the light quark hadronisation parameters are tuned to event shapes, charged-particle multiplicity and identified-particle spectra and rates which only involve light quark hadrons. This class of observables is labelled as "general" in Tab. 2.2.

2. The hadronisation parameters for bottom quarks are then tuned to the bottom quark fragmentation function, event shapes and the identified-particle spectra from $b\bar{b}$ events.

3. The hadronisation parameters involving charm quarks are then tuned to identified-particle spectra and measurements of event shapes from charm events.[1]

4. We then vary one parameter at a time to see if our tune corresponds to the minimum χ^2. In case any of the parameters are significantly far from the minimum, we retune all of them (this time considering the experimental distributions for light, bottom and charm quarks together).

5. We repeat the previous step except that now if any parameters are too far from the value that gives the minimum χ^2, their values are adjusted by hand. In particular, this is needed for bottom quark hadronisation parameters like ClMaxBottom which PROFESSOR is not able to tune: this behaviour was also found in Ref. [93].

The values of the HERWIG 7.1 default parameters and the new ones we find with our tuning procedure are shown in Tab. 2.1. The values of χ^2 per degree of freedom computed with the observables used for the tune, together with some recent data from

---

[1] Charm parameters are the last to be determined, since charm hadrons are also produced from b-hadron decays.

Preserved	$p_\perp$ in [93]	q^2 in [93]	$p_\perp$	q^2	$q_i \cdot q_j$	$q_i \cdot q_j$+veto
Light-Quark Hadronisation and Shower parameters						
AlphaMZ ($\alpha_s^{\mathrm{CMW}}(M_Z)$)	0.1087	0.1262	0.1074	0.1244	0.1136	0.1186
pTmin	0.933	1.223	0.900	1.136	0.924	0.958
ClMaxLight	3.639	3.003	4.204	3.141	3.653	3.649
ClPowLight	2.575	1.424	3.000	1.353	2.000	2.780
PSplitLight	1.016	0.848	0.914	0.831	0.935	0.899
PwtSquark	0.597	0.666	0.647	0.737	0.650	0.700
PwtDIquark	0.344	0.439	0.236	0.383	0.306	0.298
Bottom Hadronisation Parameters						
ClMaxBottom	4.655	3.911	5.757	2.900	6.000	3.757
ClPowBottom	0.622	0.638	0.672	0.518	0.680	0.547
PSplitBottom	0.499	0.531	0.557	0.365	0.550	0.625
ClSmrBottom	0.082	0.020	0.117	0.070	0.105	0.078
SingleHadronLimitBottom	0.000	0.000	0.000	0.000	0.000	0.000
Charm Hadronisation Parameters						
ClMaxCharm	3.551	3.638	4.204	3.564	3.796	3.950
ClPowCharm	1.923	2.332	3.000	2.089	2.235	2.559
PSplitCharm	1.260	1.234	1.060	0.928	0.990	0.994
ClSmrCharm	0.000	0.000	0.098	0.141	0.139	0.163
SingleHadronLimitCharm	0.000	0.000	0.000	0.011	0.000	0.000

Table 2.1: The Monte Carlo parameters obtained for different choices of the preserved quantity in the angular-ordered shower.

the ATLAS experiment [5] that is sensitive to both quark and gluon jet properties, are shown in Tab. 2.2.

From Tab. 2.1 we observe that the four reconstruction choices correspond to four significantly different values of the strong coupling, where smaller values correspond to the schemes that give a poorer description of the non-logarithmically enhanced region of the spectrum. In particular, we note that the introduction of the veto procedure to the dot-product preserving scheme induces a 4% enhancement of α_{S}.

2.7 Results

In this section we present the results of simulations produced with the tuned implementations of the recoil schemes discussed above, in order to compare the predictions obtained with each recoil scheme to experimental data. We first discuss the LEP results, for which HERWIG provides matrix-element corrections (MEC), and then LHC ones for which HERWIG does not.

Preserved	$p_\perp$	q^2	$q_i \cdot q_j$	$q_i \cdot q_j$+veto
χ^2 **per d.o.f considering several sets of observables**				
general	4.406	3.152	3.735	3.352
bottom	5.964	6.494	5.127	4.118
charm	2.306	1.725	1.838	1.912
ATLAS jets	0.1598	0.4124	0.1925	0.5396
χ^2 **per d.o.f considering sub-samples of the "general" observables**				
mult	3.031	2.757	2.822	2.776
event	6.959	3.461	5.191	3.877
ident	10.706	9.950	9.777	10.105
jet	4.579	3.226	4.093	3.638
gluon	1.128	1.174	1.237	1.216
charged	5.439	2.515	3.724	2.856

Table 2.2: The χ^2 per degree of freedom for different choices of the preserved quantity in the angular-ordered shower, obtained with the distributions we used to tune the light, bottom and charm parameters respectively. The χ^2 per degree of freedom corresponding to ATLAS jets, particle multiplicities (mult), event shapes (event), identified-particle spectra (ident), quark jets (jet), gluon jets (gluon) and charged particle distributions (charged) are also shown.

2.7.1   LEP results

The first event-shape distribution we consider is thrust, Fig. 2.4. We find the well-known behaviour of the $p_\perp$ preserving scheme, which overpopulates the non-logarithmically-enhanced region of phase space that is already filled by MEC, which corresponds to the tail of the distribution. Although the dot-product scheme performs better than the $p_\perp$ one, it still overpopulates the dead zone, however the description of the tail of the spectrum improves if we include the rejection veto described in Sec. 2.4.3. In the right panel of Fig. 2.4 an expanded view of the small $1 - T$ region is displayed, where we notice that the new choice of the recoil yields a better agreement with data.

Very similar conclusions can be drawn from the thrust major and minor (Fig. 2.5) distributions, and from the plots of the C- and D-parameters (Fig. 2.6). We see that for all the event shape distributions (except for D), in the region of phase space not populated by the angular-ordered shower, all the options over-populate the first bin. Furthermore, that the q^2 and dot-product-plus-veto are similar to each other and
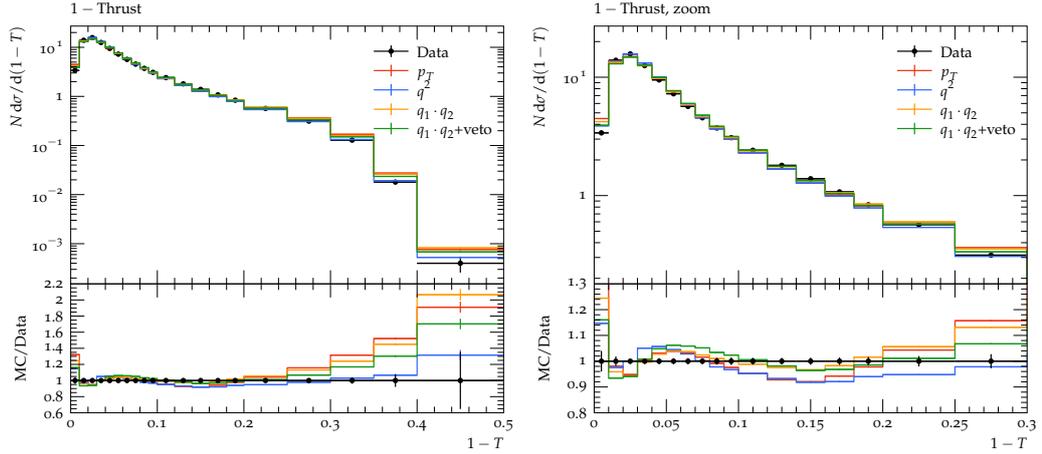
Figure 2.4: The thrust at the Z-pole compared with data from the DELPHI [1] experiment. In the right panel an expanded view of the small $1 - T$ region is shown.
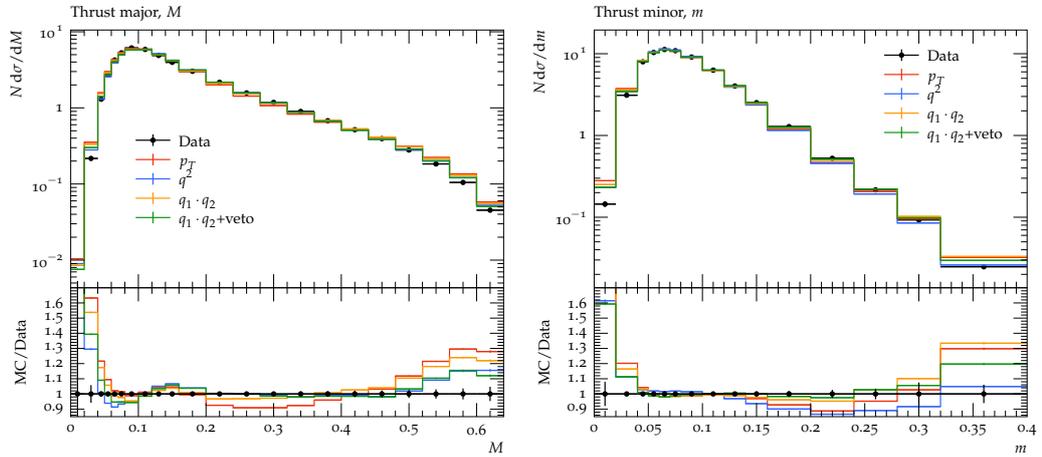
Figure 2.5: Thrust major (left) and minor (right) at the Z-pole compared with data from the DELPHI [1] experiment.

closest to the data in this region.

Looking at the behaviour of the jet resolution parameter in Fig. 2.7 we observe that the $p_\perp$ scheme most closely matches the data in the large $-\log(y_{23})$ (small y_{23}) tail of the distribution. However, in the small $-\log(y_{23})$ region the q^2 scheme yields a better description of the data. The dot-product scheme with the veto behaves very similar to the q^2 scheme over the whole spectrum, while the scheme without the veto is similar to the $p_\perp$ scheme in the tail of the distribution and to the q^2 one in the opposite limit, thus retaining the best description of the data over the whole range.

In Fig. 2.8 we show the multiplicity distributions of charged particles in gluon jets for two different gluon energies. We see that the differences between all of the recoil
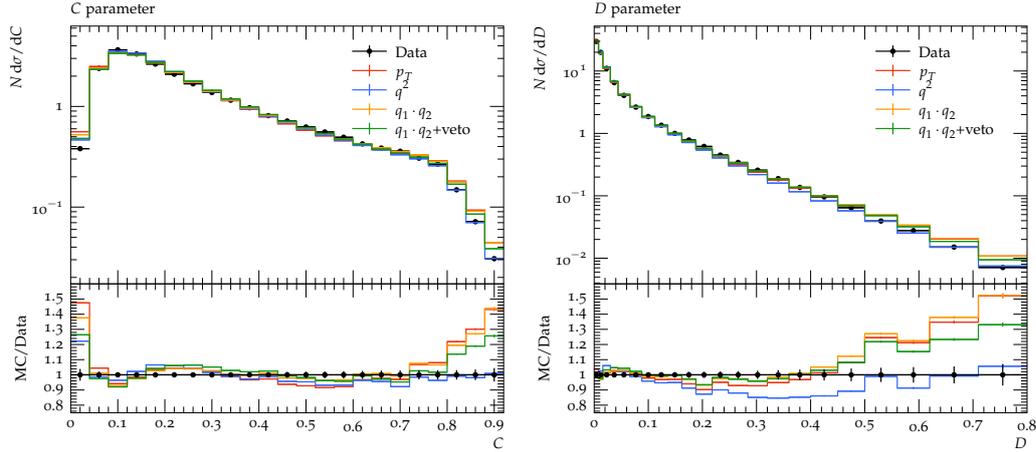
Figure 2.6: C (left) and D (right) parameters at the Z-pole compared with data from the DELPHI [1] experiment.
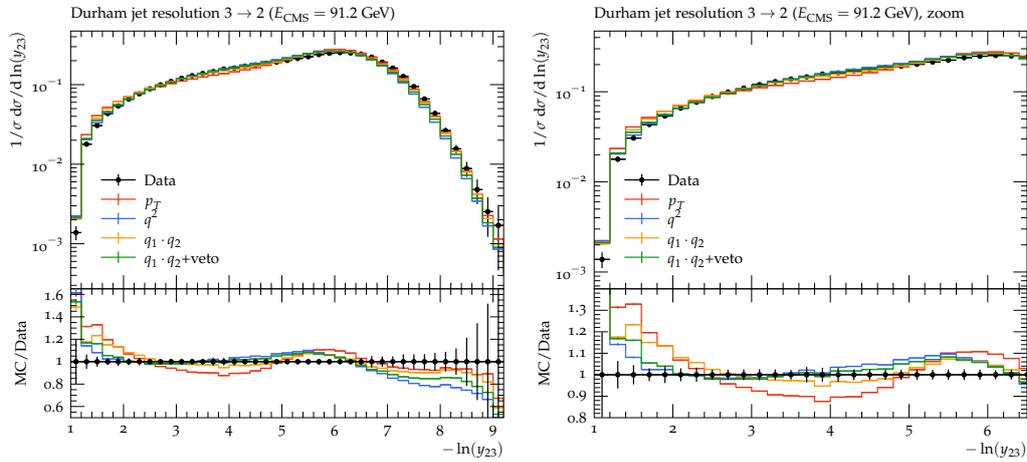
Figure 2.7: The value of jet resolution parameter that separates a 3-jet configuration and a 2-jet configuration at the Z-pole compared with data from the ALEPH [2] experiment. In the right panel an expanded section of the same plot is shown.

schemes are much smaller than the experimental error and in general they all give a good agreement with the data.

The schemes all fail to describe the peak region of the b fragmentation function, with the different options showing little difference to each other, see Fig. 2.9. Nevertheless, the dot-product-plus-veto scheme gives the best overall description of b data, as can be seen from Tab. 2.2.

Although all of the data shown for e^+e^- collisions in this section was used as part of the tuning procedure, this dataset was also used to tune and validate previous versions of the parton shower and therefore the differences seen in this version are
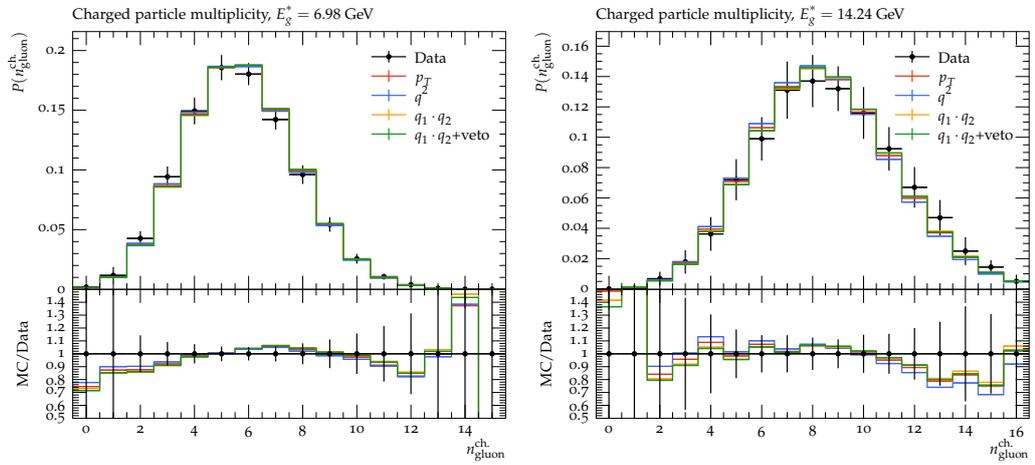
Figure 2.8: Multiplicity distributions of charged particles in gluons jets for two different gluon energies compared with data from OPAL [3].
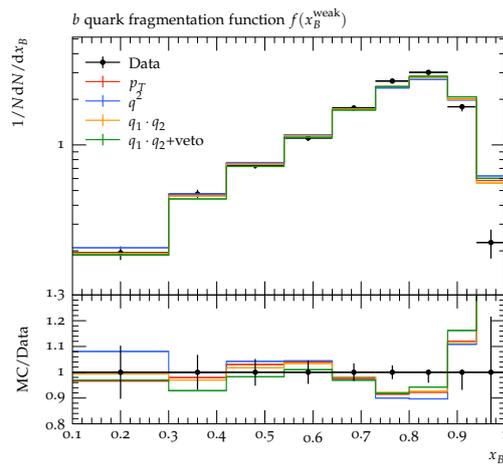
Figure 2.9: The fragmentation function of weakly-decaying B-hadrons compared with data from DELPHI [4].
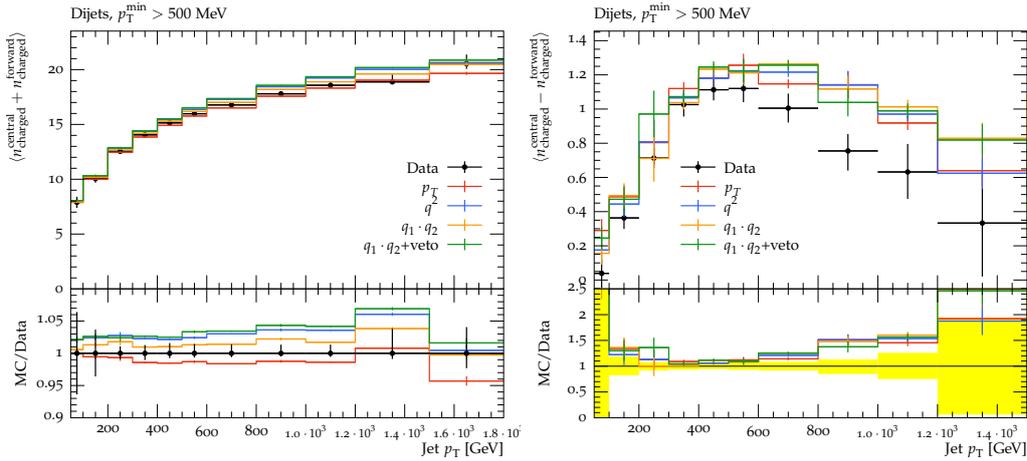
Figure 2.10: The average number of charged particles in jets (left) and the average difference between the number of particles in central and forward jets (right) as a function of the jet transverse momentum compared with data from the ATLAS experiment [5].

due to improvements made to the algorithm.

2.7.2   LHC results

Data from jets at the LHC seem to prefer the $p_\perp$ scheme as shown in Fig. 2.10. However, this behaviour is due to the absence of MEC in HERWIG for the events we have simulated. This implies that the dead zone remained unpopulated in the q^2 and dot-product schemes and that the migration of events into this region in the $p_\perp$ scheme has partially masked the lack of hard emission generation. Nevertheless we do expect that matching with higher order computations will lead to the same behaviour that we have found in LEP observables, *i.e.* that the $p_\perp$ scheme yields too much hard radiation, that the q^2 scheme, for which the kinematics of subsequent soft emissions are not guaranteed to be independent, displays worse behaviour in the opposite region of the spectrum, and that the dot-product-preserving scheme features intermediate properties. This data was not included in the tuning.

2.8   Conclusions

The pioneering work in Ref. [41] investigated the logarithmic accuracy of dipole showers by focusing on the pattern of multiple emissions. Inspired by this work, we have studied how different choices of the recoil scheme in the HERWIG angular-ordered parton shower can impact the logarithmic accuracy of final-state radiation.

We investigated the original choice of Ref. [64], where the transverse momentum of the emission is preserved during the shower evolution, and the alternative proposal to preserve the virtuality of the splitting, introduced in Ref. [93]. We observed that although the latter prescription retains, in general, a good description of the experimental data, it does not meet the formal requirement of next-to-leading logarithmic accuracy, as multiple soft emissions well separated in rapidity are not independent. On the other hand, the older recoil scheme overpopulates the non-logarithmically-enhanced region of the phase space, which should not be filled by the parton shower, but instead by higher order computations.

Due to the undesirable features of these recoil schemes, we proposed an alternative interpretation of the angular-ordering variable that well describes the process of multiple independent soft emission and retains a good agreement with data, while also considering the hard tail of the distributions. In order to enforce the correct behaviour in the hard region of phase space, we implemented a veto that suppresses large virtualities at the end of the parton shower.

This study was only concerned with final-state radiation and in the next chapter we present the results of our subsequent investigation into initial-state radiation. In this chapter we have mainly focused on the case of a massless emitter. The study of mass effects is crucial in assessing the accuracy of the parton shower and is a topic to be addressed in future works.

Chapter 3

Logarithmic Accuracy in Initial-State Radiation

3.1 Introduction

In Chapter 2 we examined how the choice of recoil scheme in the shower affects the logarithmic accuracy of final-state radiation. We have found that the q^2 preserving scheme, which was the default of HERWIG 7 prior to version 7.2, fails to meet necessary requirements to be NLL accurate that the $p_\perp$ preserving and the dot-product preserving schemes both satisfy.

In addition to FSR, there is also initial-state radiation to consider. Issues arising from transverse momentum recoil due to ISR in dipole showers were addressed in Ref. [149]. These were mainly related to the fact that a final-state singlet, such as in Drell-Yan (DY) production, only receives a non-vanishing transverse momentum contribution from the very first shower emission. The method proposed by the authors to remedy this behaviour is to allow the incoming partons to take the transverse momentum recoil, and then realign them with the beam directions at the end of the showering phase. In angular-ordered showers these issues are absent, but spurious NLL terms may arise depending on the interpretation of the ordering

variable in the presence of multiple emissions, as already found in Chapter 2 in the context of FSR. In this chapter we present the findings of our investigation into the effects of the choice of recoil scheme on the accuracy of ISR in the angular-ordered shower, focusing on the schemes which are NLL accurate for FSR.

In Sec. 3.2 we describe the implementation of the kinematic mapping for multiple emissions for different interpretations of the ordering variable. In Sec. 3.3 we discuss the radiation pattern for the case of two soft emissions, well separated in rapidity. The global recoil necessary to ensure full momentum conservation for the production of a colour singlet in hadron-hadron collisions is discussed in Sec. 3.4 (more details and the implementation for more generic processes are discussed in Appendix C). The treatment of hard emissions and other aspects of event generation for vector boson production are discussed in Sec. 3.5. In Sec. 3.6 we give an overview of our tuning procedure on the recoil schemes considered. Comparisons with experimental data for Z- and W-boson production are presented in Sec. 3.7. Finally, we present our conclusions in Sec. 3.8.

3.2   Kinematics

This study is concerned with the emission of initial-state radiation from a parton (originating from a proton) incoming to a hard scattering process. Conventionally, we consider the parton at the point of collision to be the shower progenitor and evolve the shower backwards from the scale of the hardest emission to the IR cutoff. We adopt the Sudakov decomposition for particle momenta such that

$$p_l = \alpha_l P + \beta_l n + k_{\perp l}, \tag{3.2.1}$$

where the reference vectors P and n are the momentum of the parent hadron and a light-like vector which points in the opposite direction[1], respectively. They obey the

---

[1]This direction is defined in the hadron-hadron frame if the colour partner is in the initial state, *e.g.* in a colour-singlet process such as DY. For a process with an outgoing colour partner, *e.g.* DIS, the direction of the colour partner in the Breit frame is used.

conditions

$$P^2 = 0, \qquad P \cdot n \neq 0, \qquad n^2 = 0, \qquad P \cdot k_{\perp l} = n \cdot k_{\perp l} = 0, \qquad (3.2.2)$$

so that that $k_{\perp l}$ is space-like and defined relative to the direction of P and n. For the shower progenitor, $\alpha_l = x$, where x is the fraction of the hadron's momentum that enters the hard scattering process. The parameter β_l is fixed by the requirement that the external particles are on their mass shells.

For an ISR splitting $\widetilde{ij} \to i, j$ we denote the space-like child with i and the time-like one with j. The light-cone momentum fraction of the branching is defined in the same way as for forward showers

$$z_i = \frac{p_i \cdot n}{p_{\widetilde{ij}} \cdot n}, \qquad (3.2.3)$$

and so is the relative transverse momentum of the branching

$$q_{\perp i} \equiv k_{\perp i} - z_i k_{\perp \widetilde{ij}}, \qquad (3.2.4)$$

with the magnitude being given by $p_{\perp i}^2 \equiv -q_{\perp i}^2$. Space-like partons are always considered massless, while the time-like parton can have a mass $m_j \neq 0$. This means that when a $g \to b\bar{b}$ splitting is considered, one quark is considered massless, while the other is treated as massive. The last space-like parent is required to be on-shell, and therefore the shower progenitor acquires an increasingly negative virtuality as additional emissions are added to the backwards shower.

3.2.1 One Emission

For the case where only one emission is generated, the momenta are

$$p_{\widetilde{ij}} = \frac{x}{z}P; \qquad (3.2.5a)$$

$$p_j = (1-z)p_{\widetilde{ij}} + \beta n + q_\perp; \qquad (3.2.5b)$$

$$p_i = p_{\widetilde{ij}} - p_j = zp_{\widetilde{ij}} - \beta n - q_\perp. \qquad (3.2.5c)$$

The coefficient β can be determined by requiring that p_j is on its mass shell

$$\beta = \frac{z(m_j^2 + p_\perp^2)}{2(1-z)\, x\, P \cdot n}. \tag{3.2.6}$$

The virtuality of the space-like child is

$$p_i^2 = -2p_j \cdot p_{\widetilde{ij}} + m_j^2 = \frac{-(p_\perp^2 + zm_j^2)}{(1-z)} \tag{3.2.7}$$

and the ordering variable can be defined as

$$\tilde{q}^2 = \frac{-p_i^2}{1-z} = \frac{2p_j \cdot p_{\widetilde{ij}} - m_j^2}{1-z} = \frac{(p_\perp^2 + zm_j^2)}{(1-z)^2}. \tag{3.2.8}$$

3.2.2 Multiple Emissions

When multiple emissions are considered (*i.e.* j acquires a positive virtuality p_j^2 and/or $\widetilde{ij}$ undergoes a further initial-state splitting), we cannot simultaneously preserve p_i^2, $p_j \cdot p_{\widetilde{ij}}$ and $p_\perp^2$.

It can be shown that in general the virtuality of i is

$$p_i^2 = -\frac{p_\perp^2 + zp_j^2 - z(1-z)p_{\widetilde{ij}}^2}{1-z}. \tag{3.2.9}$$

By comparing Eq. (3.2.9) with Eq. (3.2.7), we notice that the on-shell mass m_j^2 has been replaced with the virtuality p_j^2 and we have also a term proportional to $p_{\widetilde{ij}}^2$, which is zero when only one backwards emission is concerned. In order to complete the kinematic reconstruction we thus need to find an expression of $p_\perp^2$ as a function of $\tilde{q}^2$, p_j^2 and $p_{\widetilde{ij}}^2$.

$p_\perp$ Preserving Scheme

If we preserve the transverse momentum of each emission, we have

$$\tilde{q}^2 \equiv \frac{p_\perp^2 + zm_j^2}{(1-z)^2}, \tag{3.2.10}$$

which immediately yields

$$p_\perp^2 = (1-z)^2 \tilde{q}^2 - z m_j^2. \tag{3.2.11}$$

q^2 Preserving Scheme

If we instead preserve the virtuality of each emission, we obtain

$$\tilde{q}^2 \equiv \frac{-p_i^2}{1-z}, \tag{3.2.12}$$

By inverting Eq. (3.2.9) and using the above expression for p_i^2 we get

$$p_\perp^2 = (1-z)^2 \tilde{q}^2 + z(1-z) p_{\widetilde{ij}}^2 - z p_j^2. \tag{3.2.13}$$

Since $p_{\widetilde{ij}}^2 < 0$ and $p_j^2 > 0$, during the evolution $p_\perp^2$ will decrease, and can eventually become negative, as already found in the context of FSR in Chapter 2.

Dot-Product Preserving Scheme

The final choice we examine is the dot-product preserving scheme:

$$\tilde{q}^2 \equiv \frac{2 p_j \cdot p_{\widetilde{ij}} - m_j^2}{1-z}, \tag{3.2.14}$$

from which we derive

$$2 p_j \cdot p_{\widetilde{ij}} = (1-z)\tilde{q}^2 + m_j^2. \tag{3.2.15}$$

By inverting Eq. (3.2.9) and using $p_i^2 = (p_{\widetilde{ij}} - p_j)^2$,

$$p_\perp^2 = (1-z)^2 \tilde{q}^2 - p_j^2 - (1-z)^2 p_{\widetilde{ij}}^2 + (1-z) m_j^2. \tag{3.2.16}$$

In this case we see that during the forward evolution of the time-like parton j, $p_\perp$ is reduced, while during the backwards evolution of the space-like parton $\widetilde{ij}$, it is increased. We need to ensure that there is still a physical solution, *i.e.* $p_\perp^2 \geq 0$, following subsequent initial- and final-state radiation. As further space-like splittings can only increase $p_\perp^2$ there is no problem, however subsequent time-like branchings

can reduce $p_\perp^2$ and so we must ensure that further time-like radiation satisfies

$$p_j^2 \leq (1-z)^2 \tilde{q}^2. \tag{3.2.17}$$

As shown in Section 2.4.3, the angular-ordering condition for final-state radiation, $\tilde{q}_j < (1-z)\tilde{q}$, will ensure that for further time-like radiation

$$p_j^2 \leq \frac{\tilde{q}_j^2}{2}, \tag{3.2.18}$$

and therefore the angular-ordering condition ensures that

$$p_j^2 \leq (1-z)^2 \frac{\tilde{q}^2}{2}, \tag{3.2.19}$$

which ensures there will always be a physical solution for $p_\perp^2$.

Summary

Remembering that for ISR from a hard process $m_i = m_{\widetilde{ij}} = 0$, we can summarise all the $p_\perp^2$ expressions using

$$p_\perp^2 = (1-z)^2(\tilde{q}^2 - P_{\widetilde{ij}}^2) + (1-z)M_j^2 - P_j^2 - (1-z)(m_i^2 - M_{\widetilde{ij}}^2), \tag{3.2.20}$$

where

$$P_l^2 = M_l^2 = m_l^2 \tag{3.2.21}$$

in the $p_\perp$-preserving scheme,

$$P_l^2 = M_l^2 = p_l^2 \tag{3.2.22}$$

in the q^2 preserving scheme, and

$$P_l^2 = p_l^2, \ M_l^2 = m_l^2 \tag{3.2.23}$$

in the dot-product preserving scheme.

It can be shown that Eqs. (3.2.20) and (3.2.9) are also valid in case of ISR from a resonance. The derivation is identical to the pure ISR case, with the exception that

$m_i = m_{\widetilde{ij}} \neq 0$ and that the ordering variable for one emission is

$$\tilde{q}^2 = \frac{-p_i^2 + m_i^2}{1-z} = \frac{2p_j \cdot p_{\widetilde{ij}} - m_j^2}{1-z} = \frac{p_\perp^2 + zm_j^2 + (1-z)^2 m_i^2}{(1-z)^2}. \qquad (3.2.24)$$

A final point to note is that we have not implemented a veto to prevent p_i^2 from becoming too large in the $p_\perp$ and dot-product preserving schemes. This is because the large virtualities generated by these schemes are not a source of logarithmically enhanced errors and because the Jacobian to correct between the approximate and exact phase space is non-trivial for the hard processes considered in this study, such as $pp \to Z$. A further reason not to implement the veto is that too much hard radiation from the parton shower is expected to be a much smaller source of error in the description of DY events than that seen in the description of $e^+e^- \to q\bar{q}$ events in the previous chapter. This is because for $e^+e^- \to q\bar{q}$ the population of the dead zone, even after MEC or NLO matching has been implemented, should be very low. Therefore the small number of high-virtuality partons originating from the PS which do enter the region cause a significant overestimate of its population. However, for DY, the equivalent region of phase space is expected to be well populated by MEC or the NLO matching scheme, so the additional emissions entering that region from the PS are expected to produce a less significant excess.

3.3 Double Gluon Emission

To discuss the impact of the recoil scheme on the logarithmic accuracy, we focus now on the case of double soft gluon emission from an incoming quark line, as shown in Fig. 3.1.

Using the Sudakov decomposition described in the previous section:

$$p_3 = \alpha P; \qquad (3.3.1a)$$

$$k_2 = (1-z_2)p_3 + \beta_2 n + q_{\perp 2}; \qquad (3.3.1b)$$

$$p_2 = p_3 - k_2 = z_2 p_3 - \beta_2 n - q_{\perp 2}; \qquad (3.3.1c)$$
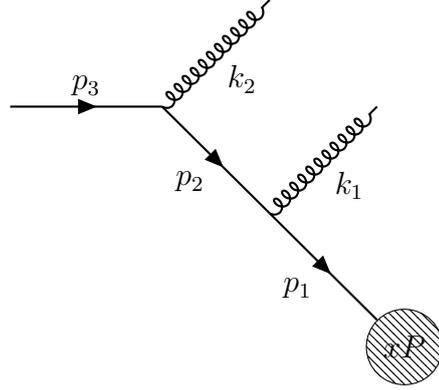
Figure 3.1: Kinematics of double soft gluon emission, in the angular-ordered parton shower, for ISR.

$$k_1 = (1 - z_1)z_2 p_3 + \beta_1 n - (1 - z_1)q_{\perp 2} + q_{\perp 1}; \qquad (3.3.1\text{d})$$

$$p_1 = p_2 - k_1 = z_1 z_2 p_3 - [\beta_1 + \beta_2]n - z_1 q_{\perp 2} - q_{\perp 1}, \qquad (3.3.1\text{e})$$

where the β_i are determined by the requirement that $k_i^2 = 0$ and $\alpha = x/(z_1 z_2)$. Due to the use of backwards evolution in a space-like shower, the partons are labelled in ascending order the further they are from the hard process.

All recoil schemes are equivalent for the emission that is generated last, therefore

$$p_{\perp 2}^2 = (1 - z_2)^2 \tilde{q}_2^2 = \epsilon_2^2 \tilde{q}_2^2, \qquad p_2^2 = -(1 - z_2)\tilde{q}_2^2 = -\epsilon_2 \tilde{q}_2^2, \qquad (3.3.2)$$

where we have introduced $\epsilon_2 = 1 - z_2 \to 0$ in the soft limit. The values of p_1^2 and $p_{\perp 1}$ depend on the interpretation of the ordering variable.

3.3.1 $p_\perp$ Preserving Scheme

For the $p_\perp$ preserving scheme, we have

$$p_{\perp 1}^2 = (1 - z_1)^2 \tilde{q}_1^2. \qquad (3.3.3)$$

Thus, from Eq. (3.2.9)

$$p_1^2 = -(1 - z_1)\tilde{q}_1^2 - z_1(1 - z_2)\tilde{q}_2^2. \qquad (3.3.4)$$

If both emissions are soft (*i.e.* $1 - z_i \equiv \epsilon_i \to 0$), we have

$$p_{\perp 1}^2 = \epsilon_1^2 \tilde{q}_1^2, \qquad p_1^2 = -\epsilon_1 \tilde{q}_1^2 - (1 - \epsilon_1)\epsilon_2 \tilde{q}_2^2 \approx -\epsilon_1 \tilde{q}_1^2 - \epsilon_2 \tilde{q}_2^2. \tag{3.3.5}$$

As we have seen for final-state radiation, this implies that the largest contribution to the virtuality can also come from subsequent emissions if for example $\epsilon_1 \ll \epsilon_2$. However, since the transverse momentum of previously emitted gluons is unchanged, this scheme will reproduce the pattern of multiple independent soft emissions widely separated in angle.

3.3.2 q^2 Preserving Scheme

For the q^2 preserving scheme, we have

$$p_1^2 = -(1 - z_1)\tilde{q}_1^2, \tag{3.3.6}$$

thus, inverting Eq. (3.2.9) gives

$$p_{\perp 1}^2 = (1 - z_1)\left[(1 - z_1)\tilde{q}_1^2 - z_1(1 - z_2)\tilde{q}_2^2\right], \tag{3.3.7}$$

which means that $p_{\perp,1}^2$ has been decreased by the subsequent emission and is not guaranteed to be positive. In the soft limit

$$p_{\perp 1}^2 \approx \epsilon_1 \left(\epsilon_1 \tilde{q}_1^2 - \epsilon_2 \tilde{q}_2^2\right), \qquad p_1^2 = -\epsilon_1 \tilde{q}_1^2. \tag{3.3.8}$$

Clearly if $\epsilon_2 \gg \epsilon_1$, the kinematics of the first emission are significantly modified. This, as we saw in Chapter 2, causes NLL issues, so we will not to consider this scheme further.

3.3.3 Dot-Product Preserving Scheme

When preserving the dot-product

$$p_1^2 = (p_2 - k_1)^2 = p_2^2 - 2p_2 \cdot k_1 = -(1 - z_2)\tilde{q}_2^2 - (1 - z_1)\tilde{q}_1^2. \tag{3.3.9}$$

From Eq. (3.2.24) we have

$$p_{\perp 1}^2 = (1 - z_1)^2 \left[\tilde{q}_1^2 - p_2^2 \right] = (1 - z_1)^2 \left[\tilde{q}_1^2 + (1 - z_2)\tilde{q}_2^2 \right]. \tag{3.3.10}$$

Thus in the soft limit

$$p_{\perp 1}^2 = \epsilon_1^2(\tilde{q}_1^2 + \epsilon_2 \tilde{q}_2^2) \approx \epsilon_1^2 \tilde{q}_1^2, \quad p_1^2 = -\epsilon_1 \tilde{q}_1^2 - \epsilon_2 \tilde{q}_2^2. \tag{3.3.11}$$

It is interesting to note that in the case of ISR, subsequent emissions tend to increase $p_{\perp 1}^2$, while in the case of FSR the opposite behaviour takes place (see Chapter 2). In any case, when ϵ_1 and ϵ_2 are both small, regardless of which one is smaller, this scheme reproduces the behaviour of the $p_\perp$ preserving one, thus it is capable of describing the matrix element for multiple independent soft gluon emissions.

3.4   Global Recoil Strategy for Z and $Z+$Jet Production

In this section we summarise the global recoil strategy applied to the cases of Z and $Z+$jet production. More details and the generalisation to an arbitrary colour structure are discussed in Appendix C. We stress that in the presence of only soft and/or collinear emissions, the global recoil strategy amounts to power suppressed changes to the rapidity and the transverse momentum of partons emitted from initial-state radiation and thus does not alter the discussion presented in the previous section.

Let us consider a Drell-Yan process, which at LO is described by the annihilation of a $q\bar{q}$ pair into a massive gauge boson. Each incoming parton is identified as a shower progenitor by the HERWIG angular-ordered shower, and thus showered independently. The two initial partons form a colour-connected neutral system so the transverse momentum of each new emission is defined with respect to the direction of the original q ($\bar{q}$) momentum. After the showering phase, the shower progenitors have

acquired a negative virtuality and a transverse momentum. The total transverse momentum imbalance is reabsorbed by the *Z* boson, but there is some freedom in how to impose longitudinal momentum conservation. Three options are possible:

1. we fix the *Z*-boson rapidity;

2. we fix the longitudinal momentum of the *Z* boson;

3. we preserve the new off-shell momentum of the shower progenitor that does not contain the hardest emission.

The last option is the default behaviour, as it allows for a simpler matching with higher order matrix elements. Indeed for one emission it exactly reproduces the kinematics of the Catani-Seymour initial-initial dipole [53] (*i.e.* the transverse recoil from the emission is passed to the emitter, while the other shower progenitor acts as a spectator and longitudinal recoil is absorbed by the *Z* boson). All of these options ensure that, in the case of multiple soft emissions well separated in rapidity, the transverse momentum of the *Z* is given by the vector sum of all the emissions' transverse momenta and that the rapidity of the *Z* can only receive suppressed power corrections $\mathcal{O}\left(p_T^2/m_z^2\right)$.

In section Sec. 3.7 we will present our results for *Z* and *Z*+jet matched predictions. In the latter case, the final-state quark (which is colour connected to an initial parton) can also be identified as a shower progenitor. The global recoil strategy applied in this case is a hybrid between the above strategy for the production of a colour singlet, and the one developed for Deep Inelastic Scattering (DIS) processes. To be concrete, let us consider the $qe^- \to qe^-$ DIS process, which proceeds through a colour-neutral t-channel exchange. The kinematic reconstruction and the transverse momentum are defined in the Breit frame [1], where the two quarks are back-to-back. Such a mapping must leave the momenta of the two electrons unchanged, thus the

---

[1]In this frame, the photon has 0 energy and causes the outgoing quark to travel back along the direction the incoming quark came from. Both quarks have energy $Q/2$. This is the analogue of the CoM frame in a DY process.

final-state quark and its children, *i.e.* the partons produced during its parton-shower evolution, need to absorb the transverse momentum imbalance due to initial-state radiation. A longitudinal boost is also applied to the incoming (outgoing) parton and its children (parents) to ensure that the *t*-channel propagator is preserved.

For *Z*+jet production, the shower progenitor which leads to the hardest emission is reconstructed first, together with its colour evolution partner. If they form an initial-initial dipole, the kinematic reconstruction devised for the Drell-Yan case is adopted, while if they form an initial-final dipole the one for DIS is implemented. This is then followed by the reconstruction of the remaining shower progenitor momentum, which is colour connected to a gluon jet that has already been reconstructed. This gluon jet will be boosted again to absorb the recoil of its second colour partner.

3.5 Matching Procedures for Initial-State Radiation

To investigate the performance of the new recoil scheme for the angular-ordered shower, we wish to compare HERWIG predictions for vector boson production, in particular the DY process, with LHC data. Before we can do so, we must outline our consideration of the aspects of event generation that are important for giving accurate predictions of this process, but are not governed by the parton shower algorithm.

There are several options in HERWIG for the treatment of the hardest emission. For leading order predictions, we use matrix element corrections to improve the description of the hardest emission and to populate the dead zone. We also use next-to-leading order predictions, obtained from MATCHBOX [62] machinery, which allows for the inclusion of next-to-leading order corrections in either the MC@NLO [20] or POWHEG [22] matching schemes. The impact of NLO matching is expected to be much more significant in DY because the $p_\perp$ of the Z boson is mainly sensitive to the

hard emissions that occur around the boundary of the PS and fixed order regimes. Therefore unlike our previous study of FSR we must consider the adjustments we have made to the PS algorithm alongside their interaction with NLO matching schemes.

For LO+MEC predictions, HERWIG uses leading-order parton distribution functions (PDFs) by default. However, the usage of NLO PDFs is also possible as the differences this introduces are beyond the level of accuracy of the calculation[1]. Thus, for illustrative purposes, in the following sections we compare LO results obtained with both LO and NLO PDFs, finding small differences as expected.

When using the POWHEG method, it is possible to separate the real emission contribution into a singular and a non-singular part, and only exponentiate the former contribution in the Sudakov form factor, while the latter part is generated as a Born-like event with a higher particle multiplicity. This separation is somewhat arbitrary and in HERWIG is controlled by the hard scale profile [150], which we turn off in our simulations (*i.e.* we adopted the strategy of exponentiating all the real corrections).

When the hardest emission generated by the POWHEG algorithm lies inside the region of phase space accessible to the parton shower algorithm (*i.e.* it is not in the dead zone), the kinematics are always reconstructed as a Z event. However, in the case that the hardest emission is in the dead zone, we consider two options. The first is to reconstruct the event as a Z+jet hard process, which we label as "POWHEG" in the plots below. We also consider the option of reconstructing such an event as a shower emission from a Z event, which we label as "POWHEG (AS)". We consider the first to be more self-consistent, but the second is actually the current HERWIG default. This choice has a negligible impact on the description of the Z

---

[1]Here we refer to the PDF employed to evaluate the matrix element and to perform the ISR evolution. The underlying event (UE) is not included, as it has no impact on the transverse momentum of the Z boson, which is only affected by ISR, in the HERWIG 7 model. For the UE, the usage of LO PDFs is recommended as the combination of LO elements and PDFs gives a better approximation of the NLO result than LO matrix elements and NLO PDFs. This is due to the different behaviour of the gluon distribution at small x for LO and NLO PDFs.

boson transverse momentum for small values of $p_\perp$ but leads to sizeable differences in the high-$p_\perp$ tails of distributions.

3.6 Tuning

Before comparing HERWIG predictions with the experimental data, we need to tune the parameters sensitive to ISR: the intrinsic $p_\perp$, *i.e.* the non-perturbative intrinsic transverse momentum for the partons inside the incoming hadron; and the strong coupling α_S (which is given in the CMW [49] scheme). To this end, we have introduced the possibility of setting the value of α_S for ISR independently from the value used for FSR. We do not consider an independent variation of the minimum transverse momentum used as a shower cutoff, $p_\perp^{\min}$, because (as was discovered during the previous study on FSR) it is strongly anti-correlated with α_S. Therefore it is sufficient only to tune α_S and set $p_\perp^{\min}$ to its FSR value of ≈ 1 GeV (as found in Chapter 2). We consider only the dot-product and transverse-momentum preserving schemes, as the virtuality preserving scheme was found to have NLL issues in Chapter 2.

The parametric dependence of the distributions is obtained from the PROFESSOR [104] program, which also finds the values of the parameters that minimise the χ^2 distribution for a given dataset. To prevent the tuning from being dominated by points with a small experimental uncertainty, we set the minimum experimental uncertainty used during the minimisation procedure to 1%. We compared the events analysed with RIVET [102] to the ATLAS Drell-Yan Z-boson production data at 7 TeV [7,151,152]. To reduce correlations in our training dataset, we considered the transverse momenta of Z bosons reconstructed from muons and the angular correlations between e^+e^- pairs produced by Z decays.

Since in our simulations we have only used the matrix elements for Z plus 0 or 1 jet, we are unable to obtain a realistic description of the high-$p_\perp$ spectrum, which would require the matching with higher multiplicity matrix elements as the parton

shower approximation is not valid in this region. For this reason, when tuning we only considered bins in which the Z transverse momentum is smaller than 50 GeV and $\phi_\eta^* < 0.8$.[1]

The results of our tuning procedure for several different HERWIG set-ups are shown in Tab. 3.1. We notice that the behaviours of the dot-product and $p_\perp$ preserving schemes are similar, except when the POWHEG (AS) scheme is adopted. For all the considered cases, the new dot-product preserving scheme always yields a better chi-squared. We also find that the value of α_S for ISR is considerably larger than the one for FSR obtained in Chapter 2. In particular, at LO (+MEC) the tuned value of α_S (which is defined in the CMW scheme) is very close to 0.1256, which corresponds to the well known value $\alpha_S = 0.118$ in the $\overline{\text{MS}}$ scheme. The usage of NLO PDFs for LO predictions does not yield a significant difference with respect to the default choice of using LO PDFs. On the other hand, when adopting the MC@NLO matching the value of the strong coupling is always smaller and the χ^2 is slightly worse. The predictions obtained with the POWHEG scheme are those with the largest chi-squared, and the tuned value of α_S is always larger than the expected value of 0.1256. When the POWHEG (AS) scheme is used, the dot-product preserving scheme yields the best chi-squared, with $\alpha_S = 0.1255$. This is in contrast with our expectations, as the treatment of emissions in the dead zone as part of the hard process is better motivated in the standard POWHEG scheme. Furthermore, as we have already said, this is the only case where we find a significant discrepancy (both in the chi-squared and in the tuned value of the strong coupling) between the $p_\perp$ and the dot-product preserving schemes.

It is not a surprise that the values of the coupling obtained by tuning the dot-product preserving scheme set-ups are typically smaller than the values from the set-ups that

---

[1]The variable ϕ_η^* is introduced in Ref. [7] and is defined as

$$\phi_\eta^* = \tan\left(\frac{\pi - \Delta\phi}{2}\right)\sin\theta^*,\tag{3.6.1}$$

with $\Delta\phi$ being the azimuthal opening angle between the two leptons and θ^* the scattering angle of the leptons with respect to the proton beam direction in the rest frame of the dilepton system.

Scheme	Dot-product Preserving					$p_\perp$ Preserving			
Accuracy	LO (NLO PDF)	LO	MC@NLO	Powheg	Powheg (AS)	LO	MC@NLO	Powheg	Powheg (AS)
ISR Shower Parameters									
α_S^{ISR}	0.1260	0.1247	0.1171	0.1341	0.1255	0.1264	0.1189	0.1352	0.1318
Intrinsic $p_\perp$	0.984	1.008	1.780	1.552	1.803	0.865	1.679	1.542	1.696
χ^2 of Best Fit Point									
χ^2	521	590	719	1528	253	658	923	2551	914
χ^2/NDOF	2.8	3.2	3.9	8.3	1.4	3.6	5.0	13.8	5.0

Table 3.1: Tuned parameters and χ^2 for Drell-Yan Z-boson production events at 7 TeV .

use the $p_\perp$ scheme, as in the latter scheme subsequent emissions tend to increase the transverse momentum of previously emitted partons (see Sec. 3.3.3). This behaviour is opposite to that seen in the FSR case, where instead the dot-product preserving scheme yields an α_S value larger than in the $p_\perp$ scheme.

In Powheg we find a larger value of α_S since for the hardest emission, which is completely handled by Matchbox, the CMW prescription is not included in the strong coupling evaluation. We have re-run the tuning procedure with the CMW prescription implemented and obtain $\alpha_S \approx 0.125$ with distributions and χ^2 values that are nearly identical.

3.7 Results

In this section we present the results of our simulations of vector boson production at the LHC and the impact of the recoil scheme and matching procedure on the accuracy of these simulations.

Z Production at 7 TeV

We begin by illustrating the distributions of Z-boson transverse momentum and ϕ_η^* at 7 TeV. We expect to find good agreement between all of our predictions and the data for small values of both transverse momentum and ϕ_η^* as we have tuned our parameters using the low-$p_\perp$ range of these distributions.

In Fig. 3.2 we show the CMS measurement [6] of the transverse momentum of the Z boson in the low-$p_\perp$ region. We can observe that the dot-product and $p_\perp$ preserving
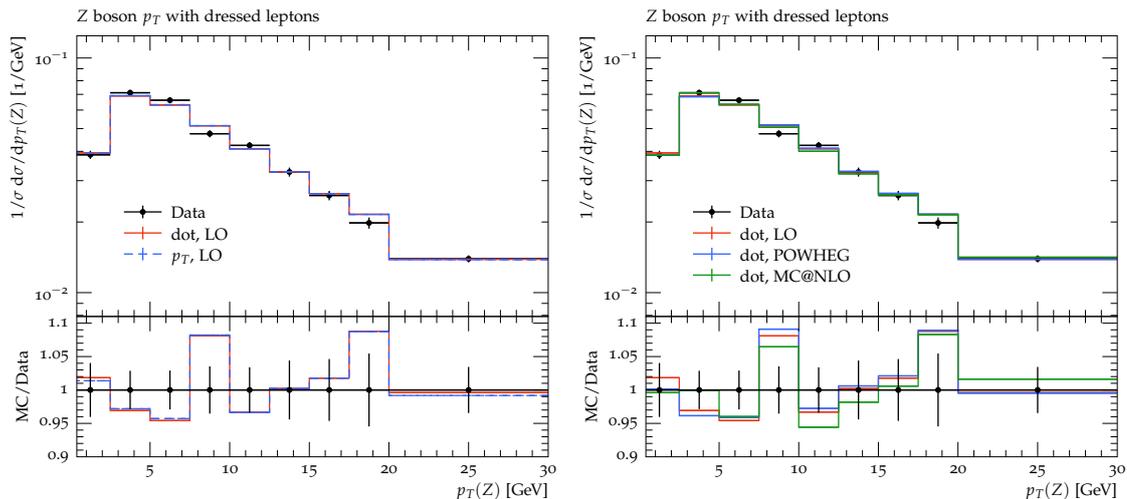
Figure 3.2: Normalised differential cross section as a function of Z $p_\perp$. CMS [6] data at 7 TeV compared to data generated by HERWIG. In the left panel, LO predictions in the dot-product and $p_\perp$ preserving schemes, in the right panel LO and NLO predictions in the dot-product preserving scheme.

schemes are almost identical (left panel), and very small differences are found by including higher order corrections (right panel).

Fig. 3.3 illustrates the distribution of the ϕ_η^* parameter of the Z boson measured by the ATLAS collaboration [7]. Like the transverse momentum results, for small values of ϕ_η^* all the theoretical predictions are very similar and agree well with data. We observe deviations between the recoil schemes (left panel) and among the several matching prescriptions (right panel) only for larger values of ϕ_η^*. We note that the LO predictions obtained using a NLO PDF (green curve in the left plot) are very similar to those obtained with the default LO PDF (red curve), as predicted in Section 3.5. We also note that, at LO, the dot-product preserving scheme yields good agreement with data up to $\phi_\eta^* \sim 0.8$, which is the upper value we used in our tuning procedure, while 5% differences with respect to the data arise at $\phi_\eta^* \sim 0.8$ in the $p_\perp$ preserving scheme (blue curve in the left plot). Both the MC@NLO and POWHEG NLO predictions (right plot) give a poorer description of the data, with small discrepancies between $\phi_\eta^* \sim 0.02$ and $\phi_\eta^* \sim 0.1$, becoming very significant for $\phi_\eta^* > 0.2$ (POWHEG) or 0.5 (MC@NLO).

In Fig. 3.4 we compare the POWHEG predictions obtained by treating hardest emis-
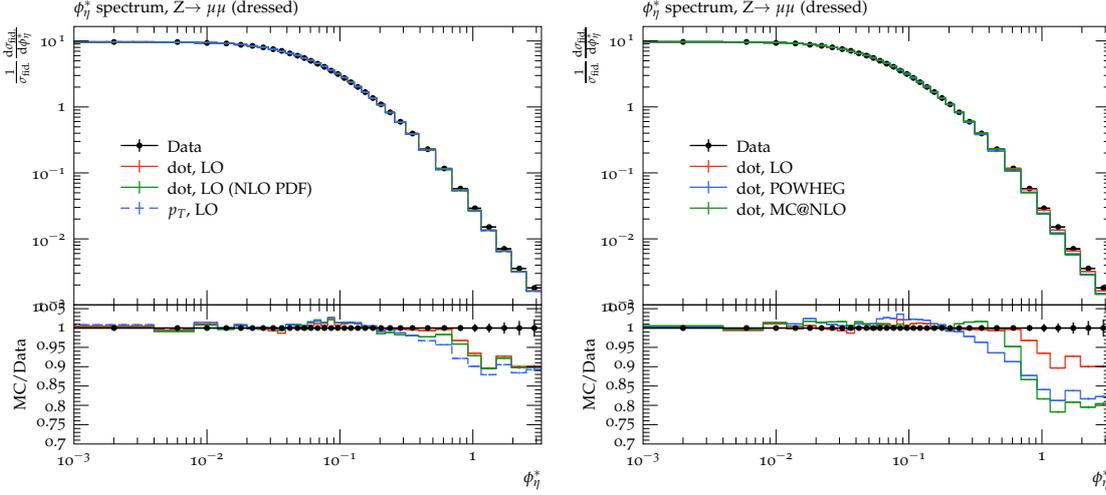
Figure 3.3: Normalised differential cross section of $Z \to \mu^+\mu^-$ as a function of the ϕ^*_η parameter of the Z boson. HERWIG results compared to ATLAS [7] data at 7 TeV. In the left panel, a comparison of LO results from the dot-product (with both LO and NLO PDFs) and $p_\perp$ preserving schemes. In the right panel, a comparison of LO and NLO results in the dot-product preserving scheme.

sions in the dead zone as part of the hard process (*i.e.* as a genuine "real emission"), with those obtained by always treating the hardest emissions as shower emissions (AS). We notice that for small values of the Z-boson $p_\perp$ (left panel), all the predictions are in good agreement. However, large differences arise when looking at the hard tail of the ϕ^*_η distribution (right panel), where all the HERWIG predictions underestimate ATLAS data. The "real-emission" scheme, which is the best theoretically motivated, leads to the largest discrepancies with respect to the data. The "as shower" treatment yields significantly different predictions from the dot-product and $p_\perp$ preserving schemes. As already seen in Tab. 3.1, POWHEG (AS) dot-product results (green curve) are the ones that yield the best description of the experimental data.

W Production at 7 TeV

As we have only used the Z-boson transverse momentum distribution to tune our shower parameters, we can use the accuracy with which our tuned showers describe the W-boson $p_\perp$ distribution to assess the universality of our tuning procedure. In
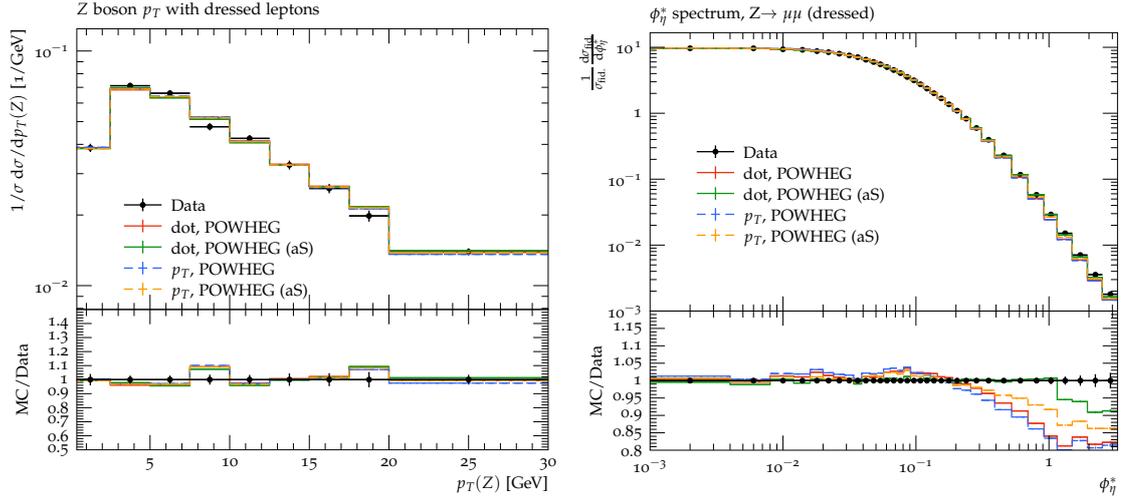
Figure 3.4: Normalised differential cross section of $Z \to \mu^+\mu^-$ as a function of Z $p_\perp$ (left panel) and of the ϕ_η^* parameter (right panel). HERWIG results, obtained using the POWHEG matching prescription, are compared to CMS [6] and ATLAS [7] data at 7 TeV.

Fig. 3.5 we compare the ATLAS 7 TeV measurements of W-boson $p_\perp$ [8] with our predictions in the dot-product (left) and $p_\perp$ (right) preserving schemes. For values of the W-boson transverse momentum smaller than 50 GeV, all the predictions agree fairly well with the data, which are however plagued by large uncertainties. For larger values we see that all of the theoretical predictions are systematically lower than the data, particularly those obtained using the NLO matched simulations.

Z Production at 8 TeV

We now examine the Z-boson distributions at 8 TeV, *i.e.* with a centre-of-mass energy slightly above the one we adopted for tuning. The ATLAS measurements of Ref. [9] allow us to investigate the behaviour below and above the Z-boson mass peak region. Predictions in the peak region are similar to those described at 7 TeV and are not shown here.

In Fig. 3.6 experimental data is compared to HERWIG results in the dot-product preserving scheme. Above the Z-mass peak we get good agreement with the data for $p_\perp < 100$ GeV and $\phi_\eta^* < 1$. However, for masses below the peak the LO predictions overpopulate the low-$p_\perp$ (ϕ_η^*) region and underpopulate the region with moderate $p_\perp$
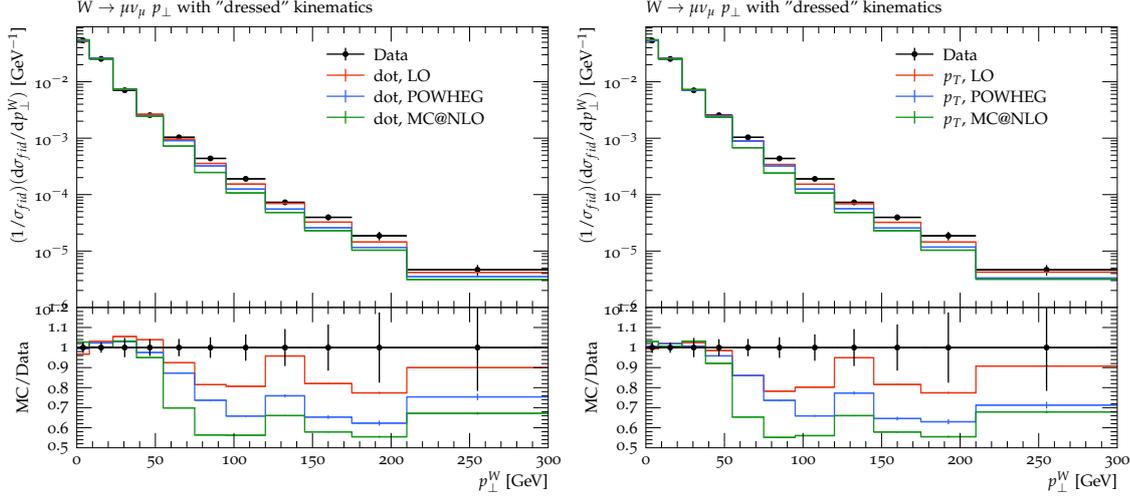
Figure 3.5: Differential normalised cross section of $W \to \mu\nu_\mu$ as a function of W $p_\perp$. HERWIG results compared to ATLAS [8] data at 7 TeV. In the left panel a comparison of LO with NLO results in the dot-product preserving scheme. In the right, the same comparison for the $p_\perp$ preserving scheme.

(ϕ_η^*) values. This feature is present also at NLO, but it is milder and discrepancies are only of the order of a few percent. In all cases, the high-$p_\perp$ (ϕ_η^*) tail is not properly described. This is not surprising, as the proper treatment of this region would require higher order matrix elements.

Z Production at 13 TeV

We conclude our phenomenological study by comparing HERWIG predictions to CMS measurements at 13 TeV [10]. Fig. 3.7 shows the distribution of the Z-boson transverse momentum for several rapidity (y) ranges, with the upper-left plot showing the inclusive case. In Table 3.2 we present the results of χ^2 calculations for the full $p_\perp$, ϕ_η^* and y distributions of Z boson production at 13 TeV. The table also shows the total χ^2 of the $p_\perp$ distributions for the y sub-ranges shown in Fig. 3.7. For these calculations we considered only $p_\perp < 50$ and $\phi_\eta^* < 0.8$.
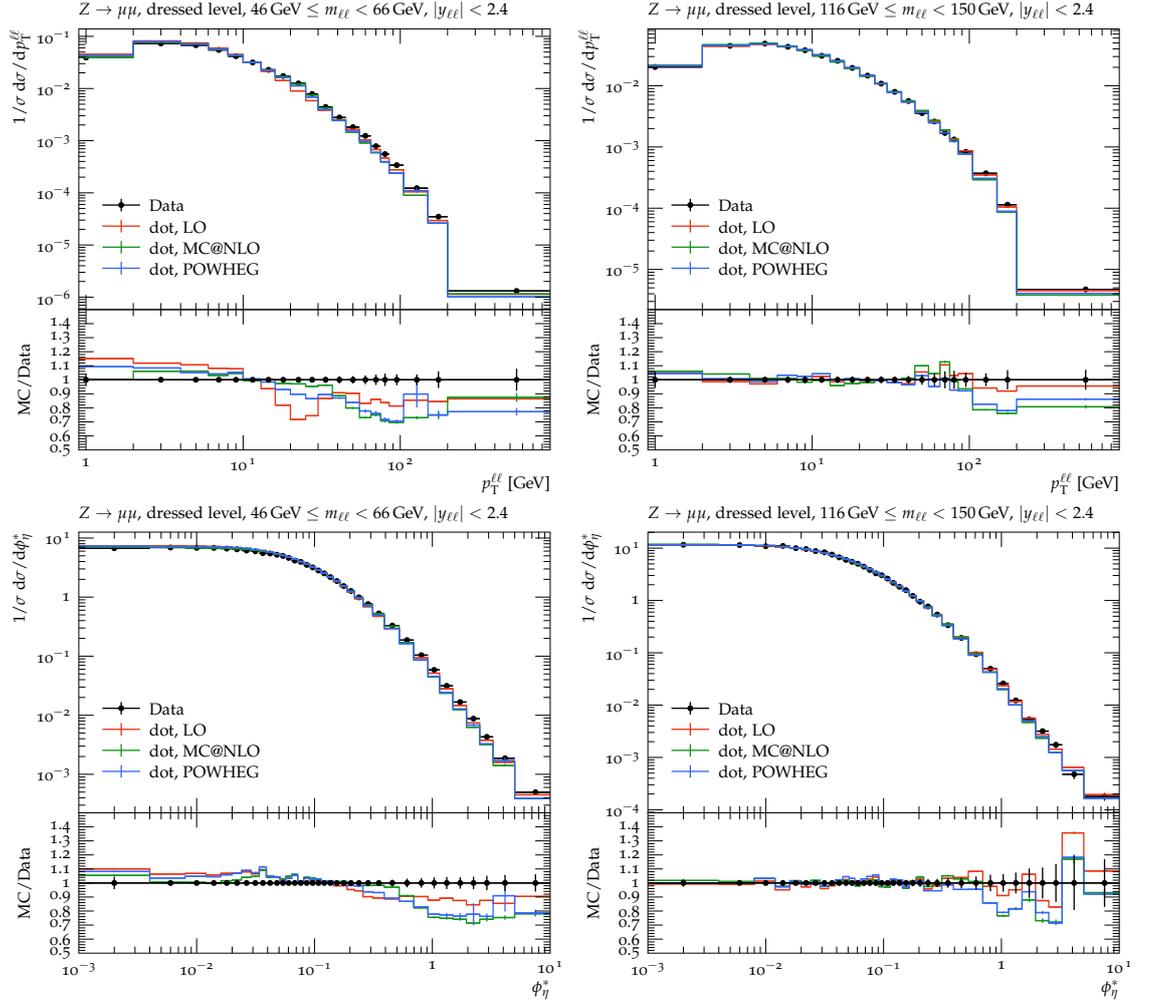
Figure 3.6: Differential normalised cross section of $Z \to \mu^+\mu^-$ as a function of the Z transverse momentum (upper panels) and ϕ^*_η (lower panels), below (left panels) and above (right panels) the Z mass peak region. HERWIG results for LO and NLO in the dot-product preserving scheme compared to ATLAS [9] at 8 TeV.
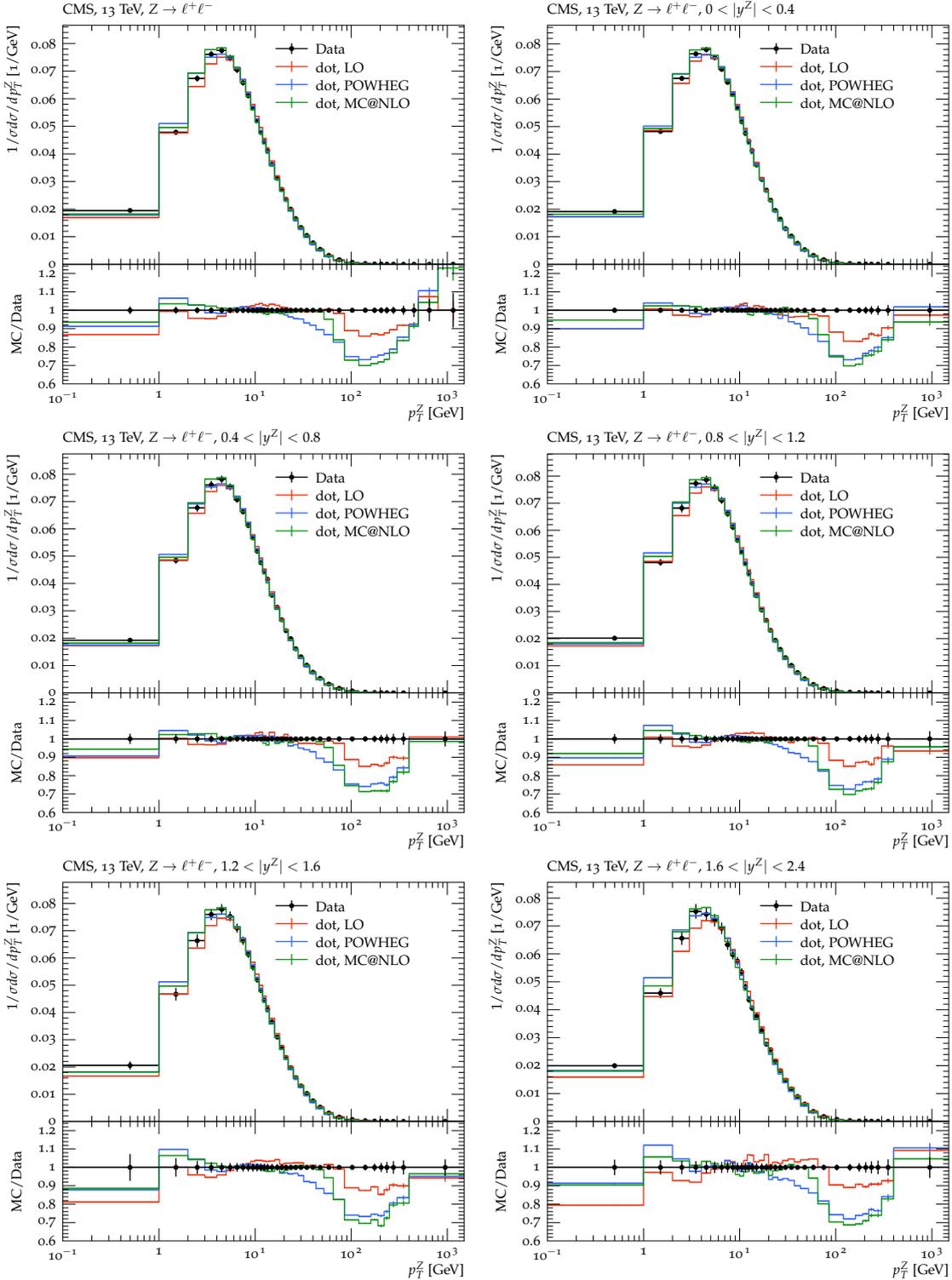
Figure 3.7: Differential normalised cross section as a function of $Z\ p_\perp$, broken down into different rapidity ranges. HERWIG results for LO and NLO in the dot-product preserving scheme are compared to CMS [10] data at 13 TeV.

Scheme	dot LO	dot MC@NLO	dot Powheg	$p_\perp$ LO	$p_\perp$ MC@NLO	$p_\perp$ Powheg
χ^2						
$p_\perp$	57.94	30.81	300.2	130.8	37.75	517.1
ϕ_η^*	36.30	683.2	1230	243.3	1164	1712
y	106.4	22.84	11.60	102.4	24.35	11.16
$p_\perp$, y bins	401.8	147.8	1355	729.8	171.8	2332
Reduced χ^2						
$p_\perp$ ($\chi^2/24$)	2.414	1.284	12.51	5.448	1.573	21.55
ϕ_η^* ($\chi^2/26$)	1.396	26.90	47.30	9.359	44.76	65.86
y ($\chi^2/12$)	8.863	1.903	0.9668	8.535	2.029	0.9298
$p_\perp$, y bins ($\chi^2/120$)	3.348	1.232	11.29	6.081	1.431	19.43

Table 3.2: χ^2 results for Z-boson distributions at 13 TeV compared to CMS data [10]. For the Z-boson transverse momentum distributions, the χ^2 is only computed for the region $p_\perp < 50$ GeV, while for ϕ_η^* we only consider $\phi_\eta^* < 0.8$. The "$p_\perp$, y bins" row refers to the $p_\perp$ distributions broken up into 5 distributions based on y.

We notice that of the all predictions, particularly those obtained using NLO matching prescriptions, track the data fairly well around the peak region, $p_\perp^Z \approx 10$ GeV, however large differences are found in both the large- and small-$p_\perp$ regions. For very small $p_\perp^Z$ values, the distribution is very sensitive to the modelling of the intrinsic $p_\perp$, which we have tuned at 7 TeV. For an improved description of the data, a new tuning could be performed for each centre-of-mass energy. Alternatively, the model of [153] could be used to predict the amount of transverse momentum built up by non-perturbative smearing throughout the perturbative evolution, as a function of the partonic and hadronic centre-of-mass energies.

Furthermore, from Table 3.2, we notice that for a given matching procedure, the results obtained in the dot-product preserving scheme always yield a smaller χ^2. The Powheg predictions always lead to the worst descriptions of the data, with the exception of the rapidity distribution of the vector boson. This is not unexpected, since the parton shower is not allowed to change the rapidity of the Z boson[1], thus the χ^2 values associated with the y distributions presented in Table 3.2 depend only on the matching procedure, and not on the recoil scheme.

---

[1]It should be noted that with the current reconstruction scheme y is not preserved, but it is subject only to minor changes as it is non-zero at leading-order

3.8   Conclusions

In this chapter we have extended the previous chapter's study on the logarithmic accuracy of angular-ordered parton showers to include initial-state radiation.

Similarly to the final-state case, the q^2 preserving scheme has problems, with later emissions being able to modify the kinematics of an earlier soft emission and degrade its logarithmic accuracy. For this reason, we have not considered it further.

We have extended the definition of the dot-product preserving scheme introduced in Chapter 2 to ISR. Like the $p_\perp$ preserving scheme, later emissions do not significantly modify the kinematics of earlier ones, so that multiple-gluon emission inherits the correct radiation pattern of single-gluon emission. One significant difference compared to the final-state case is that in the initial state, additional soft gluon emissions add to the transverse momentum generated by the first emission, while in the final-state case, they reduce it. This has an impact on the value of α_{S} fitted to data, which we allow to be different for ISR and FSR.

Based on their logarithmic accuracy, we conclude that either the $p_\perp$ preserving or dot-product preserving scheme can be used for ISR. However, based on consistency between the ISR case and the FSR case, where the dot-product preserving scheme is recommended, we recommend it also for ISR.

Based on the description of data, also, the dot-product preserving scheme is to be preferred. In fact, for each option for the hard process (LO with matrix element corrections and each of the NLO matching options), the description of data is better with the dot-product preserving scheme than with the $p_\perp$ preserving scheme.

It is impossible to consider the description of this data without also considering the choice of hard process and higher order matching scheme. Of the NLO schemes, the POWHEG (AS) scheme with the dot-product preserving shower gives the best description of data. We consider this scheme to be somewhat inconsistent, because it treats real emissions in the dead zone that the shower cannot populate, as if they were parton shower emissions. Nevertheless, because of its significantly better

description of data, we recommend that this version of POWHEG remain the default setting in HERWIG for now. The dot-product preserving recoil scheme will also become the default for ISR from the next HERWIG release.

Chapter 4

Conclusions

In this thesis we have presented our assessment of the logarithmic accuracy of the HERWIG 7 angular-ordered parton shower, as well as a new recoil prescription designed to improve this accuracy.

First we presented an analysis of the logarithmic accuracy of the HERWIG 7 angular-ordered parton shower for final-state radiation inspired by Ref. [41]. We looked at three possible interpretations of the ordering variable, $\tilde{q}$, and found that the one which had been the HERWIG 7 default, which preserves the virtuality of an emitter upon successive branchings, does not meet the requirements for NLL accuracy. This is because successive soft emissions that are strongly ordered in rapidity but are disordered in either energy or transverse momentum are not generated independently. We did, however, find that the interpretation of $\tilde{q}$ that preserves the dot product of the momenta of the child partons of a branching does pass this requirement while also somewhat mitigating problems with the scheme that preserves the $p_\perp$ of each branching. We implemented the new, dot-product preserving, scheme into HERWIG and compared tuned versions of all three showers to LEP and LHC data. We confirmed that the $p_\perp$ preserving scheme produces too many hard emissions, these emissions populating the dead zone that is meant to be filled by matrix element corrections. However, as long as a veto was included to prevent too high virtualities from being generated, we found that the dot product preserving scheme was able to

give a good agreement with the experimental data, similar to the previously used q^2 preserving scheme.

Secondly we extended our analysis to the case of initial-state radiation. We found that the same issues of NLL accuracy that affect the q^2 preserving scheme for FSR also affect it in ISR while the other two are unaffected. However we did find that due to the fact that subsequent emissions affected the kinematics differently in the final and initial-state showers, the values of α_S used in each shower should be determined separately. Since the default recoil scheme for ISR in HERWIG 7 was the $p_\perp$ preserving scheme we compared this and the new, dot-product preserving, scheme with data from the LHC for vector boson production. We found that the dot-product preserving scheme outperformed the $p_\perp$ preserving scheme in the description of the data. During this study we also examined the impact of the NLO matching schemes POWHEG and MC@NLO on the ability of the shower to reproduce experimental results. We found that the best agreement with data was given when the NLO hard process was matched to the shower using POWHEG and the hardest emission was treated as a shower emission regardless of whether such an emission was within the allowed shower phase space. This remains a slightly unsatisfactory result as we were unable to provide a theoretical motivation for this treatment of the hardest emission.

In this thesis we have shown that it is possible to adapt the techniques developed in Ref. [41] for dipole showers to the case of the angular-ordered parton shower. We have further shown that it is possible to address shortcomings in the logarithmic accuracy of such showers within the existing angular-ordered framework. The question of whether all such shortcomings could be solved within the current framework, however, remains open. This work forms the starting point for further improvements to be made with the aim of bringing the HERWIG angular-ordered parton shower up to NLL accuracy.

Appendix A

Supplementary Material for Chapter 1

A.1   The Veto Algorithm

Regardless of the type of parton shower used, the generation of each parton emission proceeds according to the veto algorithm [16], the important features of which are described in this appendix. The following explanation is derived from the one of Sec. 1.2.2 of Ref. [154], with the notation adapted to be consistent with the present thesis.

Consider a shower algorithm with ordering variable t, splitting parameter z and splitting kernel $P(t, z)$. The aim of the algorithm is to generate a set of branchings (*i.e.* a set of values of the shower parameters, $\{t_i\}$ and $\{z_i\}$) between the hard starting scale, $t_{\max}$, and the IR cut-off, $t_{\min}$, using a distribution determined by $P(t, z)$. The Sudakov form factor that gives the non-emission probability between two scales, t_{i-1} and t_i, is given by

$$\Delta^{(P)}(t_{i-1}, t_i) = \exp\left(-\int_{t_i}^{t_{i-1}} \mathrm{d}t \int_{z_-}^{z_+} \mathrm{d}z P(t, z)\right), \qquad (A.1.1)$$

where $z_\pm(t)$ gives the kinematic limits on z for a given value of t. Since $P(t, z)$ is not guaranteed to have a calculable and invertible integral, an overestimate function,

$R(t, z)$, is introduced that satisfies this condition and

$$R(t, z) \geq P(t, z) \quad \forall \quad t, z. \tag{A.1.2}$$

The overestimate function has a corresponding Sudakov form factor

$$\Delta^{(R)}(t_{i-1}, t_i) = \exp\left(-\int_{t_i}^{t_{i-1}} \mathrm{d}t \int_{z_-}^{z_+} \mathrm{d}z R(t, z)\right). \tag{A.1.3}$$

Starting at $i = 1$, at scale $t_{i-1} = t_0 = t_{\mathrm{max}}$ and setting the variable $t_{\mathrm{lim}} = t_{\mathrm{max}}$, the veto algorithm then proceeds as follows:

1. trial variables, t and z, are generated using $R(t, z)$:

   (a) t is generated by solving

   $$\frac{\Delta^{(R)}(t_{i-1}, t)}{\Delta^{(R)}(t_{i-1}, t_{\mathrm{lim}})} = r_1, \tag{A.1.4}$$

   where r_1 is a random number generated from a uniform distribution, $0 < r_1 < 1$;

   (b) z is generated by solving

   $$\int_{z_-(t)}^{z} \mathrm{d}z' R\left(t, z'\right) = r_2 \int_{z_-(t)}^{z_+(t)} \mathrm{d}z' R\left(t, z'\right), \tag{A.1.5}$$

   where r_2 is a second random number from the same distribution as r_1;

2. if $t < t_{\mathrm{min}}$, then no emission is generated and the cut-off scale, t_{min}, and an associated value of the splitting parameter, $z_{t_{\mathrm{min}}}$, are returned;

3. return $t = t_i$ and $z = z_i$, provided that the following condition is satisfied

   $$\frac{P(t, z)}{R(t, z)} > r_3, \tag{A.1.6}$$

   where r_3 is a third random number from the same distribution as before. Otherwise the trial variables are *vetoed*, and the algorithm returns to Step 1 with $t_{\mathrm{lim}} = t$.

After a set of values for t_1 and z_1 have been accepted, the algorithm is repeated for t_2 and z_2, with t_1 as the new starting scale (and setting $t_{\text{lim}} = t_1$). This process continues until the algorithm returns t_{min} and $z_{t_{\text{min}}}$, at which point the shower terminates.

Appendix B

Supplementary Material for Chapter 2

B.1 $g \to q\bar{q}$ Branching in the Dot-Product Preserving Scheme

For a $g \to q\bar{q}$ branching, the transverse momentum of the splitting, Eqn. 2.4.9, becomes

$$p_\perp^2 = z^2(1-z)^2\tilde{q}^2 - (q_1^2 - m^2)(1-z)^2 - (q_2^2 - m^2)z^2 - m^2, \quad \text{(B.1.1)}$$

where m is the quark mass. So requiring that

$$\tilde{q}^2 > 2\max\left(\frac{q_1^2 - m^2}{z^2} + \frac{m^2}{2z^2(1-z)^2}, \frac{q_2^2 - m^2}{(1-z)^2} + \frac{m^2}{2z^2(1-z)^2}\right), \quad \text{(B.1.2)}$$

is sufficient, but not necessary, for there to be a physical solution in this case. The virtuality of the branching gluon is thus given by

$$q_0^2 = q_1^2 + q_2^2 + z(1-z)\tilde{q}^2 - 2m^2 \leq \frac{\tilde{q}^2}{2}, \quad \text{(B.1.3a)}$$

which will still allow for a physical solution but gives a stricter limit than the one obtained for gluon emission.

B.2   Impact of the Recoil Scheme on the Logarithmic Accuracy of the Thrust Distribution

In the following calculation, we prove that the thrust is only described to LL accuracy in the q^2 preserving scheme, as this recoil scheme prescription introduces incorrect NLL terms at order α_S^2. To do so, we make use of the same methodology employed in Sec. 4 of Ref. [41], which relies on the CAESAR formalism [100]. We use $\Sigma(L)$, the probability an event shape has a value smaller than $\exp(-L)$, for our analysis. We have already seen in Sec. 1.1.2 that when we perform an expansion of a resummed quantity in the strong coupling, α_S, at most 2 powers of L appear for each power of α_S, *i.e.*

$$\Sigma(L) = \sum_{n=0}^{\infty} \sum_{m=0}^{2n} c_{m,n} \alpha_S^n L^m + \mathcal{O}(\alpha_S e^{-L}) \tag{B.2.1}$$

and therefore the $\alpha_S^n L^{2n}$ terms are the LL contributions and the $\alpha_S^n L^{2n-1}$ terms are the NLL ones. For many event shapes, including the thrust, $\Sigma(L)$ can be expressed as

$$\Sigma(L) = \exp\left[L g_1(\alpha_S L) + g_2(\alpha_S L) + \alpha_S g_3(\alpha_S L) + \ldots \right] + \mathcal{O}(\alpha_S e^{-L}), \tag{B.2.2}$$

where the LL terms are contained in $g_1(\alpha_S L)$, while the NLL terms are in $g_2(\alpha_S L)$.

The HERWIG single emission probability can be written as

$$dP_{\text{soft}}^{\texttt{Hw7}} = \frac{2\alpha_S C_F}{\pi} \frac{d\tilde{q}}{\tilde{q}} \frac{d\epsilon}{\epsilon} = \frac{2\alpha_S C_F}{\pi} \frac{dp_\perp}{p_\perp} dy = \bar{\alpha} \frac{dp_\perp}{p_\perp} dy \tag{B.2.3}$$

where $\bar{\alpha} = 2\alpha_S C_F/\pi$, and $p_\perp = \epsilon\tilde{q}$ and $y = \log(\epsilon Q/p_\perp)$ are the Lund variables. The impact of the incorrect shower mapping can be written as

$$\delta\Sigma(L) = \bar{\alpha}^2 \int_{-\infty}^{+\infty} dy_1 \int_{-\infty}^{-|y_1|} d\ell_1 \int_{-\infty}^{+\infty} dy_2 \int_{-\infty}^{-|y_2|} d\ell_2 \, f(y_1, y_2) \int_0^{2\pi} \frac{d\phi_{12}}{2\pi} \tag{B.2.4}$$

$$\times \left[\Theta\left(e^{-L} - X_{\text{correct}}(y_1, \ell_1, y_2, \ell_2, \phi_{12}) \right) - \Theta\left(e^{-L} - X_{\text{PS}}(y_1, \ell_1, y_2, \ell_2, \phi_{12}) \right) \right],$$

where we have replaced the $1/2!$ multiplicity factor with the ordering condition

$$
f(y_1, y_2) = \begin{cases} \Theta(y_2 - y_1) & \text{if } y_1 y_2 < 0 \\[2mm] \Theta(|y_2| - |y_1|) & \text{if } y_1 y_2 > 0 \end{cases}
\tag{B.2.5}
$$

i.e. either y_1 is in the left hemisphere and y_2 is in the right, or they are both in the same hemisphere and ordered with respect to each other. In the above expression, $\ell_i = \log(p_{\perp i}/Q)$ and X is the event-shape observable expressed in terms of the Lund variables. The subscript "correct" means that X is calculated using the correct double-soft kinematics, where $p_{\perp 1} \equiv \epsilon_1 \tilde{q}_1$ is the transverse momentum of the first emitted gluon, while "PS" denotes the result obtained using the kinematics of the HERWIG parton shower (in the double-soft limit).

In Sec. 2.5 we have shown that the double-soft kinematics are correctly mapped if the transverse momenta or the dot products of the momenta of the emitted particles are preserved, so here we only need to consider the case of the q^2 preserving scheme, which gives inaccurate kinematics when the two gluons are emitted from the same progenitor. We therefore only need to consider positive rapidities, provided we include a factor of 2

$$
\delta\Sigma(L) = 2\bar{\alpha}^2 \int_0^{+\infty} \mathrm{d}y_1 \int_{-\infty}^{-y_1} \mathrm{d}\ell_1 \int_0^{+\infty} \mathrm{d}y_2 \int_{-\infty}^{-y_2} \mathrm{d}\ell_2 \, \Theta(y_2 - y_1) \int_0^{2\pi} \frac{\mathrm{d}\phi_{12}}{2\pi}
\tag{B.2.6}
$$
$$
\times \left[\Theta\!\left(e^{-L} - X_{\mathrm{correct}}(y_1, \ell_1, y_2, \ell_2, \phi_{12})\right) - \Theta\!\left(e^{-L} - X_{\mathrm{PS}}(y_1, \ell_1, y_2, \ell_2, \phi_{12})\right) \right].
$$

The correct expression for the thrust is

$$
1 - T_{\mathrm{correct}} = \frac{p_{\perp 1} e^{-y_1} + p_{\perp 2} e^{-y_2}}{Q} = \frac{p_{\perp 1}^2}{\epsilon_1 Q^2} + \frac{p_{\perp 2}^2}{\epsilon_2 Q^2} = e^{\ell_1 - y_1} + e^{\ell_2 - y_2}.
\tag{B.2.7}
$$

In the case of the q^2 preserving scheme the contribution of the first gluon is modified: we label the new transverse momentum and rapidity as $\bar{p}_{\perp 1}$ and $\bar{y}_1$, respectively, while $p_{\perp 1}$ and y_1 denote the original values. Therefore from Eqn. (2.5.14) we derive that

$$
p_{\perp 1}^2 \to \bar{p}_{\perp 1}^2 = \max\left(p_{\perp 1}^2 - \frac{\epsilon_1}{\epsilon_2} p_{\perp 2}^2, 0 \right).
\tag{B.2.8}
$$

Utilising the fact that the recoil prescription does not affect the light-cone momentum fraction of the first gluon, *i.e.*

$$\epsilon_1 = \frac{\overline{p}_{\perp 1}}{Q} e^{\overline{y}_1} = \frac{p_{\perp 1}}{Q} e^{y_1}, \tag{B.2.9}$$

we can write

$$\begin{aligned}
1 - T_{\mathrm{PS}} &= \frac{\overline{p}_{\perp 1} e^{-\overline{y}_1}}{Q} + \frac{p_{\perp 2} e^{-y_2}}{Q} = \frac{\overline{p}_{\perp 1}^2}{\epsilon_1 Q^2} + \frac{p_{\perp 2}^2}{\epsilon_2 Q^2} \\
&= \max\left(\frac{p_{\perp 1}^2}{\epsilon_1 Q^2}, \frac{p_{\perp 2}^2}{\epsilon_2 Q^2}\right) = \max(e^{\ell_1 - y_1}, e^{\ell_2 - y_2}).
\end{aligned} \tag{B.2.10}$$

By comparing Eqn. (B.2.7) and Eqn. (B.2.10), we notice that the two expressions coincide in the strongly ordered region, thus we expect the effect of the incorrect kinematic mapping to show only at NLL. By performing the calculation we indeed find that

$$\begin{aligned}
\delta\Sigma(L) &= \bar{\alpha}^2 \int_0^{+\infty} \mathrm{d}y_1 \int_{-\infty}^{-y_1} \mathrm{d}\ell_1 \int_0^{+\infty} \mathrm{d}y_2 \int_{-\infty}^{-y_2} \mathrm{d}\ell_2 \int_0^{2\pi} \frac{\mathrm{d}\phi_{12}}{2\pi} \\
&\quad \times \left[\Theta\left(e^{-L} - e^{\ell_1 - y_1} - e^{\ell_2 - y_2}\right) - \Theta\left(e^{-L} - \max(e^{\ell_1 - y_1}, e^{\ell_2 - y_2})\right)\right] \\
&= 2\bar{\alpha}^2 \int_0^{\infty} \mathrm{d}x_1 \int_0^{(L+x_1)/2} \mathrm{d}y_1 \int_{x_1}^{\infty} \mathrm{d}x_2 \int_0^{(L+x_2)/2} \mathrm{d}y_2 \left[\Theta(1 - e^{-x_1} - e^{-x_2}) - 1\right],
\end{aligned} \tag{B.2.11}$$

where in the first line we have removed the theta function coming from the angular-ordering condition, $\Theta(y_2 - y_1)$, and included a factor of $1/2$ as the integrand is symmetric in the exchange $1 \leftrightarrow 2$. In the second line we have defined $x_i = y_i - \ell_i - L$ and reinserted an ordering condition $x_2 > x_1$. Now the dependence of $\delta\Sigma(L)$ on L comes entirely from the limits on the y integrals, which are trivial, and we can easily extract the leading power of L as follows

$$\begin{aligned}
\delta\Sigma(L) &= -\frac{\bar{\alpha}^2}{2} L^2 \int_0^{\infty} \mathrm{d}x_1 \int_{x_1}^{\infty} \mathrm{d}x_2 \, \Theta(e^{-x_1} + e^{-x_2} - 1) + \mathcal{O}(\bar{\alpha}^2 L) \\
&= -\frac{\bar{\alpha}^2}{2} L^2 \int_0^{\log 2} \mathrm{d}x_1 \left[-\log(e^{x_1} - 1)\right] + \mathcal{O}(\bar{\alpha}^2 L) \\
&= -\frac{\bar{\alpha}^2}{2} \frac{\pi^2}{12} L^2 + \mathcal{O}(\bar{\alpha}^2 L) \\
&= -\frac{C_F^2}{6} \alpha_{\mathrm{S}}^2 L^2 + \mathcal{O}(\alpha_{\mathrm{S}}^2 L),
\end{aligned} \tag{B.2.12}$$

This proves that this choice of the kinematic mapping introduces a NLL discrepancy at order α_S^2 (while for dipole showers, the first NLL discrepancy appears at order α_S^3 [41]).

Appendix C

Supplementary Material for Chapter 3

C.1 Global recoil

In this appendix we briefly describe the global recoil that is applied to hadron-collider events at the end of the showering phase to achieve momentum conservation. We closely follow the approach and notation of Sec. 6.5.2 of Ref. [44], with the recoil strategy updated for the current version of HERWIG 7.

After the parton shower evolution, the space-like shower progenitors (*i.e.* the partons colliding in the hard process) and the time-like ones (*i.e.* the final-state partons arising from the hard scattering) are no longer on their mass shell, having acquired a negative or positive virtuality. Furthermore, the colliding particles have also acquired some transverse momentum that must be redistributed among the final-state progenitors and their child partons. We therefore need to perform some momentum reshuffling to ensure momentum conservation. How this is performed depends on whether the colour partner is an initial- or final-state parton.

The details of the algorithm for final-final correlations can be found in Sec. 6.4.2 of Ref. [44], here we focus on the case where ISR is involved.

C.1.1   Drell-Yan: initial-initial correlations

When we consider the production of a colour-singlet system, such as an electroweak
gauge boson produced by the Drell-Yan process, we only have an initial-initial dipole.

We use the hadronic beam momenta $p_\oplus$ and $p_\ominus$ to define the Sudakov basis for the
initial-state shower algorithm. The subscript $\oplus$ denotes the particle incident from
the $+z$ direction, while $\ominus$ denotes the one from the $-z$ direction. The momenta of
the colliding partons, $q_\oplus$ and $q_\ominus$, can be written as

$$q_\oplus = \alpha_\oplus p_\oplus + \beta_\oplus p_\oplus + q_{\perp\oplus}, \tag{C.1.1}$$

where $q_{\perp\oplus}$ and $q_{\perp\ominus}$ are two space-like vectors orthogonal to the beam momenta.

We denote by p_{cm} the original final-state momentum, *i.e.* the momentum of the
colour singlet system prior to the inclusion of the shower

$$p_{\mathrm{cm}} = x_\oplus p_\oplus + x_\ominus p_\ominus. \tag{C.1.2}$$

After shower emissions have been generated, the sum of the momenta of the incoming
shower progenitors, $q_{\mathrm{cm}} = q_\oplus + q_\ominus$, is different from p_{cm}. We can thus introduce two
rescaling factors, $k_\oplus$ to define the shuffled momenta q'

$$q'_\oplus = \alpha_\oplus k_\oplus p_\oplus + \frac{\beta_\oplus}{k_\oplus} p_\oplus + q_{\perp\oplus}, \tag{C.1.3}$$

which satisfy the conditions $q_\oplus^{2\prime} = q_\oplus^2$ and

$$q'_{\mathrm{cm}} = q'_\oplus + q'_\ominus = \left(\alpha_\oplus k_\oplus + \frac{\beta_\ominus}{k_\ominus} \right) p_\oplus + \left(\alpha_\ominus k_\ominus + \frac{\beta_\oplus}{k_\oplus} \right) p_\ominus + q_{\perp\oplus} + q_{\perp\ominus}. \tag{C.1.4}$$

By imposing $q_{\mathrm{cm}}^{\prime 2} = p_{\mathrm{cm}}^2 = x_\oplus x_\ominus s$, where $\sqrt{s}$ in the centre-of-mass energy of the
hadronic collision, we obtain a constraint on the product of the rescaling factors
$k_{\oplus\ominus} = k_\oplus k_\ominus$:

$$\alpha_\oplus \alpha_\ominus k_{\oplus\ominus}^2 + \left(\alpha_\oplus \beta_\ominus + \alpha_\ominus \beta_\oplus - x_\oplus x_\ominus + \frac{(q_{\perp\oplus} + q_{\perp\ominus})^2}{s} \right) k_{\oplus\ominus} + \beta_\oplus \beta_\ominus = 0. \tag{C.1.5}$$

It is trivial to check that if no emission has occurred, *i.e.* $\alpha_\oplus = x_\oplus$, $\beta_\oplus = 0$ and

$q_{\perp\oplus} = 0$, then $k_\oplus = k_\ominus = 1$ is a solution of eq. (C.1.5).

By default, we set the rescaling factor of the progenitor which had the largest transverse momentum emission to $k_{\oplus\ominus}$, and the other rescaling factor to 1. This choice makes matching with higher order matrix elements simpler as for one emission it exactly reproduces the kinematics of the Catani-Seymour dipole [53].[1]

Since $q_\oplus$ and $q'_\oplus$ have the same virtuality, it is possible to define a boost to transform $q_\oplus$ to $q'_\oplus$. This boost is then applied to all the time-like children and the final space-like parent produced during the showering phase.

We then need a second boost, which is applied to the original colour-singlet final state, from p_{cm} to q'_{cm}, in order to absorb the transverse momentum $q_{\perp\oplus} + q_{\perp\ominus}$ that the colliding partons have acquired.

It is easy to check that

$$k_{\oplus\ominus} = 1 + \mathcal{O}\left(\frac{q_\oplus^2}{s}\right) + \mathcal{O}\left(\frac{q_\ominus^2}{s}\right), \tag{C.1.8}$$

i.e. that the rescaling coefficients are equal to 1 plus power-suppressed corrections, thus the boosts applied to the children of the time-like shower progenitors do not alter the logarithmic accuracy of the result.[2]

C.1.2   Deep inelastic scattering: initial-final correlations

We now consider deep inelastic processes, *i.e.* when the incoming parton with momentum p_{in} is colour-connected to an outgoing parton with momentum p_{out}. We

---

[1]A second option, which was the default in HERWIG++ and FORTRAN HERWIG, is to preserve the rapidity of the colour-singlet system, *i.e.* that the ratio of $p_\oplus$ and $p_\ominus$ is identical in q'_{cm} and p_{cm}:

$$k_\oplus^2 = k_{\oplus\ominus}\frac{x_\oplus\left(\beta_\oplus + \alpha_\ominus k_{\oplus\ominus}\right)}{x_\ominus\left(\beta_\ominus + \alpha_\oplus k_{\oplus\ominus}\right)}. \tag{C.1.6}$$

The final option is to preserve the longitudinal momentum, which leads to

$$\left(\alpha_\oplus + \frac{\beta_\ominus}{k_{\oplus\ominus}}\right)k_\oplus^2 + (x_\oplus - x_\ominus)k_\oplus - (\alpha_\ominus k_{\oplus\ominus} + \beta_\oplus) = 0. \tag{C.1.7}$$

[2]By default we boost only the time-like jet that contains the hardest emission, however if we adopt one of the other reconstruction options we need to build two separate boosts, one for each incoming shower progenitor.

want our recoil strategy to preserve the transferred momentum, defined as

$$Q^2 = -(p_{\text{in}} - p_{\text{out}})^2. \tag{C.1.9}$$

In the Breit frame

$$p_{\text{in}} = \frac{Q}{2}\left[1 + \frac{m_{\text{out}}^2}{Q^2}; \vec{0}, +1 + \frac{m_{\text{out}}^2}{Q^2}\right] \tag{C.1.10}$$

$$p_{\text{out}} = \frac{Q}{2}\left[1 + \frac{m_{\text{out}}^2}{Q^2}; \vec{0}, -1 + \frac{m_{\text{out}}^2}{Q^2}\right] \tag{C.1.11}$$

$$\Delta p = p_{\text{in}} - p_{\text{out}} = Q\left[0; \vec{0}, 1\right], \tag{C.1.12}$$

where m_{out} is the on-shell mass of the outgoing shower progenitor colour-connected to the incoming one. We introduce a set of basis vectors

$$n_1 = Q\left[1; \vec{0}, 1\right], \qquad n_2 = Q\left[1; \vec{0}, -1\right], \tag{C.1.13}$$

so that

$$\Delta p = \frac{1}{2}\left(n_1 - n_2\right), \tag{C.1.14}$$

and the momentum of the incoming jet, after the radiation, can be written as

$$q_{\text{in}} = \alpha_{\text{in}} n_1 + \beta_{\text{in}} n_2 + q_\perp. \tag{C.1.15}$$

The transverse-momentum component of q_{in} must be absorbed by the outgoing progenitor q_{out} (and its children), so we first perform a rotation that leads to

$$q_{\text{out}} = \alpha_{\text{out}} n_1 + \beta_{\text{out}} n_2 + q_\perp, \tag{C.1.16}$$

where $\beta_{\text{out}} = \frac{1}{2}$.

We introduce rescaling factors, $k_{\text{in,out}}$, that allow us to define the shuffled momenta

$$q'_{\text{in,out}} = \alpha_{\text{in,out}} k_{\text{in,out}} n_1 + \frac{\beta_{\text{in,out}}}{k_{\text{in,out}}} n_2 + q_\perp. \tag{C.1.17}$$

We impose the condition that

$$\Delta p = p_{\text{in}} - p_{\text{out}} = q'_{\text{in}} - q'_{\text{out}}, \tag{C.1.18}$$

which leads to

$$\alpha_{\text{in}} k_{\text{in}} - \alpha_{\text{out}} k_{\text{out}} = \frac{1}{2}, \qquad \frac{\beta_{\text{in}}}{k_{\text{in}}} - \frac{\beta_{\text{out}}}{k_{\text{out}}} = -\frac{1}{2}. \qquad \text{(C.1.19)}$$

Each of these rescalings can be implemented via a boost applied to the initial- and final-state showers, respectively.

If we assume that $m_{\text{out}} \ll Q^2$, we can write

$$\alpha_{\text{in}} = \beta_{\text{out}} = \frac{1}{2}, \qquad \beta_{\text{in}} = \mathcal{O}\left(\frac{p_{\text{in}}^2}{Q}\right), \qquad \alpha_{\text{out}} = \mathcal{O}\left(\frac{p_{\text{out}}^2}{Q}\right), \qquad \text{(C.1.20)}$$

which implies that

$$k_{\text{in,out}} = 1 + \mathcal{O}\left(\frac{p_{\text{in}}^2}{Q}\right) + \mathcal{O}\left(\frac{p_{\text{out}}^2}{Q}\right), \qquad \text{(C.1.21)}$$

i.e. that the boost only leads to power-suppressed corrections and does not alter the logarithmic structure of the result.

C.1.3   General case

For more complicated colour structures (*e.g.* Z+jet production) we need a more general procedure.

The default approach used by Herwig++ from version 2.3 and the one employed by FORTRAN HERWIG and Herwig++ versions prior to 2.3 are both detailed in Ref. [44], here we want to present the new approach introduced in Herwig 7, which uses information on the colour structure as much as possible.

The jet associated with the progenitor which leads to the hardest emission is reconstructed first. By default, its evolution partner is also reconstructed at this stage.[1] The procedure is then repeated with the next unreconstructed jet with the hardest emission. Since a gluon has two colour partners, its momentum is shifted twice, once by the recoil from each of its partners.

For the case of DY production with matrix element corrections, the hardest emission is considered as part of the hard process (and thus treated as a shower progenitor and

---

[1]Optionally, the evolution partner only absorbs the recoil, therefore staying on its mass shell, but the full jet arising from its evolution is not reconstructed yet.

not as a shower emission) only when it is inside the dead zone. For Powheg-matched DY production, by default a profile function is employed to decide whether the first emission should be treated as a shower emission (and exponentiated in the Sudakov) or as part of the hard process. However, in this study, we switch off this profiling mechanism, so that we always exponentiate the hardest emission and we compare whether treating the hardest emission as a shower progenitor when it is inside the dead zone or always treating it as a shower emission gives a better description of data. For MC@NLO-matched DY production, the first emitted parton is always interpreted as part of the hard process, *i.e.* as a shower progenitor.

In any of these cases, the global recoil is obtained by rescaling the momenta of the progenitors. However, since such rescalings are equal to 1 plus power-suppressed corrections, they do not interfere with the logarithmic structure of the result.

Bibliography

[1] DELPHI collaboration, P. Abreu et al., *Tuning and test of fragmentation models based on identified particles and precision event shape data*, Z. Phys. **C73** (1996) 11–60.

[2] ALEPH collaboration, A. Heister et al., *Studies of QCD at e+ e- centre-of-mass energies between 91-GeV and 209-GeV*, Eur. Phys. J. **C35** (2004) 457–486.

[3] OPAL collaboration, G. Abbiendi et al., *Experimental studies of unbiased gluon jets from e^+e^- annihilations using the jet boost algorithm*, Phys. Rev. **D69** (2004) 032002, [`hep-ex/0310048`].

[4] DELPHI collaboration, J. Abdallah et al., *A study of the b-quark fragmentation function with the DELPHI detector at LEP I and an averaged distribution obtained at the Z Pole*, Eur. Phys. J. **C71** (2011) 1557, [`1102.4748`].

[5] ATLAS collaboration, G. Aad et al., *Measurement of the charged-particle multiplicity inside jets from $\sqrt{s} = 8$ TeV pp collisions with the ATLAS detector*, Eur. Phys. J. **C76** (2016) 322, [`1602.00988`].

[6] CMS collaboration, S. Chatrchyan et al., *Measurement of the Rapidity and Transverse Momentum Distributions of Z Bosons in pp Collisions at $\sqrt{s} = 7$ TeV*, Phys. Rev. D **85** (2012) 032002, [`1110.4973`].

[7] ATLAS collaboration, G. Aad et al., *Measurement of angular correlations in Drell-Yan lepton pairs to probe Z/gamma* boson transverse momentum at sqrt(s)=7 TeV with the ATLAS detector, Phys. Lett. B* **720** (2013) 32–51, [`1211.6899`].

[8] ATLAS collaboration, G. Aad et al., *Measurement of the Transverse Momentum Distribution of W Bosons in pp Collisions at $\sqrt{s} = 7$ TeV with the ATLAS Detector, Phys. Rev. D* **85** (2012) 012005, [`1108.6308`].

[9] ATLAS collaboration, G. Aad et al., *Measurement of the transverse momentum and ϕ_η^* distributions of Drell–Yan lepton pairs in proton–proton collisions at $\sqrt{s} = 8$ TeV with the ATLAS detector, Eur. Phys. J. C* **76** (2016) 291, [`1512.02192`].

[10] CMS collaboration, A. M. Sirunyan et al., *Measurements of differential Z boson production cross sections in proton-proton collisions at $\sqrt{s} = 13$ TeV, JHEP* **12** (2019) 061, [`1909.04133`].

[11] LHCʙ collaboration, R. Aaij et al., *Measurement of CP-Averaged Observables in the $B^0 \to K^{*0}\mu^+\mu^-$ Decay, Phys. Rev. Lett.* **125** (2020) 011802, [`2003.04831`].

[12] LHCʙ collaboration, R. Aaij et al., *Test of lepton universality in beauty-quark decays*, `2103.11769`.

[13] CMS collaboration, S. Chatrchyan et al., *Observation of a New Boson at a Mass of 125 GeV with the CMS Experiment at the LHC, Phys. Lett. B* **716** (2012) 30–61, [`1207.7235`].

[14] ATLAS collaboration, G. Aad et al., *Observation of a new particle in the search for the Standard Model Higgs boson with the ATLAS detector at the LHC, Phys. Lett. B* **716** (2012) 1–29, [`1207.7214`].

[15] MUON G-2 collaboration, B. Abi et al., *Measurement of the Positive Muon Anomalous Magnetic Moment to 0.46 ppm*, *Phys. Rev. Lett.* **126** (2021) 141801, [`2104.03281`].

[16] A. Buckley et al., *General-purpose event generators for LHC physics*, *Phys. Rept.* **504** (2011) 145–233, [`1101.2599`].

[17] S. Catani, F. Krauss, R. Kuhn and B. R. Webber, *QCD matrix elements + parton showers*, *JHEP* **11** (2001) 063, [`hep-ph/0109231`].

[18] M. L. Mangano, M. Moretti and R. Pittau, *Multijet matrix elements and shower evolution in hadronic collisions: $Wb\bar{b} + n$ jets as a case study*, *Nucl. Phys. B* **632** (2002) 343–362, [`hep-ph/0108069`].

[19] L. Lonnblad, *Correcting the color dipole cascade model with fixed order matrix elements*, *JHEP* **05** (2002) 046, [`hep-ph/0112284`].

[20] S. Frixione and B. R. Webber, *Matching NLO QCD computations and parton shower simulations*, *JHEP* **06** (2002) 029, [`hep-ph/0204244`].

[21] J. Alwall, R. Frederix, S. Frixione, V. Hirschi, F. Maltoni, O. Mattelaer et al., *The automated computation of tree-level and next-to-leading order differential cross sections, and their matching to parton shower simulations*, *JHEP* **07** (2014) 079, [`1405.0301`].

[22] P. Nason, *A New method for combining NLO QCD with shower Monte Carlo algorithms*, *JHEP* **11** (2004) 040, [`hep-ph/0409146`].

[23] S. Frixione, P. Nason and C. Oleari, *Matching NLO QCD computations with Parton Shower simulations: the POWHEG method*, *JHEP* **11** (2007) 070, [`0709.2092`].

[24] S. Alioli, P. Nason, C. Oleari and E. Re, *A general framework for implementing NLO calculations in shower Monte Carlo programs: the POWHEG BOX*, *JHEP* **06** (2010) 043, [`1002.2581`].

[25] S. Jadach, W. Płaczek, S. Sapeta, A. Siódmok and M. Skrzypek, *Matching NLO QCD with parton shower in Monte Carlo scheme — the KrkNLO method*, *JHEP* **10** (2015) 052, [1503.06849].

[26] S. Hoeche, F. Krauss, M. Schonherr and F. Siegert, *QCD matrix elements + parton showers: The NLO case*, *JHEP* **04** (2013) 027, [1207.5030].

[27] K. Hamilton, P. Nason and G. Zanderighi, *MINLO: Multi-Scale Improved NLO*, *JHEP* **10** (2012) 155, [1206.3572].

[28] R. Frederix and S. Frixione, *Merging meets matching in MC@NLO*, *JHEP* **12** (2012) 061, [1209.6215].

[29] K. Hamilton, P. Nason, E. Re and G. Zanderighi, *NNLOPS simulation of Higgs boson production*, *JHEP* **10** (2013) 222, [1309.0017].

[30] S. Höche, Y. Li and S. Prestel, *Drell-Yan lepton pair production at NNLO QCD with parton showers*, *Phys. Rev. D* **91** (2015) 074015, [1405.3607].

[31] S. Alioli, C. W. Bauer, C. Berggren, F. J. Tackmann, J. R. Walsh and S. Zuberi, *Matching Fully Differential NNLO Calculations and Parton Showers*, *JHEP* **06** (2014) 089, [1311.0286].

[32] J. Bellm, S. Gieseke and S. Plätzer, *Merging NLO Multi-jet Calculations with Improved Unitarization*, *Eur. Phys. J. C* **78** (2018) 244, [1705.06700].

[33] E. Re, *Recent progress on high order calculations and matching to parton showers*, in *9th Large Hadron Collider Physics Conference*, 10, 2021, 2110.02183.

[34] J. M. Campbell, S. Höche, H. T. Li, C. T. Preuss and P. Skands, *Towards NNLO+PS Matching with Sector Showers*, 2108.07133.

[35] H. Brooks, C. T. Preuss and P. Skands, *Sector Showers for Hadron Collisions*, *JHEP* **07** (2020) 032, [2003.00702].

[36] J. R. Forshaw, J. Holguin and S. Plätzer, *Parton branching at amplitude level*, *JHEP* **08** (2019) 145, [1905.08686].

[37] J. R. Forshaw, J. Holguin and S. Plätzer, *Building a consistent parton shower*, *JHEP* **09** (2020) 014, [2003.06400].

[38] J. Holguin, J. R. Forshaw and S. Plätzer, *Improvements on dipole shower colour*, *Eur. Phys. J. C* **81** (2021) 364, [2011.15087].

[39] Z. Nagy and D. E. Soper, *Effects of subleading color in a parton shower*, *JHEP* **07** (2015) 119, [1501.00778].

[40] Z. Nagy and D. E. Soper, *Summations of large logarithms by parton showers*, *Phys. Rev. D* **104** (2021) 054049, [2011.04773].

[41] M. Dasgupta, F. A. Dreyer, K. Hamilton, P. F. Monni and G. P. Salam, *Logarithmic accuracy of parton showers: a fixed-order study*, *JHEP* **09** (2018) 033, [1805.09327].

[42] M. Dasgupta, F. A. Dreyer, K. Hamilton, P. F. Monni, G. P. Salam and G. Soyez, *Parton showers beyond leading logarithmic accuracy*, *Phys. Rev. Lett.* **125** (2020) 052002, [2002.11114].

[43] K. Hamilton, R. Medves, G. P. Salam, L. Scyboz and G. Soyez, *Colour and logarithmic accuracy in final-state parton showers*, 2011.10054.

[44] M. Bahr et al., *Herwig++ Physics and Manual*, *Eur. Phys. J.* **C58** (2008) 639–707, [0803.0883].

[45] J. Bellm et al., *Herwig 7.2 release note*, *Eur. Phys. J. C* **80** (2020) 452, [1912.06509].

[46] R. K. Ellis, W. J. Stirling and B. R. Webber, *QCD and collider physics*, vol. 8. Cambridge University Press, 2, 2011.

[47] J. Campbell, J. Huston and F. Krauss, *The Black Book of Quantum Chromodynamics: A Primer for the LHC Era.* Oxford University Press, 12, 2017.

[48] D. Amati, A. Bassetto, M. Ciafaloni, G. Marchesini and G. Veneziano, *A Treatment of Hard Processes Sensitive to the Infrared Structure of QCD*, Nucl. Phys. B **173** (1980) 429–455.

[49] S. Catani, B. R. Webber and G. Marchesini, *QCD Coherent Branching and Semi-Inclusive Processes at Large x*, Nucl. Phys. **B349** (1991) 635–654.

[50] F. Bloch and A. Nordsieck, *Note on the Radiation Field of the electron*, Phys. Rev. **52** (1937) 54–59.

[51] T. Kinoshita, *Mass singularities of Feynman amplitudes*, J. Math. Phys. **3** (1962) 650–677.

[52] T. D. Lee and M. Nauenberg, *Degenerate Systems and Mass Singularities*, Phys. Rev. **133** (1964) B1549–B1562.

[53] S. Catani and M. Seymour, *A General algorithm for calculating jet cross-sections in NLO QCD*, Nucl. Phys. B **485** (1997) 291–419, [`hep-ph/9605323`].

[54] G. Altarelli and G. Parisi, *Asymptotic Freedom in Parton Language*, Nucl. Phys. B **126** (1977) 298–318.

[55] V. N. Gribov and L. N. Lipatov, *Deep inelastic e p scattering in perturbation theory*, Sov. J. Nucl. Phys. **15** (1972) 438–450.

[56] Y. L. Dokshitzer, *Calculation of the Structure Functions for Deep Inelastic Scattering and e+ e- Annihilation by Perturbation Theory in Quantum Chromodynamics.*, Sov. Phys. JETP **46** (1977) 641–653.

[57] Y. I. Azimov, Y. L. Dokshitzer, V. A. Khoze and S. I. Troyan, *Similarity of Parton and Hadron Spectra in QCD Jets*, Z. Phys. C **27** (1985) 65–72.

[58] T. Gleisberg, S. Hoeche, F. Krauss, M. Schonherr, S. Schumann, F. Siegert et al., *Event generation with SHERPA 1.1*, *JHEP* **02** (2009) 007, [0811.4622].

[59] SHERPA collaboration, E. Bothmann et al., *Event Generation with Sherpa 2.2*, *SciPost Phys.* **7** (2019) 034, [1905.09127].

[60] T. Sjostrand, S. Mrenna and P. Z. Skands, *PYTHIA 6.4 Physics and Manual*, *JHEP* **05** (2006) 026, [hep-ph/0603175].

[61] T. Sjöstrand, S. Ask, J. R. Christiansen, R. Corke, N. Desai, P. Ilten et al., *An Introduction to PYTHIA 8.2*, *Comput. Phys. Commun.* **191** (2015) 159–177, [1410.3012].

[62] S. Platzer and S. Gieseke, *Dipole Showers and Automated NLO Matching in Herwig++*, *Eur. Phys. J. C* **72** (2012) 2187, [1109.6256].

[63] J. Alwall, M. Herquet, F. Maltoni, O. Mattelaer and T. Stelzer, *MadGraph 5 : Going Beyond*, *JHEP* **06** (2011) 128, [1106.0522].

[64] S. Gieseke, P. Stephens and B. Webber, *New formalism for QCD parton showers*, *JHEP* **12** (2003) 045, [hep-ph/0310083].

[65] T. Sjostrand and P. Z. Skands, *Transverse-momentum-ordered showers and interleaved multiple interactions*, *Eur. Phys. J.* **C39** (2005) 129–154, [hep-ph/0408302].

[66] S. Schumann and F. Krauss, *A Parton shower algorithm based on Catani-Seymour dipole factorisation*, *JHEP* **03** (2008) 038, [0709.1027].

[67] B. R. Webber, *A QCD Model for Jet Fragmentation Including Soft Gluon Interference*, *Nucl. Phys. B* **238** (1984) 492–528.

[68] J.-C. Winter, F. Krauss and G. Soff, *A Modified cluster hadronization model*, *Eur. Phys. J. C* **36** (2004) 381–395, [hep-ph/0311085].

[69] B. Andersson, G. Gustafson, G. Ingelman and T. Sjostrand, *Parton Fragmentation and String Dynamics*, *Phys. Rept.* **97** (1983) 31–145.

[70] M. Bahr, S. Gieseke and M. H. Seymour, *Simulation of multiple partonic interactions in Herwig++*, *JHEP* **07** (2008) 076, [`0803.3633`].

[71] T. Sjostrand and M. van Zijl, *A Multiple Interaction Model for the Event Structure in Hadron Collisions*, *Phys. Rev. D* **36** (1987) 2019.

[72] J. Bellm, S. Gieseke and P. Kirchgaesser, *Improving the description of multiple interactions in Herwig*, *Eur. Phys. J. C* **80** (2020) 469, [`1911.13149`].

[73] R. Corke and T. Sjostrand, *Multiparton Interactions and Rescattering*, *JHEP* **01** (2010) 035, [`0911.1909`].

[74] K. Kato and T. Munehisa, *Monte Carlo Approach to QCD Jets in the Next-to-leading Logarithmic Approximation*, *Phys. Rev.* **D36** (1987) 61.

[75] K. Kato and T. Munehisa, *Double Cascade Scheme for QCD Jets in e^+e^- Annihilation*, *Phys. Rev.* **D39** (1989) 156.

[76] K. Kato and T. Munehisa, *NLLjet : A Monte Carlo code for e+ e- QCD jets including next-to-leading order terms*, *Comput. Phys. Commun.* **64** (1991) 67–97.

[77] K. Kato, T. Munehisa and H. Tanaka, *Next-to-leading logarithmic parton shower in deep inelastic scattering*, *Z. Phys.* **C54** (1992) 397–410.

[78] W. T. Giele, D. A. Kosower and P. Z. Skands, *Higher-Order Corrections to Timelike Jets*, *Phys. Rev.* **D84** (2011) 054003, [`1102.2126`].

[79] L. Hartgring, E. Laenen and P. Skands, *Antenna Showers with One-Loop Matrix Elements*, *JHEP* **10** (2013) 127, [`1303.4974`].

[80] H. T. Li and P. Skands, *A framework for second-order parton showers*, *Phys. Lett.* **B771** (2017) 59–66, [`1611.00013`].

[81] S. Höche, F. Krauss and S. Prestel, *Implementing NLO DGLAP evolution in Parton Showers*, JHEP **10** (2017) 093, [1705.00982].

[82] S. Höche and S. Prestel, *Triple collinear emissions in parton showers*, Phys. Rev. **D96** (2017) 074017, [1705.00742].

[83] F. Dulat, S. Höche and S. Prestel, *Leading-color fully differential two-loop soft corrections to QCD dipole showers*, 1805.03757.

[84] S. Plätzer and M. Sjödahl, *Subleading N_c improved Parton Showers*, JHEP **07** (2012) 042, [1201.0260].

[85] R. A. Martínez, M. De Angelis, J. R. Forshaw, S. Plätzer and M. H. Seymour, *Soft gluon evolution and non-global logarithms*, JHEP **05** (2018) 044, [1802.08531].

[86] S. Höche and S. Prestel, *The midpoint between dipole and parton showers*, Eur. Phys. J. **C75** (2015) 461, [1506.05057].

[87] B. Andersson, G. Gustafson and C. Sjögren, *Comparison of the dipole cascade model versus $O(\alpha_s^2)$ matrix elements and color interference in e+ e-annihilation*, Nucl. Phys. **B380** (1992) 391–407.

[88] G. Gustafson, *Multiplicity distributions in QCD cascades*, Nucl. Phys. B **392** (1993) 251–280.

[89] C. Friberg, G. Gustafson and J. Hakkinen, *Color connections in e+ e-annihilation*, Nucl. Phys. B **490** (1997) 289–305, [hep-ph/9604347].

[90] P. Eden and G. Gustafson, *Energy and virtuality scale dependence in quark and gluon jets*, JHEP **09** (1998) 015, [hep-ph/9805228].

[91] B. Andersson, G. Gustafson, L. Lönnblad and U. Pettersson, *Coherence Effects in Deep Inelastic Scattering*, Z. Phys. **C43** (1989) 625.

[92] A. Banfi, G. Corcella and M. Dasgupta, *Angular ordering and parton showers for non-global QCD observables*, *JHEP* **03** (2007) 050, [`hep-ph/0612282`].

[93] D. Reichelt, P. Richardson and A. Siodmok, *Improving the Simulation of Quark and Gluon Jets with Herwig 7*, *Eur. Phys. J.* **C77** (2017) 876, [`1708.01491`].

[94] G. Marchesini and B. R. Webber, *Simulation of QCD Jets Including Soft Gluon Interference*, *Nucl. Phys.* **B238** (1984) 1–29.

[95] S. Catani, S. Dittmaier and Z. Trocsanyi, *One loop singular behavior of QCD and SUSY QCD amplitudes with massive partons*, *Phys. Lett.* **B500** (2001) 149–160, [`hep-ph/0011222`].

[96] G. Marchesini and B. R. Webber, *Simulation of QCD Coherence in Heavy Quark Production and Decay*, *Nucl. Phys.* **B330** (1990) 261–283.

[97] Y. L. Dokshitzer, V. A. Khoze and S. I. Troian, *On specific QCD properties of heavy quark fragmentation ('dead cone')*, *J. Phys.* **G17** (1991) 1602–1604.

[98] M. Cacciari, G. P. Salam and G. Soyez, *FastJet User Manual*, *Eur. Phys. J.* **C72** (2012) 1896, [`1111.6097`].

[99] S. Catani, Y. L. Dokshitzer, M. Olsson, G. Turnock and B. R. Webber, *New clustering algorithm for multi - jet cross-sections in e+ e- annihilation*, *Phys. Lett.* **B269** (1991) 432–438.

[100] A. Banfi, G. P. Salam and G. Zanderighi, *Principles of general final-state resummation and automated implementation*, *JHEP* **03** (2005) 073, [`hep-ph/0407286`].

[101] A. H. Hoang, S. Plätzer and D. Samitz, *On the Cutoff Dependence of the Quark Mass Parameter in Angular Ordered Parton Showers*, *JHEP* **10** (2018) 200, [`1807.06617`].

[102] A. Buckley, J. Butterworth, L. Lonnblad, D. Grellscheid, H. Hoeth, J. Monk et al., *Rivet user manual, Comput. Phys. Commun.* **184** (2013) 2803–2819, [1003.0694].

[103] J. Bellm, D. Grellscheid, P. Kirchgaeßer, A. Papaefstathiou, S. Plätzer, M. Rauch et al., "The physics of herwig 7.".

[104] A. Buckley, H. Hoeth, H. Lacker, H. Schulz and J. E. von Seggern, *Systematic event generator tuning for the LHC, Eur. Phys. J.* **C65** (2010) 331–357, [0907.2973].

[105] TASSO collaboration, W. Braunschweig et al., *Global Jet Properties at 14-GeV to 44-GeV Center-of-mass Energy in e^+e^- Annihilation, Z. Phys.* **C47** (1990) 187–198.

[106] JADE collaboration, P. A. Movilla Fernandez, O. Biebel, S. Bethke, S. Kluth and P. Pfeifenschneider, *A Study of event shapes and determinations of alpha-s using data of e+ e- annihilations at $\sqrt{s}$ = 22-GeV to 44-GeV, Eur. Phys. J.* **C1** (1998) 461–478, [hep-ex/9708034].

[107] JADE, OPAL collaboration, P. Pfeifenschneider et al., *QCD analyses and determinations of alpha(s) in e+ e- annihilation at energies between 35-GeV and 189-GeV, Eur. Phys. J.* **C17** (2000) 19–51, [hep-ex/0001055].

[108] L3 collaboration, P. Achard et al., *Studies of hadronic event structure in e^+e^- annihilation from 30-GeV to 209-GeV with the L3 detector, Phys. Rept.* **399** (2004) 71–174, [hep-ex/0406049].

[109] ALEPH collaboration, R. Barate et al., *Studies of quantum chromodynamics with the ALEPH detector, Phys. Rept.* **294** (1998) 1–165.

[110] OPAL collaboration, G. Abbiendi et al., *Measurement of event shape distributions and moments in $e^+e^- \rightarrow$ hadrons at 91-GeV - 209-GeV and a*

determination of alpha(s), *Eur. Phys. J.* **C40** (2005) 287–316,
[`hep-ex/0503051`].

[111] OPAL collaboration, R. Akers et al., *Measurement of the production rates of charged hadrons in e+ e- annihilation at the Z0*, *Z. Phys.* **C63** (1994) 181–196.

[112] OPAL collaboration, G. Alexander et al., Δ^{++} *production in hadronic Z0 decays*, *Phys. Lett.* **B358** (1995) 162–172.

[113] OPAL collaboration, G. Alexander et al., J/ψ *and* ψ' *production in hadronic* Z^0 *decays*, *Z. Phys.* **C70** (1996) 197–210.

[114] DELPHI collaboration, P. Abreu et al., *Strange baryon production in Z hadronic decays*, *Z. Phys.* **C67** (1995) 543–554.

[115] OPAL collaboration, G. Alexander et al., *Strange baryon production in hadronic Z0 decays*, *Z. Phys.* **C73** (1997) 569–586.

[116] OPAL collaboration, K. Ackerstaff et al., *Spin alignment of leading* $K^*(892)^0$ *mesons in hadronic Z0 decays*, *Phys. Lett.* **B412** (1997) 210–224,
[`hep-ex/9708022`].

[117] DELPHI collaboration, P. Abreu et al., *Measurement of inclusive rho0, f(0)(980), f(2)(1270), K*0(2)(1430) and f-prime(2)(1525) production in Z0 decays*, *Phys. Lett.* **B449** (1999) 364–382.

[118] OPAL collaboration, K. Ackerstaff et al., *Photon and light meson production in hadronic Z0 decays*, *Eur. Phys. J.* **C5** (1998) 411–437, [`hep-ex/9805011`].

[119] OPAL collaboration, K. Ackerstaff et al., *Production of f(0)(980), f(2)(1270) and phi(1020) in hadronic Z0 decay*, *Eur. Phys. J.* **C4** (1998) 19–28,
[`hep-ex/9802013`].

[120] OPAL collaboration, G. Abbiendi et al., *Multiplicities of pi0, eta, K0 and of charged particles in quark and gluon jets*, *Eur. Phys. J.* **C17** (2000) 373–387, [`hep-ex/0007017`].

[121] ALEPH collaboration, A. Heister et al., *Inclusive production of the omega and eta mesons in Z decays, and the muonic branching ratio of the omega*, *Phys. Lett.* **B528** (2002) 19–33, [`hep-ex/0201012`].

[122] OPAL collaboration, P. D. Acton et al., *A Measurement of $K^{*\pm}(892)$ production in hadronic Z0 decays*, *Phys. Lett.* **B305** (1993) 407–414.

[123] L3 collaboration, O. Adriani et al., *Measurement of inclusive eta production in hadronic decays of the Z0*, *Phys. Lett.* **B286** (1992) 403–412.

[124] BaBar collaboration, J. P. Lees et al., *Production of charged pions, kaons, and protons in e^+e^- annihilations into hadrons at $\sqrt{s}$=10.54 GeV*, *Phys. Rev.* **D88** (2013) 032011, [`1306.2895`].

[125] PLUTO collaboration, C. Berger et al., *Multiplicity Distributions in e+ e- Annihilations at PETRA Energies*, *Phys. Lett.* **95B** (1980) 313–317.

[126] M. Derrick et al., *Study of Quark Fragmentation in e+ e- Annihilation at 29-GeV: Charged Particle Multiplicity and Single Particle Rapidity Distributions*, *Phys. Rev.* **D34** (1986) 3304.

[127] TPC/Two Gamma collaboration, H. Aihara et al., *Pion and kaon multiplicities in heavy quark jets from e^+e^- annihilation at 29-GeV*, *Phys. Lett.* **B184** (1987) 299–304.

[128] JADE collaboration, W. Bartel et al., *Charged Particle and Neutral Kaon Production in e+ e- Annihilation at PETRA*, *Z. Phys.* **C20** (1983) 187.

[129] TASSO collaboration, W. Braunschweig et al., *Charged Multiplicity Distributions and Correlations in e+ e- Annihilation at PETRA Energies*, *Z. Phys.* **C45** (1989) 193.

[130] AMY collaboration, H. W. Zheng et al., *Charged hadron multiplicities in* e^+e^- *annihilations at* $\sqrt{s} = 50$ *GeV - 61.4 GeV, Phys. Rev.* **D42** (1990) 737–747.

[131] OPAL collaboration, K. Ackerstaff et al., *Measurements of flavor dependent fragmentation functions in* $Z^0 \to q\bar{q}$ *events, Eur. Phys. J.* **C7** (1999) 369–381, [hep-ex/9807004].

[132] SLD collaboration, K. Abe et al., *Measurement of the charged multiplicities in b, c and light quark events from Z0 decays, Phys. Lett.* **B386** (1996) 475–485, [hep-ex/9608008].

[133] SLD collaboration, K. Abe et al., *Production of* π^+, K^+, K^0, K^{*0}, ϕ, *p and* Λ^0 *in hadronic Z0 decays, Phys. Rev.* **D59** (1999) 052001, [hep-ex/9805029].

[134] SLD collaboration, K. Abe et al., *Production of* π^+, π^-, K^+, K^-, *p and* $\bar{p}$ *in light (uds), c and b jets from Z0 decays, Phys. Rev.* **D69** (2004) 072003, [hep-ex/0310017].

[135] DELPHI collaboration, P. Abreu et al., *Hadronization properties of b quarks compared to light quarks in* $e^+ e^- \to q\bar{q}$ *from 183-GeV to 200-GeV, Phys. Lett.* **B479** (2000) 118–128, [hep-ex/0103022].

[136] OPAL collaboration, G. Abbiendi et al., *Charged particle multiplicities in heavy and light quark initiated events above the Z0 peak, Phys. Lett.* **B550** (2002) 33–46, [hep-ex/0211007].

[137] ALEPH collaboration, D. Decamp et al., *Measurement of the charged particle multiplicity distribution in hadronic Z decays, Phys. Lett.* **B273** (1991) 181–192.

[138] DELPHI collaboration, P. Abreu et al., *Charged particle multiplicity distributions in Z0 hadronic decays, Z. Phys.* **C50** (1991) 185–194.

[139] OPAL collaboration, P. D. Acton et al., *A Study of charged particle multiplicities in hadronic decays of the Z0, Z. Phys.* **C53** (1992) 539–554.

[140] PARTICLE DATA GROUP collaboration, C. Amsler et al., *Review of Particle Physics, Phys. Lett.* **B667** (2008) 1–1340.

[141] OPAL collaboration, G. Abbiendi et al., *Scaling violations of quark and gluon jet fragmentation functions in e+ e- annihilations at $\sqrt{s}$ = 91.2-GeV and 183-GeV to 209-GeV, Eur. Phys. J.* **C37** (2004) 25–47, [`hep-ex/0404026`].

[142] BELLE collaboration, R. Seuster et al., *Charm hadrons from fragmentation and B decays in e+ e- annihilation at $\sqrt{s}$ = 10.6-GeV, Phys. Rev.* **D73** (2006) 032002, [`hep-ex/0506068`].

[143] BABAR collaboration, B. Aubert et al., *Inclusive Lambda(c)+ Production in e+ e- Annihilations at $\sqrt{s}$ = 10.54-GeV and in Upsilon(4S) Decays, Phys. Rev.* **D75** (2007) 012003, [`hep-ex/0609004`].

[144] CLEO collaboration, M. Artuso et al., *Charm meson spectra in e^+e^- annihilation at 10.5-GeV c.m.e., Phys. Rev.* **D70** (2004) 112001, [`hep-ex/0402040`].

[145] ALEPH collaboration, R. Barate et al., *Study of charm production in Z decays, Eur. Phys. J.* **C16** (2000) 597–611, [`hep-ex/9909032`].

[146] SLD collaboration, K. Abe et al., *Measurement of the b quark fragmentation function in Z0 decays, Phys. Rev.* **D65** (2002) 092006, [`hep-ex/0202031`].

[147] ALEPH collaboration, A. Heister et al., *Study of the fragmentation of b quarks into B mesons at the Z peak, Phys. Lett.* **B512** (2001) 30–48, [`hep-ex/0106051`].

[148] OPAL collaboration, G. Abbiendi et al., *Inclusive analysis of the b quark fragmentation function in Z decays at LEP, Eur. Phys. J.* **C29** (2003) 463–478, [`hep-ex/0210031`].

[149] S. Platzer and S. Gieseke, *Coherent Parton Showers with Local Recoils*, *JHEP* **01** (2011) 024, [`0909.5593`].

[150] J. Bellm, G. Nail, S. Plätzer, P. Schichtel and A. Siódmok, *Parton Shower Uncertainties with Herwig 7: Benchmarks at Leading Order*, *Eur. Phys. J. C* **76** (2016) 665, [`1605.01338`].

[151] ATLAS collaboration, G. Aad et al., *Measurement of the Z/γ^* boson transverse momentum distribution in pp collisions at $\sqrt{s} = 7$ TeV with the ATLAS detector*, *JHEP* **09** (2014) 145, [`1406.3660`].

[152] ATLAS collaboration, G. Aad et al., *Measurement of the transverse momentum distribution of $Z/\gamma*$ bosons in proton–proton collisions at $\sqrt{s}=7$ TeV with the ATLAS detector*, *Phys. Lett. B* **705** (2011) 415–434, [`1107.2381`].

[153] S. Gieseke, M. H. Seymour and A. Siodmok, *A Model of non-perturbative gluon emission in an initial state parton shower*, *JHEP* **06** (2008) 001, [`0712.1199`].

[154] S. J. Webster, *Improved Monte Carlo Simulations of Massive Quarks*, Ph.D. thesis, Durham U., 2019.